



Functional Properties of Superhydrophobic Textiles

Dissertation Thesis

Study programme: P3106 Textile Engineering
Study branch: Textile Technics and Materials Engineering

Author: **Muhammad Zaman Khan, M.Sc.**
Thesis Supervisor: prof. Ing. Jakub Wiener, Ph.D.
Department of material engineering



Declaration

I hereby certify I have been informed that my dissertation is fully governed by Act No. 121/2000 Coll., the Copyright Act, in particular Article 60 – School Work.

I acknowledge that the Technical University of Liberec does not infringe my copyrights by using my dissertation for internal purposes of the Technical University of Liberec.

I am aware of my obligation to inform the Technical University of Liberec on having used or granted license to use the results of my dissertation; in such a case the Technical University of Liberec may require reimbursement of the costs incurred for creating the result up to their actual amount.

I, myself, have written my dissertation as an original and primary work using the literature listed below and consulting it with my thesis supervisor and my thesis counsellor.

At the same time, I honestly declare that the texts of the printed version of my dissertation and of the electronic version uploaded into the IS/STAG are identical.

February 21, 2020

Muhammad Zaman Khan, M.Sc.

DEDICATION

I dedicate this thesis to my parents and my wife Madiha Iftikhar

ACKNOWLEDGEMENT

Firstly, I am thankful to Almighty ALLAH for giving me strength and ability to complete this research work. I would like to thank the administration of Faculty of Textile Engineering, Technical University of Liberec, for offering me scholarship for Ph.D. and for providing me the facilities to conduct this research work. Upon completing this dissertation, I owe my deepest gratitude to so many people for their immense assistance. I would like to begin by expressing my sincere gratitude to Prof. Ing. Jiří Militký, CSc. Euring and my supervisor Prof. Ing. Jakub Wiener, PhD and Dr Vijay Baheti, PhD for their continuous support, motivation, encouragement, mentoring, and cooperation throughout my PhD study. Their guidance helped me in all the time of research and writing of this thesis.

I would also like to thank Ing. Jana Drašarová, Ph.D. (Dean of Faculty of Textile Engineering), Ing. Gabriela Krupincová, Ph.D. (Vice Dean for Science and Research) and Ing. Blanka Tomkova, Ph.D. (HOD, Department of Materials Engineering) for their kind support and valued guidance. I am also very grateful to all those at the Department of Material Engineering who were always so helpful and provided me with their assistance throughout my dissertation.

I wish to extend my special thanks to Ing. Bohumila Keilová, Ing. Hana Musilová, Kateřina Nohýnková, Martina Čimbuřová, Ing. Marie Kasprova, Ph.D. and Jana Grabmüllerová for their regular help and support. I am really thankful to the following people at The Institute for Nanomaterials, Advanced Technologies and Innovation, Dr. Mateusz Fijalkowski, Dr. Kinga Adach, and Dr. Pavel Kejzlar, who provided the research facilities and helped me in the research. I am also thankful to all my Pakistani colleagues, especially to Sajid Hussain, Sajid Faheem, Qummer Zia Gilani, Azam Ali and Musaddaq Azeem for their help and support.

Last but not the least; I can never forget my parents, wife, sisters and brother for their support and motivation in my life and especially my sons Ahmad and Umar who really suffered the effects of isolation during my stay away from home.

Muhammad Zaman Khan

TABLE OF CONTENTS

ABSTRACT	XI
ABSTRAKT	XIII
LIST OF TABLES	XV
LIST OF FIGURES	XVI
LIST OF ABBREVIATIONS/ SYMBOLS	XXI
CHAPTER 1	1
1. INTRODUCTION	1
CHAPTER 2	5
2. AIMS AND OBJECTIVES	5
2.1. Superhydrophobic fabrics coated with fly ash and OTMS	7
2.2. Superhydrophobic fabrics coated with TiO₂ nanoflowers and OTMS	7
2.3. Superhydrophobic fabrics coated with ZnO nanorods and OTMS	7
CHAPTER 3	8
3. LITERATURE REVIEW	8
3.1. Self-cleaning textiles	8
3.1.1. Physical self-cleaning	8
3.1.2. Chemical self-cleaning	9
3.2. Superhydrophobicity	10

3.3. Principles of wetting states	11
3.4. Fundamentals	12
3.4.1. <i>Young's law</i>	12
3.4.2. <i>Wenzel model</i>	13
3.4.3. <i>Cassie-Baxter model.....</i>	14
3.5. Roll-off angle.....	15
3.6. Fabrication of superhydrophobic surfaces	15
3.6.1. <i>Materials for superhydrophobic surfaces.....</i>	16
3.6.2. <i>Experimental approaches to fabricate superhydrophobic surface.....</i>	19
CHAPTER 4	29
4. RESEARCH METHODOLOGY.....	29
4.1. Materials	29
4.2. Superhydrophobic fabrics coated with fly ash and OTMS.....	31
4.2.1. <i>Preparation of mechanically activated fly ash</i>	31
4.2.2. <i>Preparation of fly ash coated cotton fabrics</i>	31
4.2.3. <i>Hydrophobization of fly ash coated cotton fabrics.....</i>	31
4.3. Superhydrophobic fabrics coated with TiO₂ nanoflowers and OTMS	32
4.3.1. <i>Synthesis of flower shaped TiO₂ particles on polyester fabric</i>	32
4.3.2. <i>Superhydrophobization of TiO₂ nanoflowers coated polyester fabrics</i>	33

4.4. Superhydrophobic fabrics coated with ZnO nanorods and OTMS	34
4.4.1. <i>Preparation of ZnO nanocrystals</i>	34
4.4.2. <i>Coating method.....</i>	34
4.4.3. <i>Growth of nanorods.....</i>	34
4.4.4. <i>Superhydrophobic treatment of ZnO nanorods grown cotton fabrics.....</i>	35
4.5. Characterization of surface morphology of coated fabrics	35
4.5.1. <i>SEM and EDS analysis</i>	35
4.5.2. <i>Raman spectroscopy</i>	36
4.5.3. <i>X-Ray diffraction (XRD) analysis</i>	36
4.5.4. <i>Atomic force microscopy (AFM) analysis</i>	36
4.6. Characterization of UV protection properties.....	37
4.7. Characterization of physical properties.....	37
4.8. Characterization of superhydrophobicity of coated fabrics	38
4.8.1. <i>Contact angle measurement</i>	38
4.8.2. <i>Roll off angle measurement</i>	38
4.8.3. <i>Contact angle hysteresis</i>	38
4.8.4. <i>Durability of contact angle.....</i>	38
4.9. Characterization of self-cleaning properties of coated fabrics	39
4.9.1. <i>Physical self-cleaning</i>	39

4.9.2. <i>Chemical self-cleaning</i>	39
4.10. Oil/water separation property of the coated fabrics	40
CHAPTER 5	41
5. RESULTS AND DISCUSSION	41
5.1. Superhydrophobic fabrics coated with fly ash and OTMS	41
5.1.1. <i>Mechanical activation of fly ash</i>	41
5.1.2. <i>Surface morphology of fly ash coated cotton fabrics</i>	42
5.1.3. <i>AFM analysis of fly ash coated cotton fabrics</i>	43
5.1.4. <i>UV protection performance of fly ash coated cotton fabrics</i>	45
5.1.5. <i>Physical properties of fly ash-OTMS coated cotton fabrics</i>	46
5.1.6. <i>Superhydrophobic properties of fly ash-OTMS coated cotton fabrics</i>	47
5.1.7. <i>Analysis of superhydrophobicity of fly ash-OTMS coated cotton fabrics</i>	50
5.1.8. <i>Durability of superhydrophobic properties of fly ash-OTMS coated cotton fabrics</i> ...	53
5.1.9. <i>Oil in water removal performance of fly ash-OTMS coated cotton fabrics</i>	54
5.2. Superhydrophobic fabrics coated with TiO₂ nanoflowers and OTMS	57
5.2.1. <i>SEM analysis of polyester fabrics coated with TiO₂ nanoflowers</i>	57
5.2.2. <i>EDS analysis</i>	60
5.2.3. <i>Raman spectroscopy</i>	60
5.2.4. <i>XRD analysis</i>	61

5.2.5. AFM analysis	62
5.2.6. Physical properties of TiO ₂ -OTMS coated polyester fabrics	63
5.2.7. Superhydrophobic properties of TiO ₂ nanoflowers coated polyester fabrics	64
5.2.8. Analysis of superhydrophobicity of coated polyester fabrics	66
5.2.9. Durability of superhydrophobic properties of coated polyester fabrics	68
5.2.10. Physical self-cleaning properties of coated fabrics.....	70
5.2.11. Chemical self-cleaning properties of coated fabrics	71
5.3. Superhydrophobic fabrics coated with ZnO nanorods and OTMS	75
5.3.1. Morphological analysis and growth mechanism.....	75
5.3.2. Add-on analysis	83
5.3.3. EDS analysis	83
5.3.4. XRD analysis	85
5.3.5. Topography and roughness analysis	85
5.3.6. Superhydrophobic properties of ZnO-OTMS coated cotton fabrics.....	88
5.3.7. Durability of ZnO-OTMS coated cotton fabrics.....	92
5.3.8. Physical self-cleaning properties of ZnO-OTMS coated cotton fabrics.....	93
5.3.9. Oil in water removal performance of ZnO-OTMS coated cotton fabrics.....	94
CHAPTER 6	97
6. CONCLUSIONS AND FUTURE WORK	97

6.1. Conclusions	97
6.2. Future work	99
REFERENCES.....	100
LIST OF PUBLICATIONS	116

ABSTRACT

Over the last decades, researchers have been working to mimic the nature by inducing superhydrophobic properties into a variety of material surfaces so that they exhibit non-wetting properties. Many diverse applications have been found in the fields, such as space, defense, automotive, biomedical applications and engineering, sensors, apparels, and so on. This dissertation is about the development of superhydrophobic surfaces by inexpensive, simple and eco-friendly techniques with added functionalities (i.e. UV protection, Self-cleaning, Oil/Water separation, etc.) by deposition of fly ash, TiO_2 and ZnO particles.

The first study proposed simple and low-cost approach for improvement in UV protection and superhydrophobic properties of cotton fabrics by coating of mechanically activated fly ash particles. The maximum UV blocking was observed for 3 wt% fly ash, where UV transmittance decreased from 14.19% of untreated fabric to 0.11% of coated fabric. After subsequent treatment of Trimethoxy(octadecyl)silane (OTMS) on fly ash coated fabrics, the water contact angle was increased to 143° , 147° and 153° for fly ash concentration of 1, 2 and 3 wt% respectively. From Cassie-Baxter theories, the unwetted fraction of air pockets were estimated to be 43%, 55% and 67% respectively for 1, 2 and 3 wt% of fly ash particles. Furthermore, the coated fabrics showed great potentials for separation of floating oil layer, underwater oil droplet or oil/water mixture. The separation efficiency of 98%, 96%, 97% and 95% was obtained for selected model oils toluene, n-hexane, chloroform and petrol ether, respectively.

In second study, the growth of 3D shaped TiO_2 flower particles on surface of polyester fabrics using two step approaches of sol-gel technology and hydrothermal method was successfully achieved. The scanning electron microscopy, EDS analysis, Raman spectroscopy, and X-ray diffraction techniques were employed to study the effect of Titanium isopropoxide (TTIP) concentration on the growth of flower-like TiO_2 microstructures. Atomic force microscopy (AFM) was carried out to evaluate the surface topography and roughness. Later, the layer of Trimethoxy(octadecyl)silane was applied on TiO_2 coated polyester fabrics to fabricate the self-cleaning textiles. The physical self-cleaning properties were examined based on superhydrophobicity and contact angle measurements where maximum static contact angle of 160.1° and minimum roll off angle of 3° was found for 2 mL TTIP dose. The degradation of

methyl orange dyes under UV light irradiation was observed to confirm the photocatalytic chemical self-cleaning behavior, where the samples coated with 2 mL TTIP decolorized the dye solution in 150 min, whereas the samples coated with 1 mL and 1.5 mL TTIP took almost 300 and 210 min respectively.

In third study, a novel microwave hydrothermal method was employed on cotton fabrics to develop superhydrophobic surface by rapid synthesis of aligned ZnO nanorods on surface of the cotton fabric. Two step approaches was used for the growth of ZnO nanorods. First, cotton fabric was coated by seed layer of ZnO nanocrystals synthesized using microwave-assisted sol gel method. Secondly, ZnO nanorods were grown rapidly on the seeded cotton fabrics by microwave hydrothermal method. At last, layer of non-fluorinated silane was applied on as-grown nanorods to fabricate a superhydrophobic surface. The non-fluorinated silane was selected as this is less hazardous to skin compared to fluorinated silanes. The effect of zinc nitrate hexahydrate ($\text{Zn}(\text{NO}_3)_2 \cdot 6\text{H}_2\text{O}$) concentration, reaction time and microwave power on the growth of ZnO nanorods were investigated in detail using scanning electron microscopy (SEM). To study the structural properties of ZnO nanorods EDS analysis and X-ray diffraction (XRD) techniques were used. Surface topography and roughness of the nanorods grown fabrics were studied using AFM. The superhydrophobic properties were examined based on contact angle and roll off angle measurements where maximum water contact angle of 170.2° and minimum roll off angle of 1° was found for 25 mM zinc nitrate hexahydrate ($\text{Zn}(\text{NO}_3)_2 \cdot 6\text{H}_2\text{O}$) concentration. The physical self-cleaning property was examined by using methyl orange dye as debris particles. The ZnO-OTMS coated fabrics were evaluated for superhydrophobic durability against mechanical abrasion, laundering, chemical and UV action. Moreover, the ZnO-OTMS coated fabrics showed excellent potentials for separation of floating and underwater oil layers or oil in water mixture. The oil in water separation efficiency of 99%, 98%, 98% and 96% was obtained for chloroform/water, n-hexane/water, petro ether/water and toluene/water, respectively.

Keywords: Fly ash particles; Superhydrophobicity; UV protection; Roughness; Oil water separation, TiO_2 nanoflowers; Physical self-cleaning; Chemical self-cleaning, ZnO nanorods; Microwave hydrothermal synthesis; Contact angle

ABSTRAKT

V posledních desetiletích se vědci snaží napodobovat přírodu tak, že připravují super hydrofobní povrchy různých materiálů, které mají nesmáčivé projevy. Tyto materiály nacházejí mnoho různých aplikací v řadě oborů a výrobků. Příkladem jsou kosmická technika, vojenský a automobilový průmysl, biomedicínské obory a strojírenství, čidla, speciální oděvy atd. Tato disertační práce se zabývá vývojem superhydrofobních povrchů s multifunkčními projevy (tj. UV ochrana, samočištění, separace olej / voda atd.) pomocí levných, jednoduchých a ekologicky orientovaných technik. Je využito ukládání částic popílku, strukturovaných nanočástic TiO_2 a ZnO s následnou silanizací.

V první studii je navržen jednoduchý a levný postup ke zlepšení ochrany proti UV záření a získání superhydrofobních vlastností bavlněných tkanin povrchovým nánosem mechanicky aktivovaných částic popílku. Maximální UV blokování bylo pozorováno pro 3 hmotnostní % popílku, kde propustnost UV klesla ze 14,19% pro neošetřené textilie na 0,11% pro upravené textilie. Po následné silanizaci pomocí trimethoxy (oktadecyl) silanu (OTMS) byl kontaktní úhel pro vodu zvýšen na 143° , 147° respektive 153° pro koncentrace 1, 2 a 3 hmotnostní % popílku. Z teorie Cassie-Baxtera byl odhadnut podíl nesmočených vzduchových prostor (kapes) 43%, 55% a 67% pro 1, 2 a 3 hmotnostní % popílku. Kromě toho upravené textilie umožňovaly oddělení olejové vrstvy, kapiček oleje ve vodě nebo směsi oleje a vody. Účinnost separace 98%, 96%, 97% a 95% byla získána pro vybrané modelové oleje, toluen, n-hexan, chloroform a petroléter.

Ve druhé studii byl realizován růst částic TiO_2 tvaru nano květin na povrchu polyesterových tkanin pomocí dvou stupňového procesu sol-gel a hydrotermálního působení. Ke studiu účinku izopropoxidu titanu (TTIP) byly použity skenovací elektronová mikroskopie, EDS analýza, Ramanova spektroskopie a rentgenová difrakce. Pro vyhodnocení topografie povrchu a drsnosti byla použita mikroskopie AFM. Polyesterové textilie s nánosem TiO_2 tvaru nano květin byly následně silanizovány pomocí trimethoxy (oktadecyl) silanu s cílem přípravy samočisticích textilií. Fyzikální samočisticí schopnosti byly zkoumány na základě měření superhydrofobicity pomocí kontaktního úhlu. Pro dávku 2 ml TTIP byl nalezen maximální statický kontaktní úhel $160,1^\circ$ a minimální úhel skoulení kapky (roll off) 3° . Pro potvrzení fotokatalytického chemického samočisticího chování byla hodnocena rychlost degradace barviva Metyl-oranž na

upravených vzorcích při ozáření ultrafialovým světlem. U vzorku, kde byly pro růst TiO_2 nanočástic použity 2 ml TTIP došlo odbarvení za 150 minut, zatímco u vzorků, kde bylo použito 1 ml a 1,5 ml TTIP došlo k odbarvení po 300 a 210 min.

Ve třetí studii byla použita nová mikrovlnná hydrotermální metoda rychlé tvorby uspořádaných nano tyčinek ZnO pro vytvoření superhydrofobního povrchu na bavlněných tkaninách. Pro růst nano tyčinek ZnO byly použity dva kroky. Nejprve byla bavlněná tkanina potažena zárodečnou vrstvou nanokrystalů ZnO syntetizovaných metodou sol-gel s využitím mikrovlnného ohřevu. Růst nano tyčinek ZnO byl realizován na zárodečné povrchové vrstvě bavlněných tkanin mikrovlnnou hydrotermální metodou. Následně byla provedena silanizace pomocí prekurzoru neobsahujícího fluor, tak aby byl vytvořen superhydrofobní povrch. Vliv koncentrace hexahydrátu dusičnanu zinečnatého ($\text{Zn}(\text{NO}_3)_2 \cdot 6\text{H}_2\text{O}$), reakční doby a mikrovlnné energie na růst nano tyčinek ZnO byl podrobně zkoumán pomocí skenovací elektronové mikroskopie (SEM). Ke studiu strukturních vlastností nano tyčinek ZnO byly použity EDS analýza a rentgenové difrakce (XRD). Povrchová topografie a drsnost textilií obsahujících nano tyčinky ZnO byla studována pomocí AFM. Superhydrofobní vlastnosti byly zkoumány na základě měření kontaktního úhlu a měření úhlu náběhu. Byl nalezen maximální kontaktní úhel vody $170,2^\circ$ a minimální úhel skoulení kapky 1° pro koncentraci hexahydrátu dusičnanu zinečnatého ($\text{Zn}(\text{NO}_3)_2 \cdot 6\text{H}_2\text{O}$) 25 mM. Fyzikální samočisticí vlastnosti byly zkoumány pomocí částic nečistot simulovaných barvivem Metyl-oranž. Byly hodnoceny také odolnosti proti mechanickému oděru, praní, chemickému a UV působení. Bylo také nalezeno, že upravené textilie mají schopnost separace různých směsí vody a olejů. Účinnost separace oleje od vody 99%, 98%, 98% a 96% byla získána pro směs chloroform/voda, n-hexan/voda, petroléter/voda a toluen/voda.

Klíčová slova: Částice popílku; superhydrofobita; ochrana proti UV záření; drsnost; oddělení oleje a vody; nano květiny TiO_2 ; fyzikální samočištění; chemické samočištění; nano tyčinky ZnO; mikrovlnná hydrotermální syntéza; kontaktní úhel

LIST OF TABLES

Table 1. Parameters of fabric used.....	30
Table 2. UV transmission of fly ash coated cotton fabrics	45
Table 3. Add-on (%) of FA+OTMS coated cotton fabrics	46
Table 4. Stiffness of the FA+OTMS coated cotton fabrics	47
Table 5. Add-on (%) of TiO ₂ -OTMS coated polyester fabrics.....	63
Table 6. Stiffness of the TiO ₂ -OTMS coated polyester fabrics	64
Table 7. Dimension of nanorods grown at various concentrations.....	78
Table 8. Add-on (%) of ZnO-OTMS coated cotton fabrics	83
Table 9. Elemental composition of ZnO nanorods coated cotton fabrics	84
Table 10. Analysis of surface roughness	86

LIST OF FIGURES

Figure 1. Superhydrophobicity in nature [14].	2
Figure 2. Self-cleaning lotus surface, flowering plant of Lotus (<i>Nelumbo nucifera</i>) is shown in (a). Lotus leaf contaminated with clay (b) and self-cleaning action of lotus leaf (c). The SEM images (d–f) show the lotus leaf surface in different magnifications [16]	3
Figure 3. Summary of aims and objectives of this thesis.	6
Figure 4. Physical self-cleaning on (a) a superhydrophilic and (b) a superhydrophobic surface [29].	9
Figure 5. Reactions during the photoexcitation of titanium dioxide using UV/vis light [28].	10
Figure 6. Schematic representation of wetting states of surfaces with different WCA [33].	11
Figure 7. Water droplets on flat, nano, micro and hierarchical structures [35].	11
Figure 8. A drop of water on an ideal smooth surface (Young’s model) [36].	13
Figure 9. (a) Wenzel droplet, (b) Cassie-Baxter droplet [37].	14
Figure 10. Typical methods to fabricate micro/nanorough surfaces [41].	16
Figure 11. Multi-step and single-step processes used for development of superhydrophobic surfaces [85].	20
Figure 12. Low surface energy coating materials used for hydrophobic coating [85].	20
Figure 13. SEM images of (a) pristine cotton fiber, (b) cotton fibers treated with silver particles and (c) higher magnification image of (a); (d) image of water droplet on surface treated with silver particles and HDTMS [86].	21
Figure 14. Schematic of superhydrophobic OTMS/TCPP/TiO ₂ -coated cotton and inset is the WCA image on OTMS/TCPP/TiO ₂ -coated cotton [13].	22

Figure 15. Procedure employed to fabricate superhydrophobic TiO ₂ particles decorated cotton fabric with fluoroalkylsilane modification. SEM images of pristine and coated fabric, and droplet behavior (insets) on corresponding fabric surface [87].	23
Figure 16. (a) Structural schematic , (b) Photograph of cotton fabric coated with Nafion-MWCNTs, (c) SEM images of coated cotton fiber and (d) contact angle results with various numbers of deposition [46].	24
Figure 17. SEM images of ZnO-coated cotton fabrics with different mesh density at two reaction temperatures 70 °C (sparse (a), medium (b) and dense (c)) and 80 °C (sparse (d), medium (e) and dense (f)). In the inset are water contact angles for the corresponding [89].	25
Figure 18. (a) Schematic diagram of the fabrication process for superamphiphobic cotton fabrics. (b) Photographs of water, cooking oil and hexadecane droplets on the coated cotton fabrics [90].	26
Figure 19. Illustration of the fabrication of multifunctional superhydrophobic fabrics [91].	26
Figure 20. (a) Experimental strategy for the fabrication of superhydrophobic cotton fabrics, (b) SEM micrographs superhydrophobic cotton fabric and, (c) Photographs of the static water droplets on corresponding surface [5].	27
Figure 21. Microscopic images of (a) cotton, and (b) polyester fabric	30
Figure 22. Fabrication of fly ash-OTMS coated superhydrophobic cotton fabric	32
Figure 23. Schematic of deposition of TiO ₂ flower shaped particles on polyester fabric	33
Figure 24. Shows the schematic of development of superhydrophobic cotton fabrics	35
Figure 25. Effect of ball milling on fly ash	42
Figure 26. Surface structure of fly ash coated cotton fabrics	43
Figure 27. AFM images and representative surface profiles of the pristine and coated fabrics ...	44

Figure 28. Effect of fly ash concentration on contact angle	49
Figure 29. Self-cleaning property of 3 wt% fly ash-OTMS coated cotton fabric.....	49
Figure 30. Analysis of superhydrophobicity of fly ash-OTMS coated cotton fabrics	53
Figure 31. Durability of fly ash-OTMS coated cotton fabrics	54
Figure 32. Oil in water removal performance of fly ash-OTMS coated cotton fabrics	56
Figure 33. SEM micrographs of polyester fabric	58
Figure 34. Effect of Titanium isopropoxide dose on growth of TiO ₂ nano flowers	59
Figure 35. EDS spectrum of flower-like TiO ₂ nanoparticles coated on polyester.....	60
Figure 36. Raman spectra of flower-like TiO ₂ nanoparticles coated on polyester fabric	61
Figure 37. XRD pattern of flower-like TiO ₂ nanoparticles coated on polyester fabric	62
Figure 38. AFM analysis of the flower-like TiO ₂ nanoparticles coated polyester.....	63
Figure 39. Effect of Titanium isopropoxide dose on contact angle	65
Figure 40. Analysis of superhydrophobicity of TiO ₂ -OTMS coated polyester fabrics	68
Figure 41. Durability of surface microstructure TiO ₂ -OTMS coated fabrics.....	69
Figure 42. Durability of TiO ₂ -OTMS coated polyester fabrics	70
Figure 43. Physical self-cleaning property of TiO ₂ -OTMS coated polyester fabric	71
Figure 44. Photocatalytic stain degradation of TiO ₂ -OTMS coated polyester fabric	72
Figure 45. Evaluation of TiO ₂ -OTMS coated polyester fabric after photocatalytic degradation .	73
Figure 46. Solution discoloration properties of TiO ₂ -OTMS coated polyester fabrics	74

Figure 47. SEM image of the (a) pristine cotton fabric, (b) ZnO nanorods grown fabric surface and (c) 3D AFM image of the ZnO nanorods decorated fabric surface. Insets (a) and (b) are images of water droplet on the corresponding fabric surfaces..... 75

Figure 48. SEM images of (a) ZnO seeded cotton fiber and, (b) 10 mM zinc nitrate hexahydrate concentration treated cotton fiber 77

Figure 49. SEM images of ZnO nanorods grown onto cotton fabric in microwave reactor at 360 W (60 %) for 10 min under various concentration of zinc nitrate hexahydrate/HMTA: (a) 25 mM, (b) 50 mM, (c) 75 mM, and (d) 100 mM. Insets are the corresponding low magnification images 79

Figure 50. SEM images of ZnO nanorods grown on cotton surfaces treated with 25 mM of Zinc nitrate hexahydrate/HMTA in microwave reactor at 360 W (60 %) for different reaction time: (a, b) 10 min, (c, d) 20 min and (e, f) 30 min..... 80

Figure 51. SEM images of ZnO nanorods grown on cotton surfaces treated with 25 mM of Zinc nitrate hexahydrate/HMTA in microwave reactor for 10 min at different microwave powers (watt): (a, b) 360 W (60 %) , (c, d) 420 W (70 %) and (e, f) 480 W (80 %). Magnifications: 10.00 KX (a, c, e) and 25.00 KX (b, d, f) 82

Figure 52. EDS spectra of ZnO nanorods coated cotton fabrics at various concentration of Zinc nitrate hexahydrate/HMTA for 10 min: (a) 25 mM, (b) 50 mM, (c) 75 mM, and (d) 100 mM ... 84

Figure 53. XRD patterns of the ZnO nanorods grown at 25 mM and 100 mM concentration of zinc nitrate hexahydrate/HMTA. All peaks are indexed according to ICDD Card No. 01-083-6338..... 85

Figure 54. AFM images and surface profiles of ZnO nanorods grown fabrics at various concentration of zinc nitrate hexahydrate, (a) 25 mM, (b) 50 mM, (c) 75 mM, and (d) 100 mM 87

Figure 55. Effect of zinc nitrate hexahydrate concentration on water contact angle 89

Figure 56. Analysis of superhydrophobicity of ZnO-OTMS coated cotton fabrics 92

Figure 57. Durability of ZnO-OTMS coated cotton fabrics 93

Figure 58. The self-cleaning process of ZnO-OTMS coated cotton fabric (a–d). The high magnify optical images of ZnO-OTMS coated cotton fabric before self-cleaning (e), and after self-cleaning (g), and corresponding schematic illustration of the self-cleaning process (f) 94

Figure 59. Oil in water removal performance of ZnO-OTMS coated cotton fabrics 95

LIST OF ABBREVIATIONS/ SYMBOLS

Abbreviations

AFM	Atomic Force Microscopy
CAH	Contact Angle Hysteresis
CVD	Chemical Vapor Deposition
EMI	Electromagnetic Interference
EDS	Energy-dispersive X-ray spectroscopy
FA	Fly Ash
HDTMS	Hexadecyltrimethoxysilane
HMTA	Hexamethylenetetramine
OTMS	Trimethoxy(octadecyl)silane
SEM	Scanning Electron Microscopy
TTIP	Titanium Isopropoxide
UPF	Ultraviolet Protection Factor
UV	Ultraviolet
WCA	Water Contact Angle
XRD	X-Ray Diffraction

Symbols

w/w	Weight by weight
-----	------------------

Ra	Average roughness
g/L	Grams per liter
v/v	Volume by volume
mM	Millimole
μL	Microliter
θ_R	Roll-off angle
F_e	Force of attraction
W_{ad}	Work of adhesion
γ_{SV}	Solid vapor interfacial tension
γ_{SL}	Solid liquid interfacial tension
γ_{LV}	liquid vapor interfacial tension

CHAPTER 1

1. INTRODUCTION

The superhydrophobicity of solid surfaces has been investigated with considerable attention over the past few years due to the increased demands of impermeable textiles, self-cleaning coatings, non-adhesive coatings, microfluidic devices, biosensors and outdoor antennas [1, 2]. Based on superhydrophobic species existing in nature (e.g. lotus leaves, butterfly wings, and water strider legs), surface roughness and low surface energy of materials can be considered as the two important factors to obtain superhydrophobic surfaces [3]. The different methods such as electrospinning deposition, layer-by-layer assembly, chemical etching, phase separation, chemical vapor deposition, colloid assembly have been employed to obtain superhydrophobic surfaces [4, 5].

The self-cleaning textiles also hold great promise for military applications where there is a lack of time for laundering at severe conditions, and in business life when clothes get stained accidentally [6]. Currently, there are two main concepts used in developing self-cleaning textiles [7]. The first concept (physical self-cleaning) is based on the superhydrophobic approach where water droplets attain the spherical shape and then they roll off the surface carrying away the dirt particles [8]. The second concept (chemical self-cleaning) is based on the process of photocatalysis where the dirt/stain molecules break down to simpler species (such as CO₂ and water) on exposure to light [9]. For physical self-cleaning, the surface roughness and low surface energy of materials are the two important factors to control the wettability of a surface and to obtain water contact angles greater than 150° [3]. As an inspiration from nature (e.g. lotus leaves, butterfly wings, and water strider legs), scientists have fabricated superhydrophobic textiles by creating surface roughness in combination with low surface energy materials such as organic silanes, fluorinated silanes, alkyl amines and silicates [10–12]. For chemical self-cleaning, polycrystalline semiconductor oxides have been applied in the form of nano-coatings, leading to the successful development of a number of UV-active self-cleaning textiles [13].

In early 90s, the researchers started to explore the natural surfaces having superhydrophobic and self-cleaning properties. These natural surfaces include the lotus plant, rice and Colocasia esculenta etc. Figure 1 shows the superhydrophobic and self-cleaning surfaces present in nature. These surfaces have micro/nano hierarchical structures on their surfaces [14].

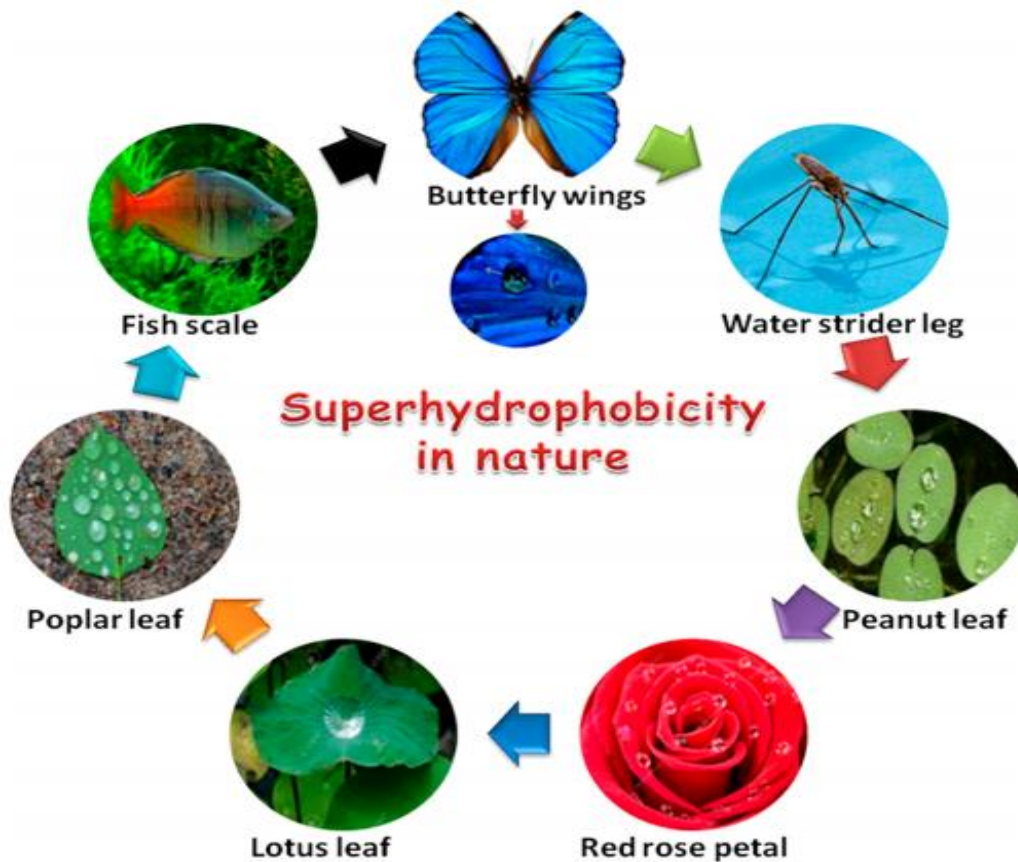
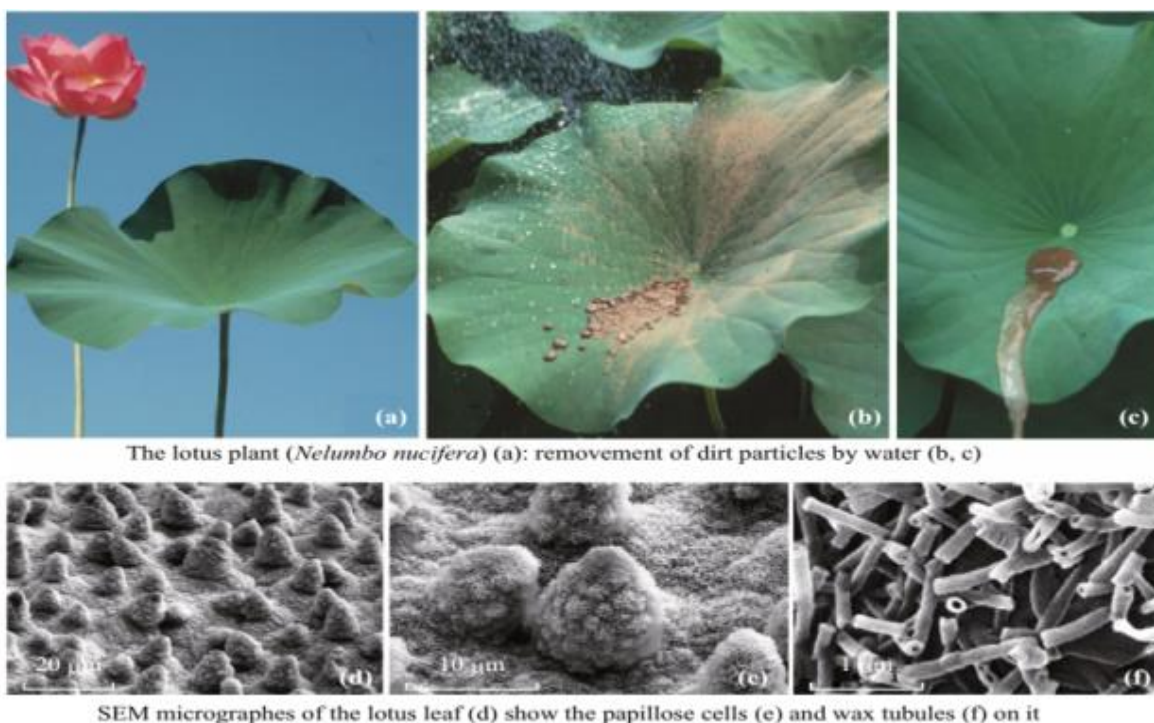


Figure 1. Superhydrophobicity in nature [14].

Lotus effect refers to cleaning of lotus leaves by rain water droplets (see Figure 2). When water droplets fall on the lotus leaves, the water droplets attain the spherical shape and then they roll off the surface carrying away the dirt particles leaving neat and clean surface. The physical self-cleaning phenomenon has two important properties; superhydrophobicity and low water roll off angle. The lotus leaf contains 3-10 μ m hills and valley which are covered with nanocrystals of wax of size 70-100nm [15].



The lotus plant (*Nelumbo nucifera*) (a): removal of dirt particles by water (b, c)

SEM micrographs of the lotus leaf (d) show the papillose cells (e) and wax tubules (f) on it

Figure 2. Self-cleaning lotus surface, flowering plant of Lotus (*Nelumbo nucifera*) is shown in (a). Lotus leaf contaminated with clay (b) and self-cleaning action of lotus leaf (c). The SEM images (d–f) show the lotus leaf surface in different magnifications [16]

In 1963, DuPont introduced its fluorochemical based product for treating fabrics which was called Zepel fabric fluoridizer. After treatment, the fabric exhibited water and oil repellency. The launch of this product followed by several other similar chemicals and research works to improve the durability as well as the repellency characteristics. The first time lotus effect mechanism was studied and reported by Barthlott and Neinhuis in 1997 [17]. During this study, it was found that self-cleaning property is due to presence of hierarchical rough surface structure of plant leaves. Since then, this type of self-cleaning of plant leaves is called lotus effect.

During last two decade research interests on superhydrophobicity and self-cleaning surfaces have grown tremendously. Numerous studies have been done related to mimicking of natural plants and animals. Great work has been reported on understanding of the structures and special wettability of the natural superhydrophobic surfaces and development of artificial anti-wetting surfaces. Such superhydrophobic surfaces have many applications such a self-cleaning,

anti-corrosion, anti-fogging/frosting, oil/water separation, and anti-bio adhesion applications. Superhydrophobic textiles having oil in water separation ability are valuable to overcome the problems caused by oil spillage accidents. Furthermore, many other novel multifunctional applications for superhydrophobic surfaces have started to gain attention, like UV-protection, photocatalytic activity, anti-bacterial, EMI shielding, flame-retardant and anti-adhesion [18]. In order to defend other properties against damage, it has become an increasing trend to integrate the superhydrophobicity with additional functionalities. Thus, attention should be paid to research on environmentally friendly preparation methods, as well as durability and mechanical stability of the textiles. In this context, this research work is focused on the development of superhydrophobic textiles with added functionalities (i.e. UV protection, Self-cleaning, Oil/Water separation) by deposition of fly ash, TiO_2 and ZnO nanostructures.

CHAPTER 2

2. AIMS AND OBJECTIVES

The superhydrophobic surfaces exhibits the water contact angles greater than 150° and roll-off angle less than 10° . Over the past decade, there have been many successful attempts at artificially reproducing the surface structures found on natural superhydrophobic surfaces. Currently, the most superhydrophobic surfaces are developed by using expensive, time consuming methods, precious equipment, high energy and less eco-friendly conditions. There are still many challenges on large scale fabrication of superhydrophobic surfaces by inexpensive, simple and eco-friendly techniques [19–22].

Great attention must be given to develop simple and environment friendly methods, also durability and stability of the textiles under various ageing conditions. Moreover, other novel multifunctional applications for superhydrophobic textiles started to merge, including UV-blocking, photocatalytic, antibacterial, flame-retardant, anti-fogging/frosting, oil/water separation, and anti-bio adhesion. Among all properties, the integration of UV protection on superhydrophobic surfaces is of great concern in present work. This is because, the risks of UV radiations to induce acute and chronic illnesses, when they interact with skin, increased significantly in recent years [23]. Recently, numerous efforts have been made to simultaneously create superhydrophobic and photocatalytic surfaces which not only repel water but also decompose organic contaminates at the same time. However, the fabrication of superhydrophobic and photocatalytic surface is challenging because this surface either loses its superhydrophobicity upon irradiation with light or does not show a photocatalytic property [24].

The overall objectives of this research work are to develop the superhydrophobic textiles with added functionalities (i.e. UV protection, Self-cleaning, Oil/Water separation, etc.) by deposition of fly ash, TiO_2 and ZnO nanostructures. The main purpose and aim of the thesis is shown as tree diagram in Figure 3.

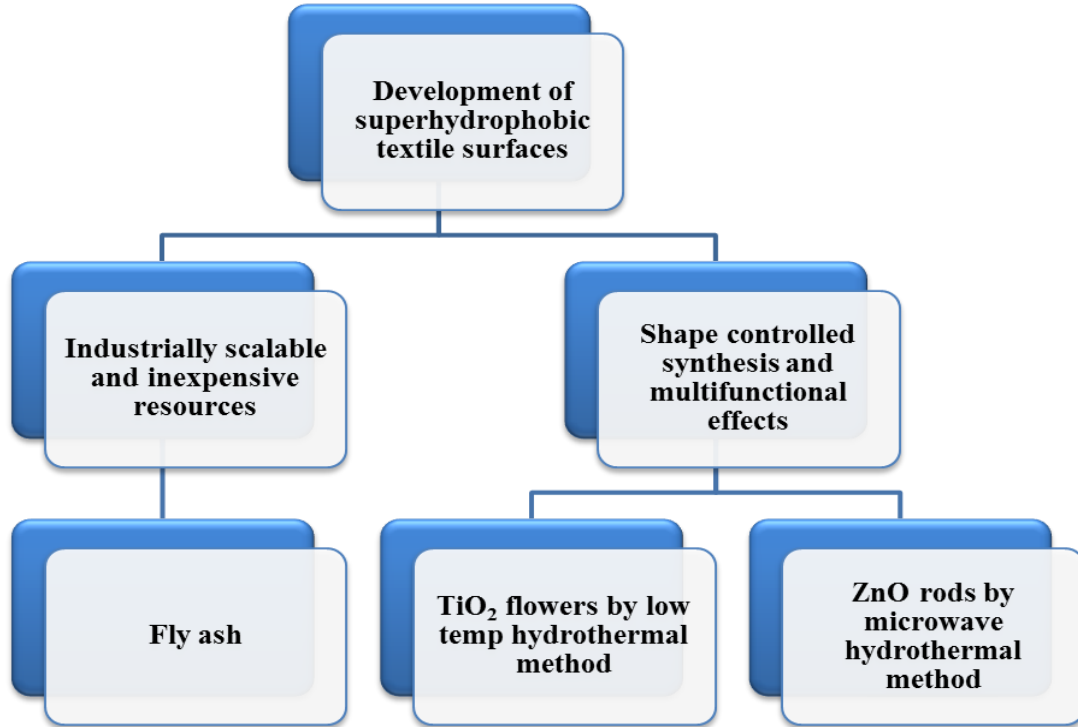


Figure 3. Summary of aims and objectives of this thesis.

The specific objectives are as follow;

- Deposition of nanoparticles by different methods to achieve hierarchical surface roughness.
- Application of non-fluorinated silane (i.e. Trimethoxy(octadecyl)silane) to modify the surface chemistry.
- Characterization of surface morphology and topography of nanoparticle coated fabrics by different microscopy techniques.
- Evaluation of superhydrophobic properties from contact angle, sliding angle and contact angle hysteresis tests, and the validation of results by Cassie-Baxter model.
- Characterization of superhydrophobic durability against chemical and mechanical treatments.
- Evaluation of other essential properties, such as UV protection, Physical self-cleaning, Chemical self-cleaning, Oil-water separation and durability properties.

2.1. Superhydrophobic fabrics coated with fly ash and OTMS

Aim of first study was to use mechanically activated fly ash to create effective and durable coating on cotton fiber surface for enhancing superhydrophobicity, UV protection, physical self-cleaning and oil in water separation. To the best of the author's knowledge, this is the first study on fly ash coated cotton fabrics. The coating of fly ash particles has never been studied for UV blocking properties of textiles despite their high refractive index and presence of metal oxide constituents in chemical composition.

2.2. Superhydrophobic fabrics coated with TiO₂ nanoflowers and OTMS

Aim of second study was to fabricate the polyester based self-cleaning textiles which are simultaneously superhydrophobic and photocatalytic. The 3D shaped TiO₂ flower particles grown on surface of polyester fabrics using two step approaches of sol-gel technology and hydrothermal method with subsequent silanization by Trimethoxy(octadecyl)silane (OTMS) were proposed as active layer. The flower-like TiO₂ hierarchical structure was proposed for obtaining excellent photocatalytic properties and inhibit defects of micron and nanometer structures due to their more abundant porous structure, larger specific surface area, lower density, better surface permeability, greater light-harvesting capacity, good light absorption efficiency, and appropriate refractive index [25].

2.3. Superhydrophobic fabrics coated with ZnO nanorods and OTMS

Aim of third study was to develop superhydrophobic cotton fabrics by using of a novel microwave hydrothermal method to grow vertically aligned ZnO nanorods on cotton fibers surfaces with subsequent silanization by Trimethoxy(octadecyl) silane (OTMS). This novel microwave hydrothermal method to grow ZnO nanorods is a simple, inexpensive, and time saving, low temperature and affective control over morphology. The study of effect of salt concentrations, reaction time and microwave power on the morphology of ZnO nanorods was proposed.

CHAPTER 3

3. LITERATURE REVIEW

3.1. Self-cleaning textiles

The research related to self-cleaning surfaces has received considerable attention within the scientific community due to their potential applications in industry and daily life [26]. For example, it is useful for the textile products which are endangered by staining with heavy contaminants such as soot, oils, lubricants or those not capable of washing due to their size or water and/or detergent sensitivity (i.e. umbrellas, canopies, shade shelters, camps, curtains, blinds, roller blinds or external sunshades) [27]. The self-cleaning textiles also hold great promise for military applications where there is a lack of time for laundering at severe conditions, and in business life when clothes get stained accidentally [6]. Currently, there are two main concepts used in developing self-cleaning textiles [7].

3.1.1. Physical self-cleaning

The first concept (physical self-cleaning) is based on the superhydrophobic approach where water droplets attain the spherical shape and then they roll off the surface carrying away the dirt particles [8]. For physical self-cleaning, the surface roughness and low surface energy of materials are the two important factors to control the wettability of a surface and to obtain water contact angles greater than 150° [3]. It was observed that the sliding angles decrease with increasing contact angle depending on the surface roughness. The superhydrophobic approach of physical self-cleaning surfaces exhibits high water contact angle ($WCA > 150^\circ$), low contact angle hysteresis and low roll off angle. During superhydrophilic approach ($WCA < 5^\circ$) where water droplets are spread, producing a film on the surface transport on the top dirt particles (see Figure 4) [28, 29].

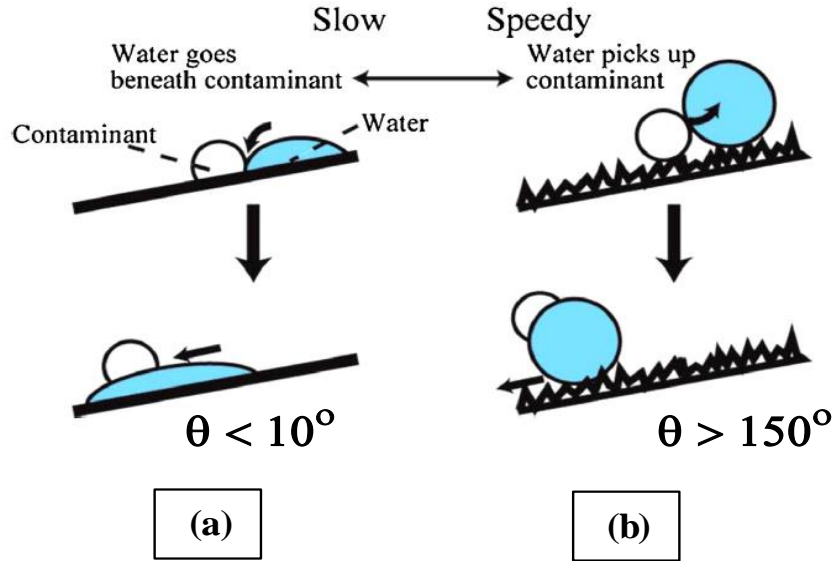


Figure 4. Physical self-cleaning on (a) a superhydrophilic and (b) a superhydrophobic surface [29].

3.1.2. Chemical self-cleaning

The second concept (chemical self-cleaning) is based on the process of photo-catalysis where the dirt/stain molecules break down to simpler species (such as CO_2 and water) on exposure to light. The UV radiation activates the photocatalyst deposited on surface which generates the active species capable of degrading organic chemicals. In photocatalytic reaction the electromagnetic radiation with phonon energy (given by its wavelength λ (nm)) at least equal to the band gap of semiconductor E_g (eV) should be used. The required wavelength for just overcoming band gap is simply given by Equation (1).

$$\lambda = \frac{1240}{E_g} \quad (1)$$

For the visible light range this is from 3.1 eV to 1.8 eV.

One of most efficient materials for chemical self-cleaning (photochemical oxidation/reduction) is TiO_2 nanoparticles of different shape and size. TiO_2 is a versatile

photocatalyst degrading a wide range of organic pollutants, bacteria, cancer cells, and viruses and has applications in air and water remediation, and self-sterilizing surfaces as well [28, 30–32]. The processes of photoexcitation for TiO_2 promoted by sun radiation are shown in Figure 5. When TiO_2 was illuminated by light energy higher than its band gaps, the electrons in TiO_2 jumped from the valence band to the conduction band and then formed electron (e^-) and electric hole (h^+) pairs on the surface of the photocatalyst. The negative electrons and oxygen combined into O_2^- , whereas the positive electric holes and water generated hydroxyl radicals. When the organic compound falls on the surface of the photocatalyst, it can combine with O_2^- and OH^- respectively, and turn into carbon dioxide and water.

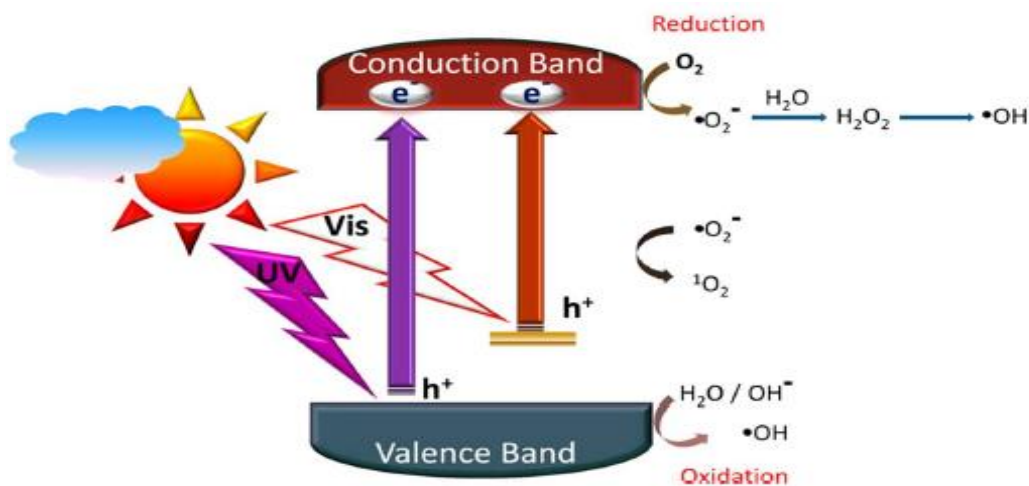


Figure 5. Reactions during the photoexcitation of titanium dioxide using UV/vis light [28].

3.2. Superhydrophobicity

Superhydrophobicity is the tendency of a surface to repel water drops. Hydrophobicity comes from the Greek hydro that means *water* and phobos means *fear*. Therefore, a hydrophobic surface is one which repels the water while hydrophilicity is directly opposite of it. To develop superhydrophobic structures modification of surface chemistry is necessary in combination with micro-nano surface roughness.

Before going into details of superhydrophobicity, it is better to understand wetting phenomenon. A surface is considered as a superhydrophobic surface only if the surface having

extremely high water contact angle (WCA $> 150^\circ$), low contact angle hysteresis (CAH $< 10^\circ$), low sliding angle (SA $< 10^\circ$) and high stability of Cassie model state. The surface with a water contact angle of less than 90° is considered as hydrophilic and with contact angle greater than 90° is defined hydrophobic [33, 34]. The contact angle of a water droplet on a hydrophilic, hydrophobic, and superhydrophobic surface is illustrated in Figure 6.

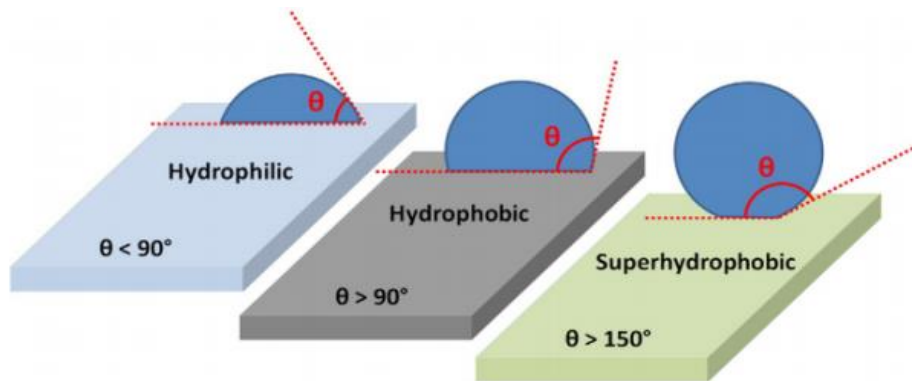


Figure 6. Schematic representation of wetting states of surfaces with different WCA [33].

3.3. Principles of wetting states

Superhydrophobicity is the intrinsic property of hierarchical structure. These structures are able to increase the superhydrophobicity by reducing the contact between the water droplet and the surface [35]. The roughness of the surface plays a vital role for hydrophobicity. This roughness can be divided into two types; unitary roughness which can be micro or nano-roughness and hierarchical roughness which is the micro-roughness covered by nano-roughness as shown in Figure 7.

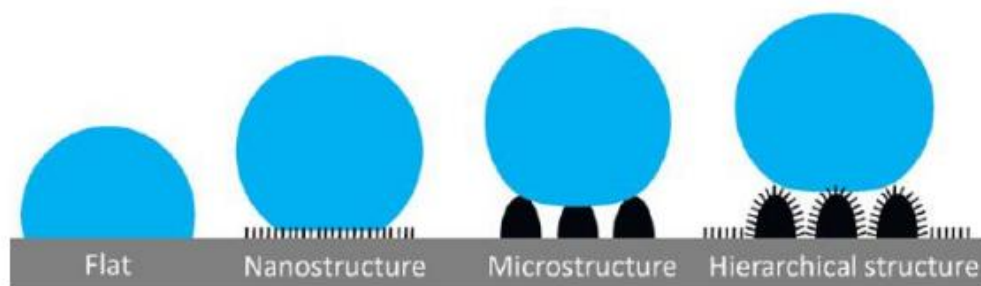


Figure 7. Water droplets on flat, nano, micro and hierarchical structures [35].

According to the affinity with vapor and solid, the liquid spread over the surface. Therefore, there are three types of wetting; total, partial and nonwetting. In order to determine if droplet spreads over the surface or not, we take into consideration the parameter of spreading “S” which depends on the surface energy of solid and liquid (Equation 2).

$$S = \gamma_{SV} - (\gamma_{SL} + \gamma_{LV}) \quad (2)$$

Where, γ_{SV} , γ_{SL} and γ_{LV} are the interfacial tensions between solid and vapor, solid and liquid, and liquid and vapor respectively. If “S” is positive, the liquid spreads over the completely. If “S” is negative, the liquid does not spread and forms a droplet with a contact angle θ on the solid surface. The line at the interface of three phases, liquid, gas and solid is called triple line.

3.4. Fundamentals

3.4.1. Young’s law

Wetting is commonly characterized by the contact angle, which is defined as the angle between the tangent to the liquid/vapor interface and the solid surface at the three-phase contact line. In 1805, Thomas Young proposed a model (Equation 3) to determine the contact angle of the liquid on a homogeneous and perfectly smooth surface [2].

$$\cos\theta = \frac{\gamma_{SV} - \gamma_{SL}}{\gamma_{LV}} \quad (3)$$

Young’s equation is a basic and classical wetting model used to evaluate wetting of flat surface. According to his law, the droplet can only be in equilibrium if the forces acting on the triple are equal (see Figure 8). By convention, the contact angle is measured from the liquid side. For a smooth and chemically homogeneous solid surface, the contact angle of a drop can be calculated theoretically by using the Young’s equation [36].

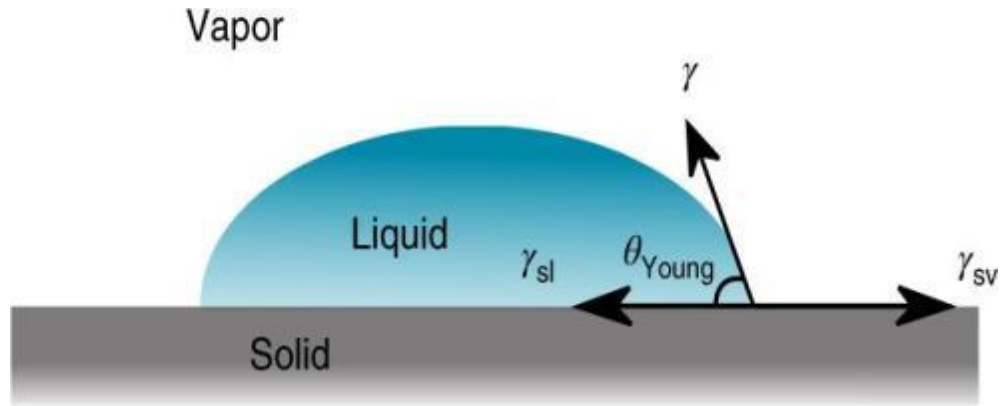


Figure 8. A drop of water on an ideal smooth surface (Young's model) [36].

Where; θ is the Young contact angle on ideally smooth surface, γ_{SV} and γ_{SL} refer to the solid/vapor and solid/liquid interfacial tensions, respectively, and γ_{LV} is the liquid/vapor interfacial tension (i.e, surface tension of the liquid). From the Young equation, it is well known that solid surfaces having high surface energy show a low contact angle, whereas solid surfaces with low surface energy tends to exhibit a high contact angle value. The contact angle depends on the difference of interfacial tension between solid, gas and solid, liquid. A high quality silicon wafer is considered close to the ideal smooth surface.

3.4.2. Wenzel model

In 1936, Wenzel proposed a new model (Figure 9a) for rough surfaces. In the Wenzel model, the liquid is in contact with the entire solid surface and completely penetrates into cavities. The Wenzel model states that a rough material has a higher surface area than a smooth one, which modifies the contact angle [2, 37].

There is not a single surface in nature which is completely homogeneous and perfectly smooth. So, there is always more or less roughness present on the surface. Therefore, the Young's law does not give the exact value of contact angle. In order to calculate the contact angle on rough surface, Wenzel put forward the following equation (Eq. 4).

$$\cos\theta_w = r \cos\theta \quad (4)$$

Where; θ_w is the contact angle on a surface with roughness, and θ is that of on an ideal surface and r is roughness fraction which is defined as the ratio between contact area to projected area of the surface. The "r" is either equal to 1 or more than 1. If it is equal to 1 that means the surface is 100% homogeneous and smooth which is not possible. If the surface is already hydrophilic (WCA $<90^\circ$), the introduction of roughness to the surface will increase its hydrophilicity. The surface having water contact angle less than 10° is refer to superhydrophilic surface. Similarly, if the surface is already hydrophobic, the roughness to the surface will increase the hydrophobicity and the surface will become superhydrophobic, having contact angle greater than 150° [38]. This equation is valid only when the water droplet penetrates into the asperities of roughness as shown in Figure 9a.

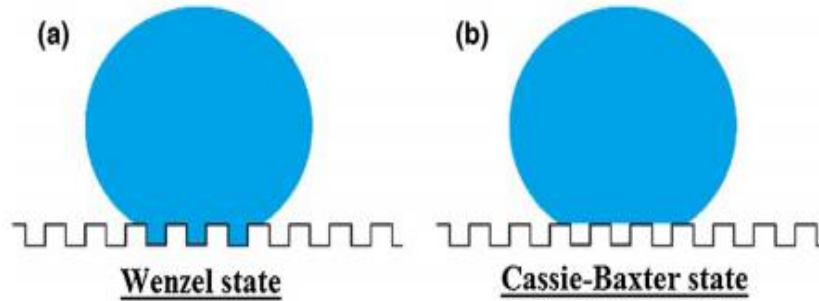


Figure 9. (a) Wenzel droplet, (b) Cassie-Baxter droplet [37].

3.4.3. Cassie-Baxter model

The Cassie model (1944) is based on water contact with a composite surface of the solid and air that is trapped into the microgrooves of the rough surface. In this state, the droplet of liquid does not make a complete contact with the surface that is due to the presence of air pockets underneath. The drops of liquid rest on the heterogeneous composite interface of the surface that consists of the peaks of patterned rough surface and air pockets trapped between them, which a drop of liquid cannot penetrate as shown in Figure 9b [39, 40]. Therefore, for a surface composed of two fractions, one with the fractional area f_1 and the contact angle θ_1 and the other with f_2 and θ_2 , respectively (so that $f_1 + f_2 = 1$), the contact angle for the heterogeneous interface is given by the Cassie-Baxter equation (Eq. 5) [41].

Where; $f_2 = 1 - f_1$

$$\cos\theta^* = f_1 \cos\theta_1 + (1 - f_1) \cos\theta_2 \quad (5)$$

On applying this equation to air/solid composite interface, the equation becomes (Eq. 6).

$$\cos\theta^* = f_1(\cos\theta_1 + 1) - 1 \quad (6)$$

Where, apparent contact angle (θ^*) observed on a rough surface and the equilibrium contact angle (θ_1) obtained on a smooth surface without roughness. The f_1 is surface fraction of solid in contact with the droplet. The Cassie–Baxter model given in Equation (6) can be used to estimate the area fraction of a water droplet (f_1) in contact with a surface (i.e. wetted solid fraction). The superhydrophobicity of a surface is due to roughness, when roughness of the surface increases, the value of f_1 decreases. The air pockets can lead to the surface being superhydrophobic. As the droplet of liquid do not penetrate between the cavities of roughness, therefore, water beads up into a spherical shape and roll off the surface.

3.5. Roll-off angle

The angle at which a water drop rolls off a tilted flat surface is known as the roll-off angle (θ_R). Generally, superhydrophobic surfaces have a static contact angle above 150° and a roll off angle of less than 10° . But very high quality superhydrophobic surfaces can exhibit roll-off angles of less than 1 degree [42] . A low roll-off angle is crucial to self-cleaning application. The roll-off angle, also known as “sliding” angle, is the one of the inclinations when the water droplet completely rolls off the surface without an external force [18].

3.6. Fabrication of superhydrophobic surfaces

Fabrication of superhydrophobic surfaces has been an area of active research since the mid-1990s. In general, different techniques that is used for the micro and nanostructure fabrication, such as lithography, etching, and deposition and self-assembly, has been utilized for producing superhydrophobic surfaces (Figure 10). There are two main requirements for the

development of superhydrophobic surface, such as roughness of the surface and it should be hydrophobic (low surface energy). These two things lead to two methods for the fabrication of superhydrophobic surface: first, it is possible to make a rough surface from an initially hydrophobic material and secondly to modify a rough hydrophilic surface by modifying surface chemistry or by applying low surface energy material on it. Roughness is usually a more critical property than the low surface energy, since both moderately hydrophobic and very hydrophobic materials can exhibit similar wetting behavior when roughened [41]. Surface modification of the surface having roughness is carried out by using low surface energy materials such as fluorocarbon, organic silanes, fluorinated silanes, alkyl amines and silicates [13, 43–45]. In order to defend other properties against damage, it has become an increasing trend to integrate the superhydrophobicity with additional functionalities [46]. Several methods are reported for the development of superhydrophobic surfaces including hydrothermal technique [8, 47], sol gel method [48], dip coating [10, 49], electro-chemical method [50], layer-by-layer method [51], chemical vapor deposition [52, 53], and spray coating [54–56].

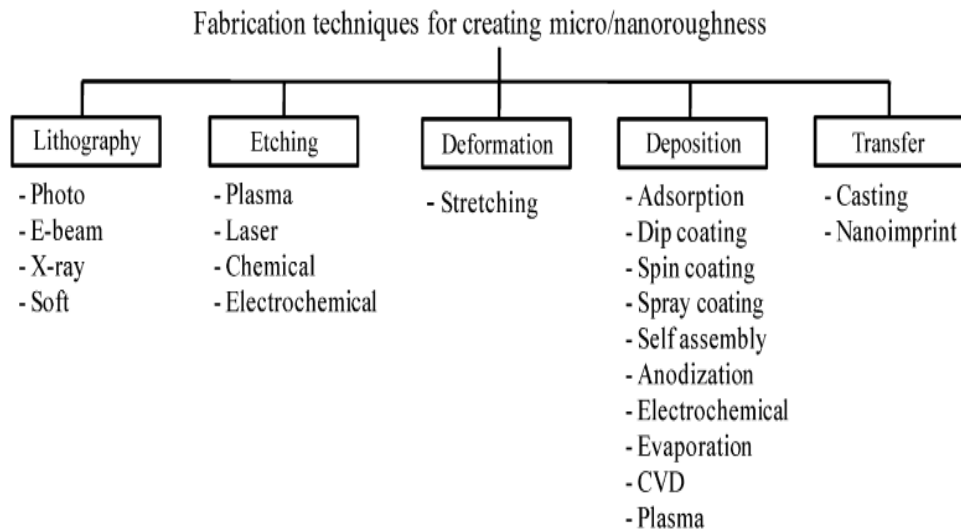


Figure 10. Typical methods to fabricate micro/nanorough surfaces [41].

3.6.1. Materials for superhydrophobic surfaces

Due to growing market demand, the researchers have focused their attention on development of superhydrophobic textiles using non-conventional techniques. These techniques

include the use of nanotechnology or nanomaterials either to deposit nanoparticles on textiles to functionalize them or to develop nanofibers which are used for manufacturing of fabrics with functional characteristics. The use of various nanoparticles is easiest ways to fabricate superhydrophobic and superoleophobic surfaces with high resistance against various environments [52, 57, 58]. The use of nanoparticles, nanofinishes and nanostructures is very useful for enhancing and developing superior performance characteristics of conventional textiles including superhydrophobicity, self-cleaning, UV blocking, antimicrobial activity, soil-resistance, anti-static, anti-infrared and flame-retardancy. The superhydrophobicity or superhydrophilicity of textile materials can also be enhanced by creating nanostructure surfaces [59]. UV protection property of a textile fabric can be achieved by dye, pigment, metal oxides or UV absorber finish. These materials can provide protection against UV radiation by absorbing and blocking its penetration through a fabric.

In recent years, lot of research has been done to develop superhydrophobic textiles using nanoparticles of ZnO, TiO₂, and SiO₂, etc. Excellent UV protection was achieved by deposition of TiO₂ on polyester fabric [60]. TiO₂ and ZnO nanoparticles are also used for this purpose as they have good UV protection properties. They give protection by reflecting, scattering or absorbing harmful UV radiations of sun. They are more stable when compared to organic UV-blocking agents. Nanoparticles of ZnO can be prepared by wet chemical technique followed by application on fabrics for enhanced UV protection [61–64]. Antibacterial effects on textile fabric can be maximized using nanoparticles because of the increased surface area [65–68]. Nano-rough superhydrophobic surfaces can be prepared by controlling surface topography by many processing methods which include sol–gel technique, organic/inorganic hybrid method, CVD, electrochemical deposition, embossing, plasma processing and phase separation technique. The incorporation of TiO₂ nanoparticles by titania sol-gel coating can cause surface roughness for enhancing the superhydrophobicity of the fabric [69]. Carbon fabric was coated with silica nanoparticles to make it superhydrophobic [70]. For physical and chemical self-cleaning, polycrystalline semiconductor oxides have been applied in the form of nano-coatings, leading to the successful development of a number of UV-active self-cleaning textiles [13]. Although TiO₂ or ZnO are widely used inorganic UV blockers, but they accelerate the photo damage of human skin due to high photocatalytic activity [71]. Therefore, the searches on safe UV shielding agents

that possess superior shielding efficiency with poor photocatalytic property have become an urgent necessity.

a) Fly ash

Ash residues are wastes of coal-fired power plants and they are produced at the boiler outlet of the plants, these including fly ashes and bottom ashes. They can be beneficially used in the building industry and road construction applications such as cement or asphalt additive, autoclaved aerated concrete block, concrete admixture, highway ice control, and hazardous waste removal [72–74]. In spite of these applications, the large quantities produced by industry create environment and waste management issues. Therefore, the development of alternative potential applications and further means to facilitate the recycling of incineration ashes are urgently needed.

Fly ashes (FA) are aluminosilicate rich by-products generated in coal firing powder plants. They are unique, non-toxic, chemically and physically stable, abundant and cheap, low density particles. In these circumstances, fly ash can be utilized as simple and low-cost approach for improvement in UV protection and superhydrophobic properties of cotton fabrics by coating of mechanically activated fly ash particles. Interestingly, fly ash particles have been reported to create micro/nanoscale roughness on the surface of fibers economically, however the researchers did not mention the additional benefits of fly ash coated fabrics [75].

b) Titanium dioxide

Titanium dioxide (TiO_2) has become the most popular high efficiency catalyst due to the advantages of its high refraction coefficient, absorption in the UV range, strong photocatalytic effect, biological inertness and low cost [76, 77]. The different methods such as electrospinning deposition, layer-by-layer assembly, chemical etching, phase separation, chemical vapor deposition, colloid assembly, etc. have been employed to obtain superhydrophobic surfaces [4, 5]. It was reported that the particle size, crystal structure, and the morphology play important roles on photocatalytic activity of TiO_2 , which are mainly depended on synthetic method and reaction conditions including titanium salt, pH value, reaction temperature, time, additives, etc. [78]. To further improve their performance and the durability, a considerable amount of research

is also focused on the controllable synthesis of TiO_2 with aligned one/three-dimensional nanostructures such as nanorods, nanowires, nanoflowers, nanotubes because of their high specific surface area and favored charge-transfer rate [79, 80].

c) Zinc oxide

Zinc oxide (ZnO) has many functional properties such as nontoxic, photocatalytic activity, UV resistant, antibacterial and piezoelectric properties. Zinc oxide nanostructures are used in catalytic reaction process due to its large surface area and high catalytic activity [81, 82]. In recent years, a lot of research has been done for the synthesis of zinc oxide nanostructures such as nanoflowers, nanowires, nanorodes, nanotubes, nanopillars and hollow spheres by using various hydrothermal techniques.

There are many challenges to development a cost effective, simple, energy efficient and time saving method for the synthesis of ZnO nanostructures. Microwave assisted heating methods are considered promising way of rapid heating, volumetric, high reaction rate and less reaction time as compared to the conventional heating methods [83, 84]. In recent years, a lot of research has been done for the synthesis of zinc oxide nanostructures such as nanoflowers, nanowires, nanorodes, nanotubes, nanopillars and hollow spheres by using various hydrothermal techniques. There are many challenges to development a cost effective, simple, energy efficient and time saving method for the synthesis of ZnO nanostructures.

3.6.2. Experimental approaches to fabricate superhydrophobic surface

As discussed earlier, synthesis and fabrication of any superhydrophobic surface require a combination of rough surface morphology and low overall surface energy. Several chemical and physical techniques have been used to fabricate such surfaces [85]. The methods can be broadly classified into two processes; multi-step process and single-step process (Figure 11).

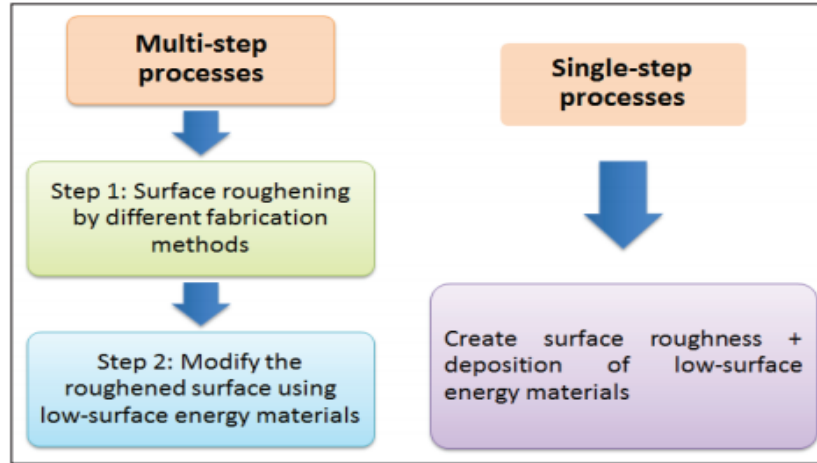


Figure 11. Multi-step and single-step processes used for development of superhydrophobic surfaces [85].

Several low surface energy materials are used for modification of surface chemistry. Long chain fatty acids, organic silanes, thiols and azides are most commonly used materials for modification of surface properties (Figure 12).

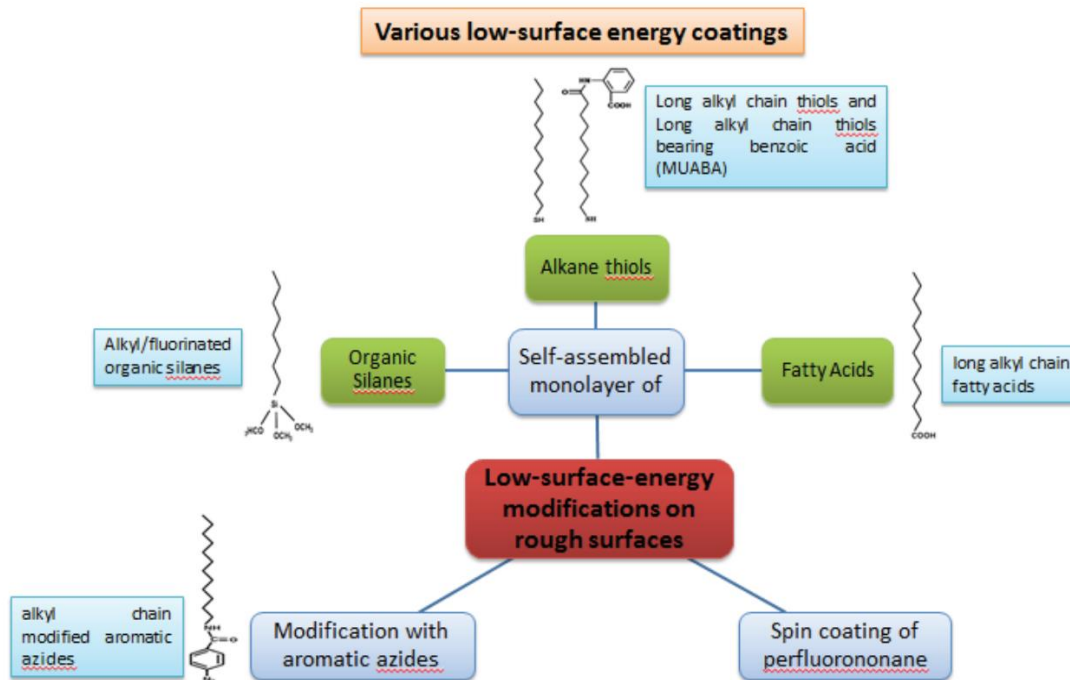


Figure 12. Low surface energy coating materials used for hydrophobic coating [85].

In order to defend other properties against damage, it has become an increasing trend to integrate the superhydrophobicity with additional functionalities [46]. For instance, Xue et al. fabricated superhydrophobic antibacterial surfaces on cotton textiles by introducing silver nanoparticles followed by surface hydrophobization of silane based low surface energy agents [86]. SEM images of the pristine cotton fiber and coated cotton fiber shown in Figure 13(a-c). They developed superhydrophobic surface having a water contact angle of 157.3° for cotton treated with silver particles and HDTMS, as shown in Figure 13(d).

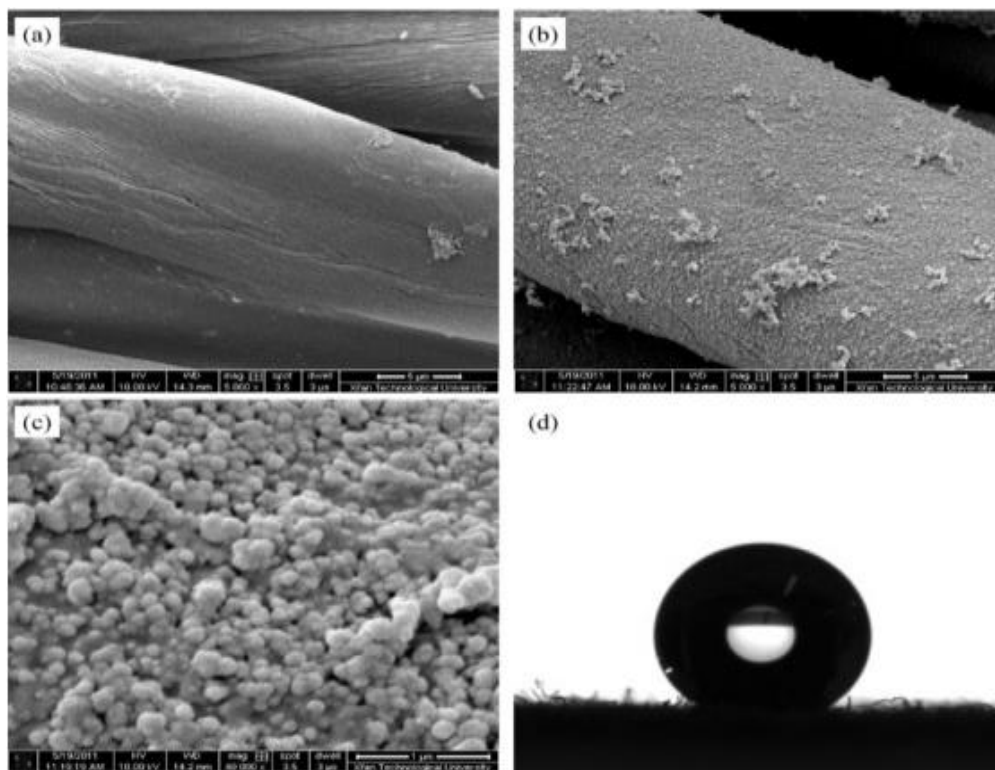


Figure 13. SEM images of (a) pristine cotton fiber, (b) cotton fibers treated with silver particles and (c) higher magnification image of (a); (d) image of water droplet on surface treated with silver particles and HDTMS [86].

Afzal et al. prepared a superhydrophobic and photocatalytic cotton fabric by step-wise deposition of anatase TiO_2 , mesotetra (4-carboxyphenyl) porphyrin and Trimethoxy(octadecyl)silane (OTMS) (Figure 14). The modified cotton fabrics exhibited

excellent superhydrophobicity with a water contact angle of 156° , but also showed significant photocatalytic degradation of methylene blue under visible-light irradiation [13].

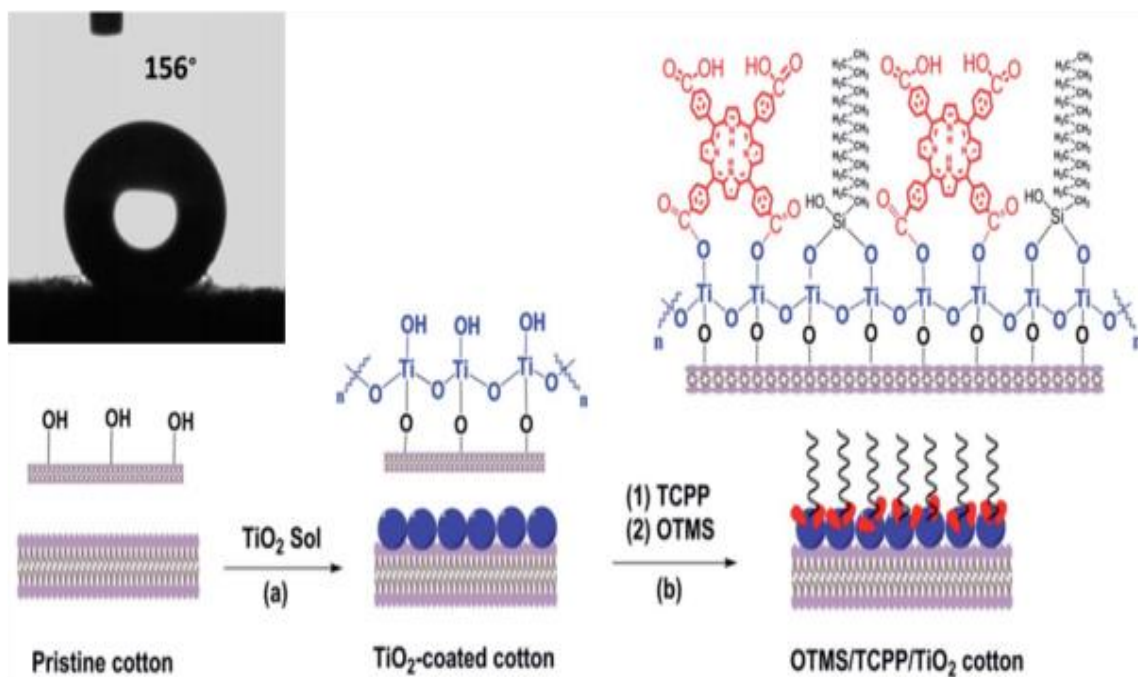


Figure 14. Schematic of superhydrophobic OTMS/TCPP/TiO₂-coated cotton and inset is the WCA image on OTMS/TCPP/TiO₂-coated cotton [13].

In another study, superhydrophobic surfaces with good UV protection and oil/water separation properties have been reported by hydrothermal deposition of TiO₂ nanoparticles on the cotton fabric followed by coating of fluorinated silanes [8]. Huang et al, results showed TiO₂ particles were uniformly distributed on the fiber surface with a high coating density (Figure 15). In comparison with hydrophobic cotton fabric, the TiO₂ coated cotton fabric exhibited a high superhydrophobic activity with a contact angle of 160° and a sliding angle lower than 10° [87].

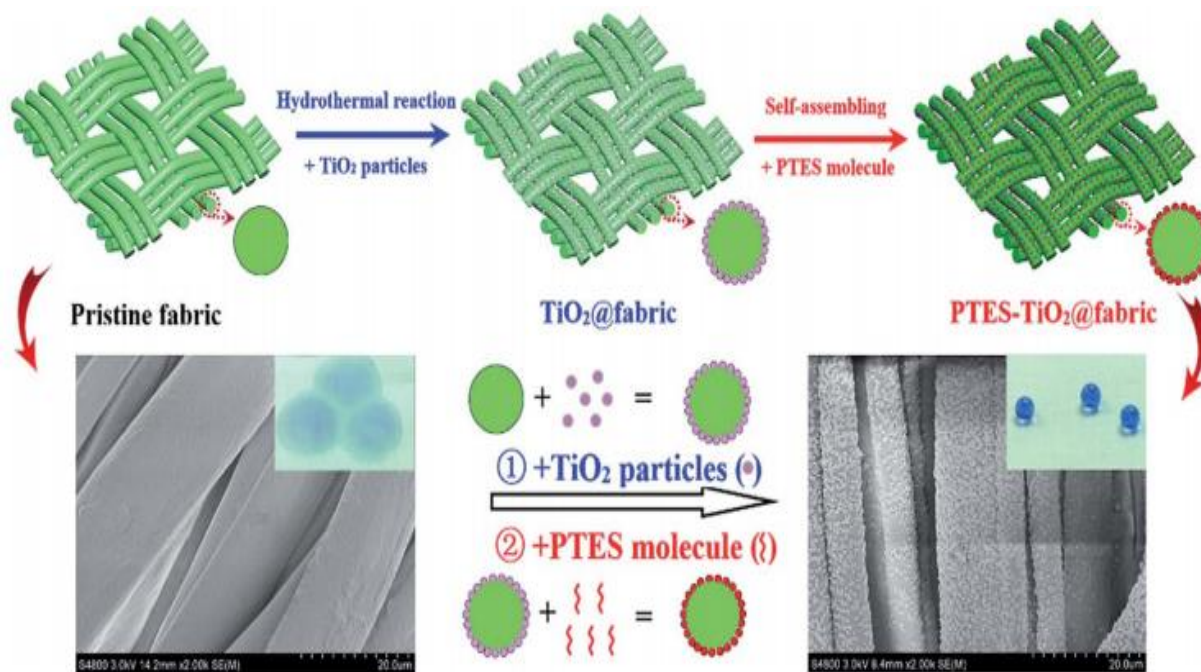


Figure 15. Procedure employed to fabricate superhydrophobic TiO_2 particles decorated cotton fabric with fluoroalkylsilane modification. SEM images of pristine and coated fabric, and droplet behavior (insets) on corresponding fabric surface [87].

Recently, Zou et al. coated cotton fabrics with perfluorosulfonated polymer and carbon nanotubes for development of superhydrophobic, electrically conductive and EMI shielding fabrics [46]. Figure 16a represent schematic diagram for the fabrication of the superhydrophobic fabric. Photograph and SEM images of cotton fabric coated with Nafion-MWCNTs can be seen from Figure 16(b-c). The contact angle of the resultant fabric was measured for various numbers of depositions (Figure 16d). The resultant fabric showed the favorable shielding effectiveness of 9.0 dB and a water contact angle of 154.6° .

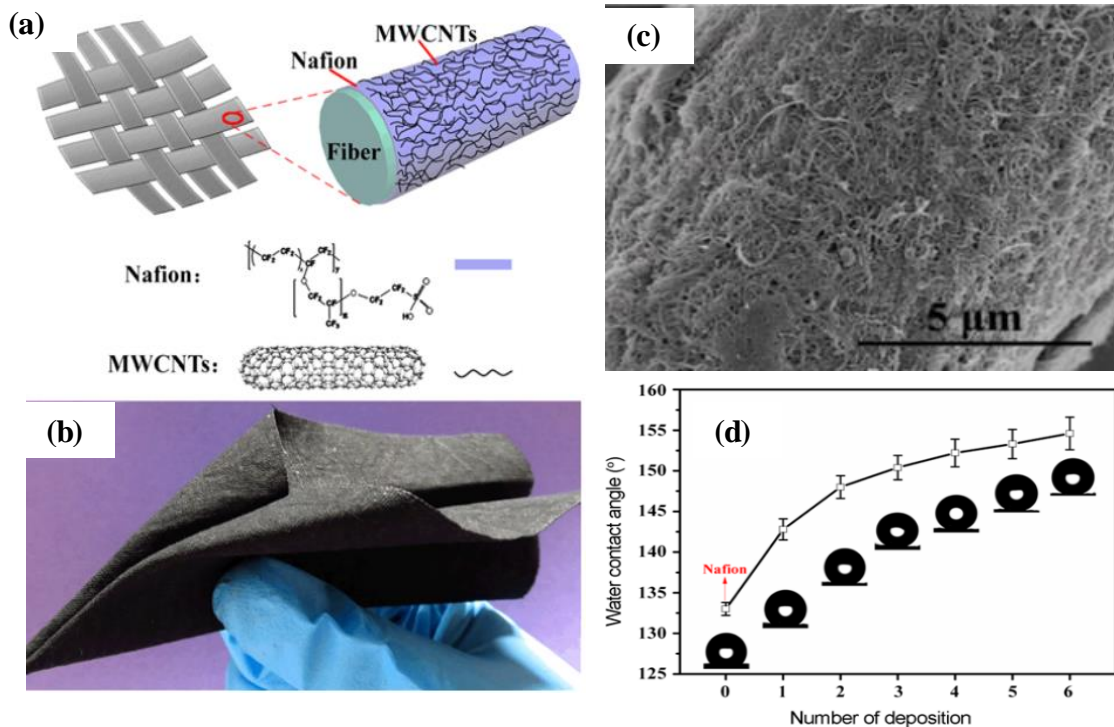


Figure 16. (a) Structural schematic , (b) Photograph of cotton fabric coated with Nafion-MWCNTs, (c) SEM images of coated cotton fiber and (d) contact angle results with various numbers of deposition [46].

In another study, self-cleaning, lotus effect and antibacterial properties have been developed on polyester fabric by growing ZnO nanorods [88]. Recently, Preda et al. developed superhydrophobic cotton fabrics through electroless deposition of ZnO hexagonal prisms (Figure 17). The ZnO functionalized cotton fabrics showed superhydrophobicity, with water contact angles exceeding 150° . In this study they did not evaluate the durability of the ZnO coated cotton fabrics [89].

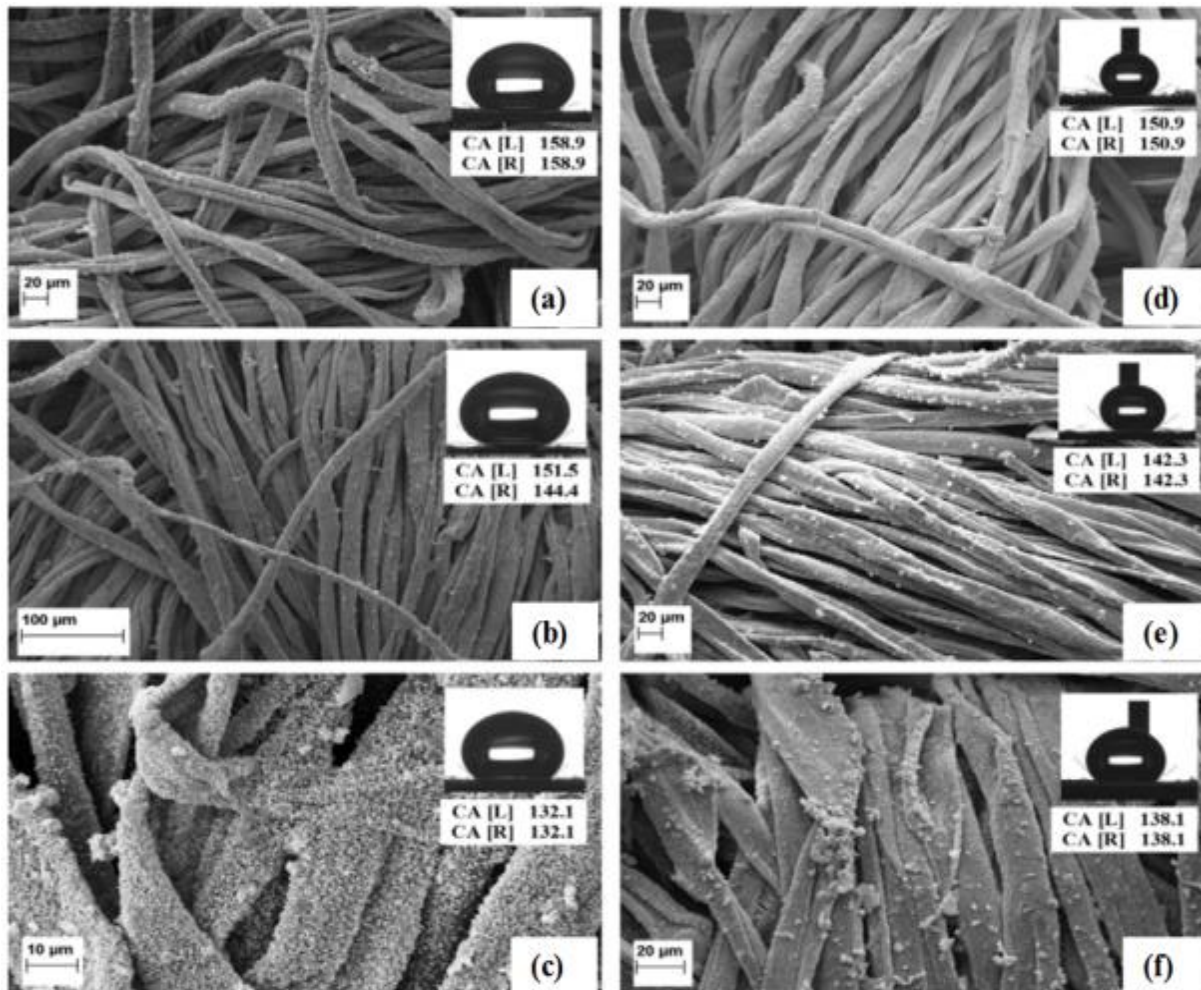


Figure 17. SEM images of ZnO-coated cotton fabrics with different mesh density at two reaction temperatures 70 °C (sparse (a), medium (b) and dense (c)) and 80 °C (sparse (d), medium (e) and dense (f)). In the inset are water contact angles for the corresponding [89].

In a previous study, the cotton fabrics coated with Ormosil (*organically modified silica*) clusters with subsequent fluoridization showed superamphiphobicity and the contact angles of water, cooking oil and hexadecane reach to 164.4°, 160.1° and 156.3°, respectively. Figure 18a shows the graphical representation of the methods used for the fabrication of superamphiphobic cotton fabric. The superamphiphobic cotton fabric showed contact angles of 164.4°, 160.1°, and 156.3° corresponding to water, cooking oil and hexadecane (Figure 18b). Water drops immediately rolled off the cotton fabric after deposition because of the extremely low adhesion of the coating to water [90].

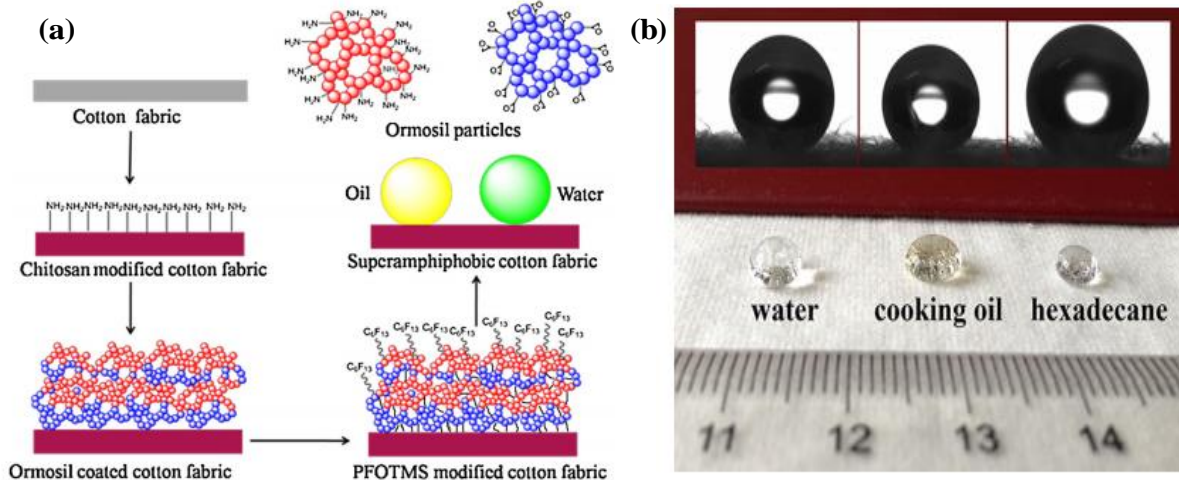


Figure 18. (a) Schematic diagram of the fabrication process for superamphiphobic cotton fabrics. (b) Photographs of water, cooking oil and hexadecane droplets on the coated cotton fabrics [90].

Guo et al. reported a layer by layer electrostatic assembly method to develop superhydrophobic fabric by coating carbon nanotubes (CNTs) on polyester fabrics using poly(dimethyl diallyl ammonium chloride) as a polyelectrolyte, followed by post-treatment with poly(dimethylsiloxane) (PDMS) (Figure 19). The developed fabric exhibited superhydrophobicity, UV blocking properties and electrical conductivity [91].

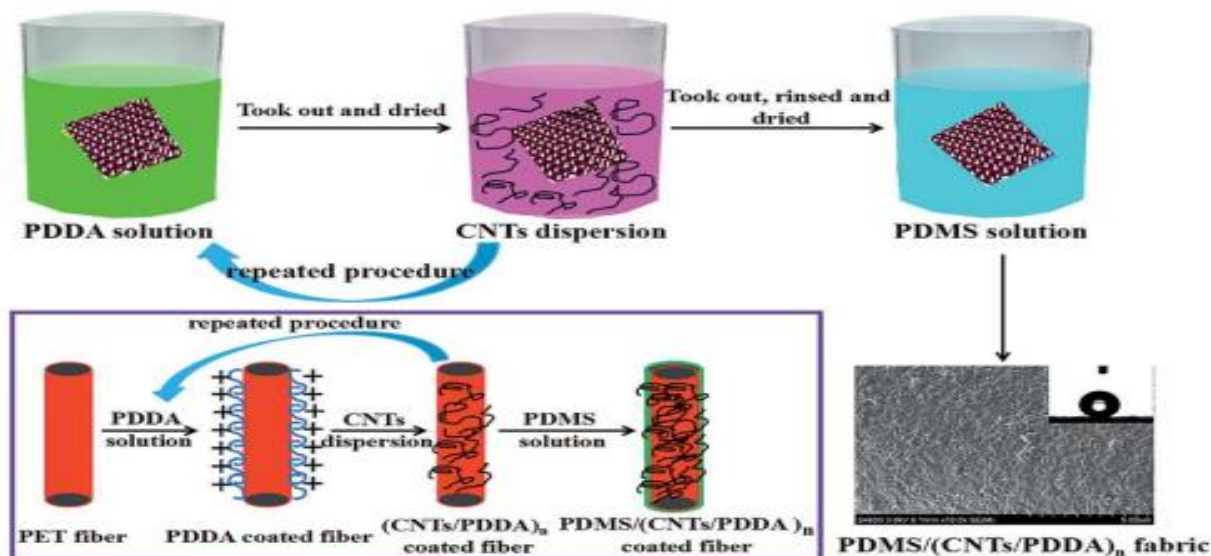


Figure 19. Illustration of the fabrication of multifunctional superhydrophobic fabrics [91].

Zhang et al. developed superhydrophobic cotton fabrics coated with stearic acid modified ZnO/polystyrene nanocomposite coating (Figure 20a). The superhydrophobic cotton textiles displayed a good property in water/oil separation. The Figure 20b shows the SEM image of the superhydrophobic cotton fabric. Whereas, image of water droplet on the developed surface can be seen in Figure 20c. The static water contact angle on the superhydrophobic cotton sample surface was arranged from 153° to 155° [5].

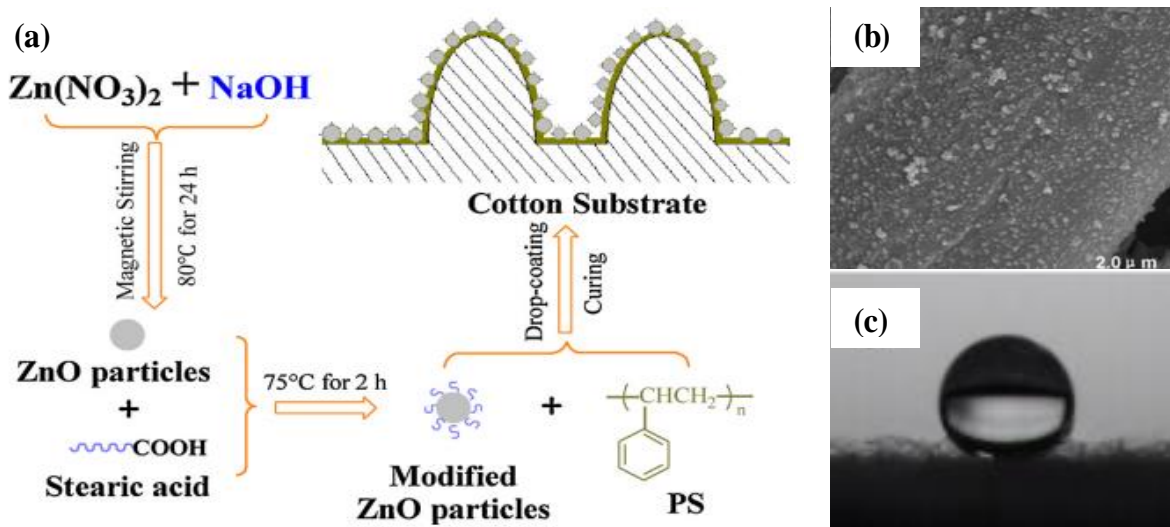


Figure 20. (a) Experimental strategy for the fabrication of superhydrophobic cotton fabrics, (b) SEM micrographs superhydrophobic cotton fabric and, (c) Photographs of the static water droplets on corresponding surface [5].

In another study, superhydrophobic cotton fabrics were developed by the combination of photoactive TiO_2 and superhydrophobic SiO_2 . The as-prepared nanocomposite coated fabrics were tested for superhydrophobic and chemical self-cleaning properties [24]. There are still many challenges exist, like physical, chemical stability and cost of materials. These problems are needed to be solved before large scale production of these special surfaces. The development of highly robust superhydrophobic surfaces is important issue for future research [50].

Recently, microwave assisted synthesis has attracted many researcher due to its advantages over conventional synthesis techniques. Microwave assisted heating methods are considered promising way of rapid heating, volumetric, high reaction rate and less reaction time

as compared to the conventional heating methods [83, 84]. It has reduced energy consumption, time, cost and waste materials. Microwave assisted synthesis has also increased reaction rate, synthesis rate, bulk production rate, purity of material and homogeneity of the reaction [92]. During microwave-assisted synthesis microwaves can penetrate through the material and supply energy [93]. In microwave heating electromagnetic energy is converted to thermal energy. During this phenomenon the heat caused by the electric component of an electromagnetic field is due to two main mechanisms; dipolar polarization mechanism and conduction mechanism [94].

CHAPTER 4

4. RESEARCH METHODOLOGY

This chapter consists the materials and methodology for the development of superhydrophobic fabrics coated with fly ash, TiO₂ nanoflowers by low temperature hydrothermal method and ZnO nanorods by microwave hydrothermal method that has been divided into three sections respectively.

4.1. Materials

Fly ash was obtained from the city of Plzeň located in the Czech Republic with the help of SILO Transport organization. The fly ash was light gray in color with density of 2 g/cc. The main constituents of fly ash as determined by elemental analysis are 53.80% O, 20.25% Si, 14.27% Al, 4.72% Fe, 1.95% Ti, 1.84% Na, 1.06% Mg, 0.94 %Ca, 0.34% Zr, 0.25% K, 0.19% S, 0.16% Cu, 0.15% As, and 0.09% P. According to the composition, fly ash was classified in class-F category (ASTM C618) based on more than 70% total content of silica and alumina together. Titanium isopropoxide Ti[OCH(CH₃)₂]₄, Titanium butoxide Ti(OBu)₄, Hydrochloric acid, Caustic soda, Ethanol, Acetic acid, Zinc acetate dihydrate [Zn(CH₃COO)₂·2H₂O, ≥99% purity], Hexamethylenetetramine (HMTA, C₆H₁₂N₄, 99%) and OTMS (analytical grade) were purchased from Merck (Sigma Aldrich) and used as received. Zinc nitrate hexahydrate (ZnN₂O₆·6H₂O, 99% pure) was obtained from Alfa Aesar. To investigate oil in water separation performance, four model oils of varying density (i.e. toluene, n-hexane, chloroform, petro ether) were used from laboratory.

Plain woven bleached 100% cotton fabric and plain woven 100% polyester fabric was used as substrate to create superhydrophobic surfaces. The detailed specifications of cotton and polyester fabrics are given in Table 1. The porosity of the fabric was calculated by dividing the fabric density by the relative density of the fibers. The optical micrographs of cotton and polyester fabrics are shown in Figure 21.

Table 1. Parameters of fabric used

Fabric	Weave	Warp Count (Tex)	Weft Count (Tex)	Warp Sett (ends/cm)	Weft Sett (picks/cm)	Areal Density (g/m^2)	Thickness (mm)	Porosity (%)
Cotton	1/1 Plain	14	10	48	46	120	0.25	69
Polyester	1/1 Plain	9.8	18.5	52	27	97	0.18	61

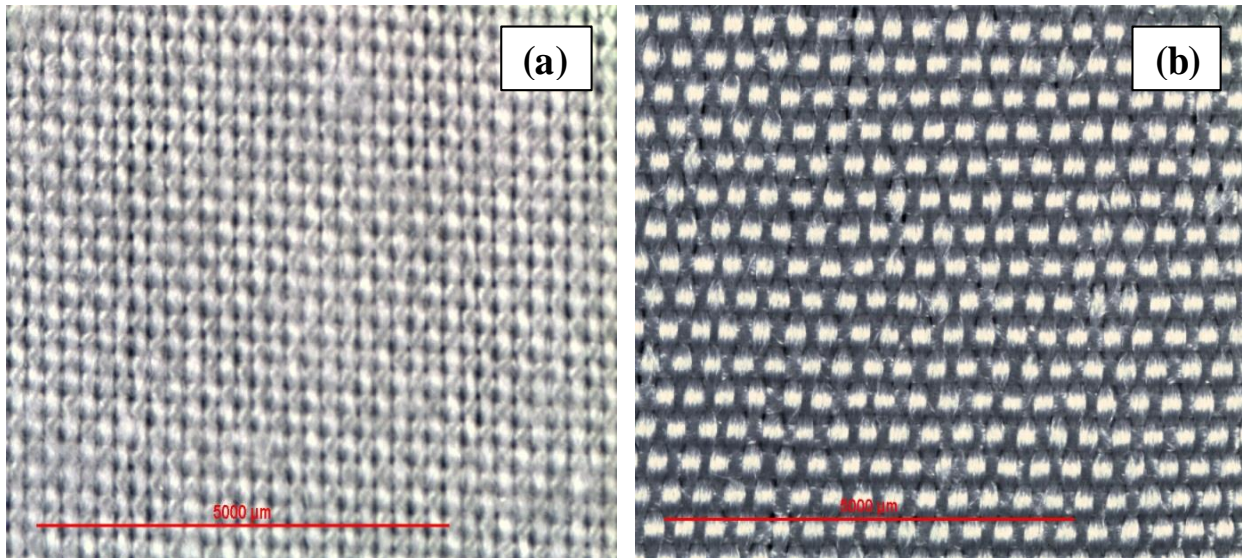


Figure 21. Microscopic images of (a) cotton, and (b) polyester fabric

4.2. Superhydrophobic fabrics coated with fly ash and OTMS

4.2.1. Preparation of mechanically activated fly ash

Mechanical activation of fly ash was carried out using high-energy planetary ball mill of Fritsch Pulverisette 7 in a sintered corundum container of 80 ml capacity using zirconia balls of 10 mm diameter for the duration of 30 min. The ball mill was loaded with ball to fly ash weight ratio of 5:1. The rotation speed of the planet carrier was kept at 850 rpm. During milling, fly ash particles were subjected to a severe plastic deformation due to the repetitive compressive loads arising from the impacts between balls and fly ash. The milled fly ash particles were taken out to test particle size distribution on Malvern Zetasizer Nano based on dynamic light scattering principle. The deionized water was used as dispersion medium. The dispersion was ultrasonicated for 5 min under Bandelin ultrasonic probe before characterization. Refractive index of 1.55 was used for fly ash to calculate particle size. In addition, morphology of fly ash after ball milling was observed on Scanning electron microscope (SEM) TS5130-Tescan at 30 kV accelerated voltage.

4.2.2. Preparation of fly ash coated cotton fabrics

Mechanically activated fly ash particles were added at 1, 2 and 3 wt% concentration into distilled water and the dispersion was sonicated for 15 min using ultrasonic system (Bandelin Sonopuls HD 3200, 20 kHz, 200 W, 50% efficiency). Then, the fly ash dispersion was applied on bleached cotton fabric through a dip-pad-dry-cure process. The fabric was immersed into the dispersion for 1 min, subsequently passed through a padder, dried at 80°C in a drying oven and finally cured at 120 °C for 3 min.

4.2.3. Hydrophobization of fly ash coated cotton fabrics

For fabrication of superhydrophobic surfaces, OTMS was applied on fly ash coated cotton fabrics to lower their surface energy. The OTMS has very long chain of carbon atoms which impart hydrophobicity. The OTMS (8%, w/w) was added drop wise into ethanol, and acetic acid was employed to promote the hydrolysis of OTMS by adjusting pH values in 4-5 range. The solution was stirred at room temperature for 45 min. The fly ash coated cotton fabrics were then immersed in hydrolyzed OTMS solution, dried in air and cured at 120 °C for 1 hr. One

control sample was also prepared without any surface decoration of fly ash particles. Figure 22 shows the schematic of fabrication of superhydrophobic surfaces.

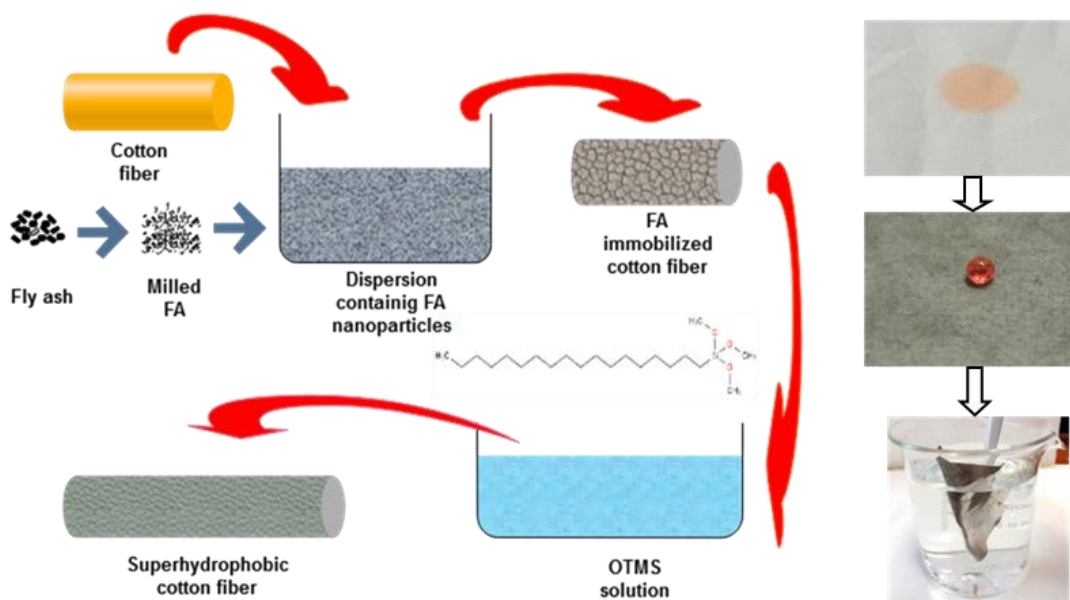


Figure 22. Fabrication of fly ash-OTMS coated superhydrophobic cotton fabric

4.3. Superhydrophobic fabrics coated with TiO₂ nanoflowers and OTMS

4.3.1. Synthesis of flower shaped TiO₂ particles on polyester fabric

At the beginning, the surface of polyester fabric was cleaned by petroleum ether for 2 hr at 60 °C in Soxhlet apparatus and later treated with 20 g/L caustic soda solution at 80 °C for 30 minutes. Then, the flower shaped TiO₂ particles were grown on surface of polyester fibers using two step approaches of sol-gel technology and hydrothermal method. In the first step, a semitransparent TiO₂ sol was formed by continuously stirring a mixed solution of Titanium butoxide (6 mL), ethanol (60 mL) and acetic acid (2 mL) for 3 h at 60 °C. The caustic soda treated polyester fabric was immersed in the prepared TiO₂ sol for 5 min, padded with a wet pickup of 70–80% and dried at 110 °C. This process was repeated 3 times and the samples were cured at 140 °C. In the second step, hydrothermal method was used to grow the flower shaped TiO₂ particles on the already TiO₂ seeded fabric. Here, different amounts of titanium isopropoxide were added drop wise into the aqueous hydrochloric acid solutions (i.e. 10 mL HCl

and 60 mL distilled water), and the mixtures were stirred for 10 min until the solutions turned clear. The resulting solution was further transferred into 150-mL Teflon-lined stainless-steel autoclave and TiO₂ seeded polyester fabric was placed in it. The autoclave was placed in an oven for 1 h at 125 °C. Finally, the polyester fabric was removed from the autoclave, rinsed with deionized water and dried at room temperature.

4.3.2. Superhydrophobization of TiO₂ nanoflowers coated polyester fabrics

The OTMS was applied on TiO₂ coated polyester fabrics for fabrication of superhydrophobic surfaces by lowering the surface energy. The OTMS solution was prepared by addition of (8%, w/w) OTMS drop wise into ethanol and stirring it at room temperature for 45 min. The hydrolysis of OTMS was promoted by use of acetic acid and by adjusting pH values in 4-5 range. The polyester fabrics decorated with different concentrations of 3D shaped TiO₂ flowers were then immersed in hydrolyzed OTMS solution, dried in air and cured at 120 °C for 1 hr. One control sample was also prepared by just coating of OTMS alone and without any surface decoration of TiO₂ nanoflowers. The schematic of fabrication of superhydrophobic surfaces can be seen as continued process to decoration of TiO₂ flowers from Figure 23.

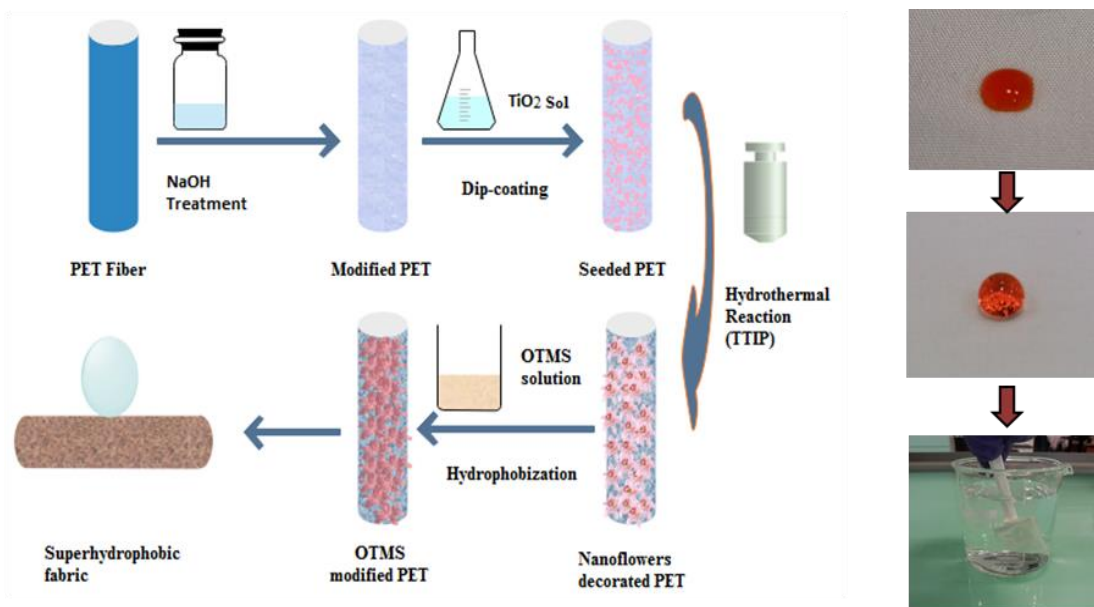


Figure 23. Schematic of deposition of TiO₂ flower shaped particles on polyester fabric

4.4. Superhydrophobic fabrics coated with ZnO nanorods and OTMS

4.4.1. Preparation of ZnO nanocrystals

Two step processes was used to grow ZnO nanorods on cotton fabric. In first step the Zinc oxide nanocrystals were prepared by microwave-assisted sol gel method. Zinc acetate dihydrate (25 mM) was dissolved in ethanol under stirring at room temperature followed by addition of sodium hydroxide (75 mM) in ethanol solution. Then the 50 mL resultant solution was transfer to Teflon reaction container and closed firmly. The reaction container was put into the microwave reactor (Magnum II reactor, 600 W, 2.45 GHz, ERTEC, Poland) and reaction was carried out at 60 °C (360 W) for 10 min. Finally, a transparent ZnO seed solution was obtained.

4.4.2. Coating method

The as-prepared ZnO nanocrystals seed solution was deposited onto the cotton fabric by dip-pad-cure process. The cotton fabric was dipped into solution, then dried at 110 °C and cured at 150 °C for 5 min in an oven to ensure ZnO nanocrystal particles adhere to cotton fiber surface.

4.4.3. Growth of nanorods

In second step, ZnO nanorods were grown on these seed layer deposited cotton fabrics through microwave hydrothermal synthesis. Equimolar aqueous solutions of zinc nitrate hexahydrate and hexamethylenetetramine (HMTA) were prepared by mixing 25 mL of each solution to make 50 mL solution. The cotton fabric seeded with ZnO nanocrystals and resultant solution was transferred to Teflon reaction container and container was put into the microwave reactor (Magnum II reactor, 600 W, 2.45 GHz, ERTEC, Poland). In situ synthesis of ZnO nanorods on cotton fabric was carried out using microwave hydrothermal technique under various conditions. The effect of zinc nitrate hexahydrate concentration (10mM, 25mM, 50mM, 75mM, and 100mM), reaction time (10 min, 20 min, 30 min) and microwave power (360 W, 420 W, 480 W) was studied in detail. After reaction, the samples were taken out and rinsed in deionized water for 3 times and dried at 100 °C for 10 min.

4.4.4. Superhydrophobic treatment of ZnO nanorods grown cotton fabrics

The OTMS was applied on ZnO nanorods coated cotton fabrics for development of superhydrophobic surfaces by lowering the surface energy. The OTMS solution (8%, w/w) was prepared by stirring at room temperature for 45 min. The ZnO nanorods coated cotton fabrics were then immersed in the OTMS solution, air dried and then cured at 120°C for 1 hr. One control sample was also prepared by coating of OTMS alone on cotton fabric. The schematic showing methods used for development of superhydrophobic cotton fabrics (see Figure 24).

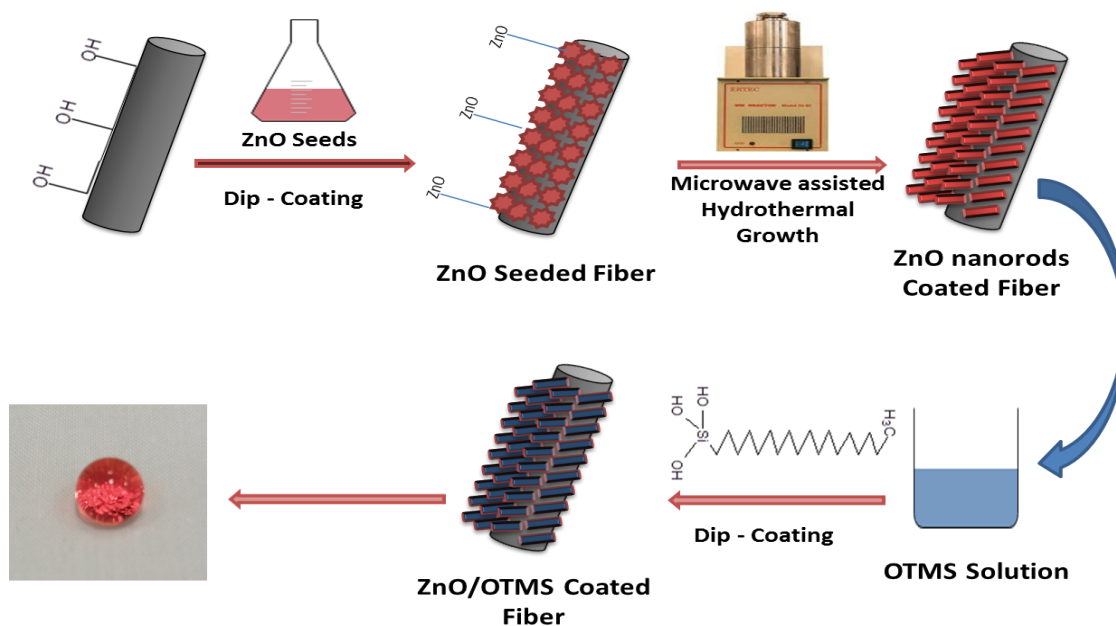


Figure 24. Shows the schematic of development of superhydrophobic cotton fabrics

4.5. Characterization of surface morphology of coated fabrics

4.5.1. SEM and EDS analysis

The scanning electron microscope (SEM) of TS5130 Vega Tescan was employed to observe the surface morphology of coated fabrics at 30 kV acceleration voltages. The gold sputtering was performed to develop the conductive layer on surface of samples before SEM analysis. For better resolution, the surface structure of coated samples was also seen under the

field emission scanning electron microscope of Zeiss Ultra Plus at an accelerating voltage 2 kV equipped with an Energy Dispersive X-ray spectrometer Oxford X-max 20.

4.5.2. Raman spectroscopy

For characterization of crystal phases, the Raman spectra were recorded by DXR Raman Microscope (Thermo Scientific, USA) with 532 nm laser, grating 900 lines/mm in spectral range of 3500-50 cm^{-1} and objective Olympus LMPlanFL 10x and 50x. The 25 and 50 μm slit spectrograph aperture was used with 0.9 to 5.0 mW level of laser power, 1 sec exposure time and 50 exposures.

4.5.3. X-Ray diffraction (XRD) analysis

The crystalline structure of material was studied on X-Ray diffraction (XRD) analysis of PAN analytical X'pert PRO equipment. The XRD analysis was performed with a diffractometer equipped with a conventional X-ray tube Cu $\kappa\alpha_1$ radiation ($\lambda=1.5406 \text{ \AA}$) power condition (40 KV/30 mA). The XRD pattern was measured in the 2θ range of 20-70 with the step size of 0.02.

4.5.4. Atomic force microscopy (AFM) analysis

In this study, NanoWizard 3 NanoScience AFM from JPK Instruments was used in non-contact mode to determine the surface roughness and to observe the topography of the coated samples. For all samples, at least three topographic images were obtained and surface roughness was calculated. The software calculates the surface roughness average (Ra) directly from AFM signals using the Equation (7).

$$R_a = \frac{1}{L} \int_0^L |Z(x)| dx \quad (7)$$

Where $Z(x)$ is the function that describes the surface profile analyzed in terms of height (Z) and position (x) of the sample over the evaluation length (L).

4.6. Characterization of UV protection properties

UV protection behavior of the coated fabrics was determined by measuring percentage transmission of UV radiations on UV-vis-NIR Spectrophotometer (UV-3101PC) as per AATCC 183-2000 standard. The samples were conditioned for 4 hours at 21 ± 1 °C temperature and 65 ± 2 % relative humidity. For each sample, four measurements were performed and the average of scans was taken to calculate the UPF factor from Equation (8).

$$UPF = \frac{\sum_{280nm}^{400nm} E_{\lambda} S_{\lambda} \Delta_{\lambda}}{\sum_{280nm}^{400nm} E_{\lambda} S_{\lambda} T_{\lambda} \Delta_{\lambda}} \quad (8)$$

Where S_{λ} is the solar spectral irradiance, E_{λ} is the relative erythral spectral response, T_{λ} is the average spectral transmittance of the sample and Δ_{λ} is the measured wavelength interval in nanometres.

4.7. Characterization of physical properties

The uptake (i.e. add on percentage) of coated fabric was calculated using the Equation (9).

$$Add\ on\ (\%) = \frac{w_f - w_i}{w_i} \times 100 \quad (9)$$

Where w_i is weight of fabric before coating and w_f is weight of fabric after coating.

Furthermore, the coated fabrics were investigated for the comfort properties based on the measurements of stiffness from the TH-7 instrument which is similar to standard Kawabata KES-FB 2 device used for testing of low stress mechanical properties [95].

4.8. Characterization of superhydrophobicity of coated fabrics

4.8.1. Contact angle measurement

Surface energy evaluation system of Advex instrument was employed to measure the contact angle of the coated fabrics. It is a computer-aided instrument which uses the sessile drop method to calculate the contact angle between liquid and solid. . Six measurements were made on each sample with 5 μL of water droplet and average contact angle was determined.

4.8.2. Roll off angle measurement

The roll off angle was measured by using a custom-made device, which can measure the roll off angle with an accuracy of 1° . The spirit level was used to balance the apparatus on table. Sample was fixed on device and 5 μL water droplet was dropped from a syringe on the fabric. Then, the plate was inclined slowly (1°), until the droplet started to move. On each sample, six measurements were made and mean value was taken.

4.8.3. Contact angle hysteresis

The advancing contact angle was measured when needle was brought in close proximity to the sample surface, and the deionized water was pumped until the drop reached a size of approximately 25 μL . Subsequently, the receding angle was measured when the liquid was pumped in at the same rate until the detached drop from the needle or all of the liquid returned to the syringe. Then, the contact angle hysteresis was estimated from the difference between the advancing and the receding contact angles. The test was repeated three times for each specimen at different locations.

4.8.4. Durability of contact angle

The mechanical abrasion durability of the coated fabrics was studied from the sand paper test. The coated fabric was dragged against sand paper surface after putting 100 g load on the top of the sample and the change in contact angle after 20 abrasion cycles was examined [96–98]. Further, the washing durability was examined by measuring the contact angle after five laundering cycles according to ISO 105 C06 (B1M) standard (4 g L^{-1} detergent, 60°C temperature and 45 min time). The chemical durability was evaluated by measuring the contact

angle after immersing the coated fabrics into acidic (pH=1) and alkaline (pH=13) solutions for the duration of 24 h. For evaluation of UV durability, the coated cotton fabrics were placed under ultraviolet lamp Philips TL 6W UV tubes (315-400 nm) for 24 h and then their contact angle was measured. The durability against a jet of water was also studied by observation of the bouncing of water droplets. A jet of water was impacted on the fabric surface with speed of 3 m/s by a syringe kept at 4 cm above the sample with an angle of 45° for 1 min, and the bouncing of water droplets was captured in the high-speed camera (Olympus, *i-SPEED 3*) at 5000 frame s⁻¹.

4.9. Characterization of self-cleaning properties of coated fabrics

4.9.1. Physical self-cleaning

The 0.5 g methyl orange dye was used as contaminant and it was randomly sprinkled over the coated fabric surface. Then, the physical self-cleaning property was studied by rolling the water over the dye contaminated surfaces. The directed movement of water droplets was observed in digital camera by introduction of water droplets at an angle of 45° on the coated fabric surface using micropipette.

4.9.2. Chemical self-cleaning

As the coated fabrics were superhydrophobic in nature, therefore they were not immersed directly in aqueous solution of methyl orange dye. The superhydrophobic fabrics were first soaked in acetone and then immersed in dye solution for the chemical self-cleaning behavior using two different experiments (i.e. stain degradation and solution discoloration). For stain degradation, the dyed samples were irradiated under the UV light of Philips TL 6W UV tubes (315-400 nm) and the stain degradation performance was evaluated as a function of exposure time to UV light. Later, the fabric surfaces discolored after the tests were scanned with 300 dpi and the scanned images were analyzed to calculate the color intensity by Image J software [99]. For solution discoloration experiments, the coated samples with diameter 2.8 cm were placed in a beaker having 15 ml of methyl orange dye solution. This beaker was then placed below the light source Philips TL 6W UV tubes (315-400 nm) at a distance of 18 cm. To estimate the photo catalytic discoloration effect, an aliquot was removed from the solution after a pre-set time

interval and its absorbance was measured at λ_{\max} (485 nm) using UV-Vis Spectrophotometer (UV-1600PC).

4.10. Oil/water separation property of the coated fabrics

The coated superhydrophobic fabrics were tested for oil in water separation performance using four model oils of different densities (n-hexane, toluene, chloroform, petro ether) mixed in water (50% v/v). The coated fabric was placed on top of the small beaker which was mounted in another big beaker. When oil/water mixture was poured onto the surface of coated fabric, oil penetrated through the fabric into small beaker whereas water flowed into the big beaker. The oil/water separation efficiency (%) was calculated from the ratio of volume of oil remaining after separation to initial volume of oil mixed with water. The reusability of contaminated fabrics was also investigated by measuring their separation efficiency after numerous of water–oil separation recycles. For measurement of oil absorption capacity, the coated fabric samples were immersed in an oil/water mixture for 5 s, removed, and then weighed immediately. The oil absorption capacity (Q) of the fabric was calculated from weights measured at room temperature using Equation (10).

$$Q = \frac{(W_t - W_i)}{W_i} \times 100 \quad (10)$$

Where W_t is the weight of the saturated coated fabrics after immersing in oil/water, and W_i is the weight of the fresh coated fabrics.

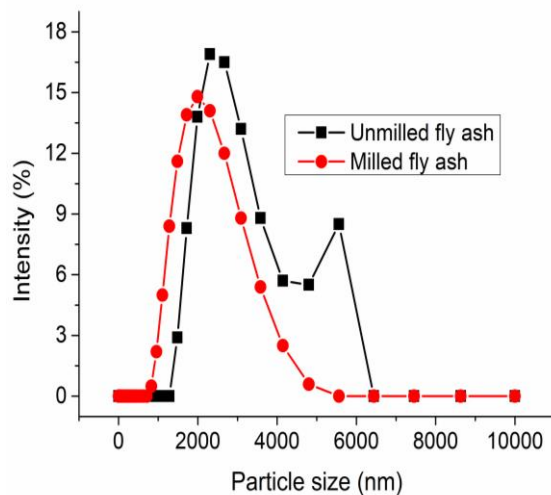
CHAPTER 5

5. RESULTS AND DISCUSSION

5.1. Superhydrophobic fabrics coated with fly ash and OTMS

5.1.1. Mechanical activation of fly ash

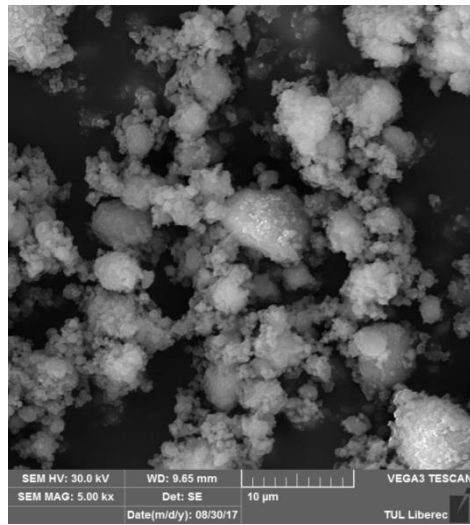
Figure 25 (a) shows the particle size distribution of fly ash after 30 min of dry milling. It can be seen that the size of fly ash particles was greatly reduced after the grinding. The unmilled fly ash with mean particle diameter of 3547 nm was converted to smaller particles of mean below 1000 nm diameter. When milling was continued for longer time, the temperature of milling container was increased. This resulted in sticking of fly ash layer on surface of milling container, and therefore further grinding of fly ash was not continued. For observation of surface morphology of fly ash particles, SEM images of unmilled and 30 min milled fly ash particles were taken. Figure 25 (b) and Figure 25 (c) showed that the milling destroyed a large proportion of the spherical morphology of unmilled fly ash and subsequently resulted into nano/micro fly ash with more active surfaces [100].



(a) Particle size distribution of fly ash



(b) SEM image of unmilled fly ash

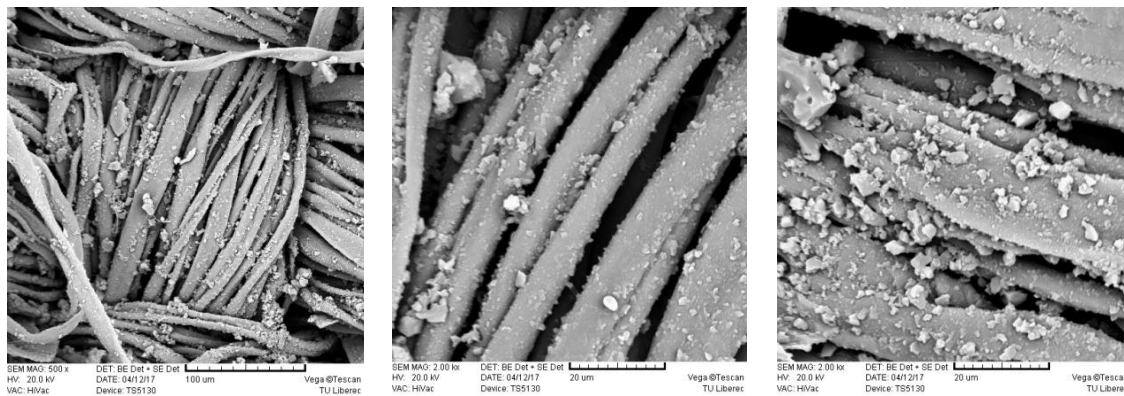


(c) SEM image of milled fly ash

Figure 25. Effect of ball milling on fly ash

5.1.2. Surface morphology of fly ash coated cotton fabrics

The surface hierarchical structure is important to obtain the superhydrophobic property. Figure 26 show the SEM images of fly ash coated fabric surfaces. The surface of cotton fiber was uniformly covered by fly ash particles. Moreover, dense coatings with obvious hierarchical structures were formed when increasing the fly ash concentration. A micro/nanoscale surface mimicking the surface of lotus leaf was formed with each fiber of approximately 10 μm diameter, and the fly ash particles of below 1000 nm size. A good adhesion between the fly ash particles and cotton fibers can be attributed to the presence of hydroxyl groups and formation of hydrogen bonds between them. Nevertheless, large particles observed on the textile surface with increase of fly ash concentration indicated their agglomeration tendency at high fly ash concentration [75].



(a) 1 wt% fly ash

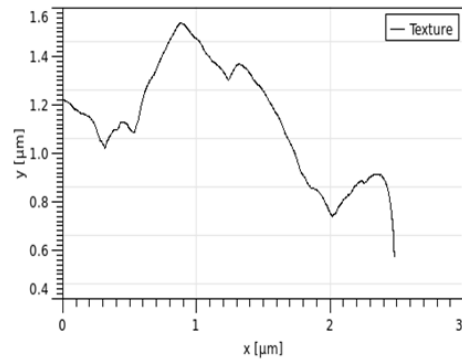
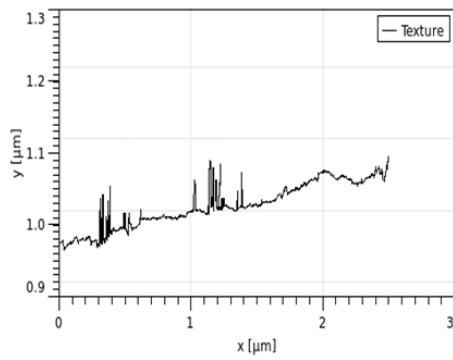
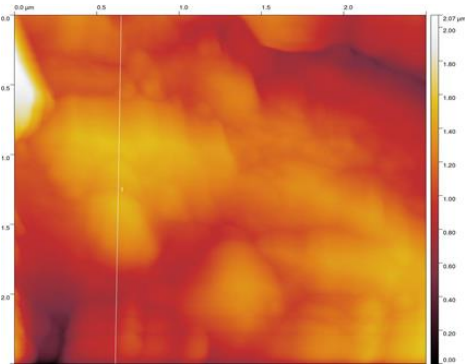
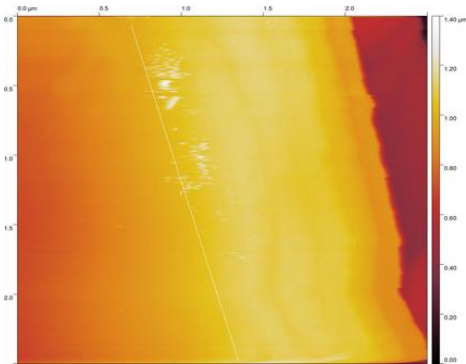
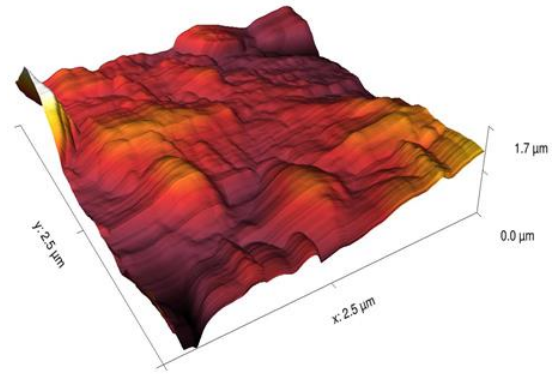
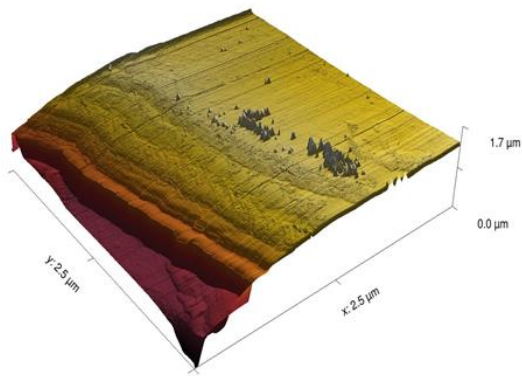
(b) 2 wt% fly ash

(c) 3 wt% fly ash

Figure 26. Surface structure of fly ash coated cotton fabrics

5.1.3. AFM analysis of fly ash coated cotton fabrics

The generation of surface roughness due to fly ash coating was further estimated using AFM. The AFM images and surface profiles of pristine and fly ash coated cotton fabrics are shown in Figure 27. For the pristine cotton fabric, the average roughness (R_a) was 22.56 ± 11.5 nm, and for fly ash coated cotton fabric, it was increased to 182.9 ± 15.7 nm, respectively. The pristine cotton fabric surface showed relatively smooth surface. It can be seen that after coating of fly ash particles, the surface roughness of the fabric increased manifold. According to the Cassie-Baxter model, increasing surface roughness would increase the water contact angle of the surface [101–103].



(a). Pristine cotton fabric

(b). FA coated cotton fabric

Figure 27. AFM images and representative surface profiles of the pristine and coated fabrics

5.1.4. UV protection performance of fly ash coated cotton fabrics

Table 2 provides the average transmittance values of UV-A (315–400 nm), UV-B (280–315 nm) and the whole UV range (280–400 nm). The UV transmittance was found to reduce with increase in concentration of fly ash particles on fabric surface. The maximum UV blocking was observed in case of cotton fabric coated with 3 wt% fly ash, where the average transmittance decreased from 15.64%, 9.28% and 14.19% of the untreated fabric to 0.12%, 0.07% and 0.11% for UV-A region, UV-B region and the whole UV range, respectively. This behavior can be attributed to the absorbance of UV light by fly ash particles for transferring the electron from the valance band to the conduction band [104].

Table 2. UV transmission of fly ash coated cotton fabrics

Sample	UV-A (%)	UV-B (%)	Whole UV (%)	UPF
Without FA	15.64	9.28	14.19	9.49
1% MFA	0.56	0.33	0.50	299.4
2% MFA	0.23	0.14	0.21	801.44
3% MFA	0.12	0.07	0.11	1777.43

The ultraviolet protection factor (UPF) is another important parameter to assess the UV-blocking property of a fabric, which indicates the ability of fabrics to protect the skin against sun burning. It is defined as the ratio of potential erythema effect to actual erythema effect by the radiation transmitted through the fabric [105]. From Table 2, the untreated cotton fabric showed a low UPF of 9.49, however all the cotton fabrics decorated with fly ash particles exhibited large increase in UPF values. The maximum increase in UPF was observed for 3 wt% fly ash

concentration, where the UPF value was increased to 1777.43. The great scattering of UV rays can be attributed to large refractive index of fly ash particles accompanied with constituents of metal oxides in their chemical composition [106].

5.1.5. Physical properties of fly ash-OTMS coated cotton fabrics

The add-on of coated fabrics at different fly ash-OTMS coatings were calculated, and it was found to increase in linear pattern with increase in fly ash concentration (Table 3). The final dry add-on of the coated fabrics was measured as 2.5% for 1% FA+OTMS, 6.3% for 2% FA+OTMS and 9.2% for 3% FA+OTMS.

Table 3. Add-on (%) of FA+OTMS coated cotton fabrics

Sample	Add-on (%)
1% FA+OTMS	2.5 (± 0.16)
2% FA+OTMS	6.3 (± 0.30)
3% FA+OTMS	9.2 (± 0.25)

Subsequently, the hand (i.e. comfort) properties of the coated fabrics were assessed from the measurements of stiffness values. Stiffness is a tendency of the fabric to keep standing without support. It is a special property of the fabric for desirable draping and also influences the physical comfort of clothing [107–109]. It can be evaluated from bending properties of the fabric using bending length and flexural rigidity. Despite large increments in add-on of coated fabrics at higher fly ash concentration, the stiffness values were found to increase marginally. The stiffness of uncoated cotton fabric was 0.86 N m, whereas it was measured as 1.09, 1.23 and 1.31 N m for 1%, 2% and 3% FA+OTMS coated cotton fabrics respectively (see Table 4). This indicated no loss in draping behavior of fly ash-OTMS coated cotton fabrics and therefore satisfactory physical comfort behavior.

Table 4. Stiffness of the FA+OTMS coated cotton fabrics

Sample	Stiffness (N m)
Control	0.86 (± 0.13)
1% FA+OTMS	1.09 (± 0.10)
2% FA+OTMS	1.23 (± 0.11)
3% FA+OTMS	1.31 (± 0.08)

5.1.6. Superhydrophobic properties of fly ash-OTMS coated cotton fabrics

The effect of fly ash particles on surface wettability of fly ash-OTMS coated cotton fabrics was investigated from measurements of static water contact angle, roll-off angle and contact angle hysteresis (see Figure 28). The surface of uncoated cotton fabric was completely wetted by the water droplet without any contact angle, whereas the water droplet exhibited a spherical shape on the surface of fly ash-OTMS coated textile (see Figure 22). For OTMS coated cotton fabrics, the static water contact angle and roll off angle were measured around 130° and 21° respectively. This indicated the hydrophobic behavior of cotton fabrics with OTMS coating alone, however the water droplets were difficult to roll off on this surface showing the strong adhesion between the water droplet and the coating surface. When fly ash particles were applied on cotton fabric with subsequent treatment of OTMS, the contact angle was enhanced and roll off angle was further decreased. The static contact angle of 143°, 147° and 153° and roll off angle of 13°, 8° and 5° was measured for fly ash concentration of 1, 2 and 3 wt% respectively (see Figure 28a). These results demonstrated the improvement in water repellency from surface hydrophobicity to superhydrophobicity when cotton fabric was coated with 3 wt% fly ash and then OTMS. From Figure 26, the enhancement in water repellency can be attributed to the

formation of unique two-tier structural surface combined with the microscaled cotton fibers (10 μm) and the nanoscaled fly ash particles (below 1 μm).

Due to surface roughness and heterogeneity of textile surfaces, the coated fabrics were further tested to measure their dynamic wetting behaviors. This is important because the measured contact angle after the liquid drop advances is usually greater than the contact angle that results after the droplet recedes from a previously wetted surface due to the change in surface energy or the surface roughness [70, 106]. Further, the contact angle hysteresis (i.e. difference between the advancing and receding contact angles) plays an important role in the sliding behavior of water droplets for self-cleaning effect [44, 110, 111]. Therefore, the advancing and receding angles of fly ash-OTMS coated cotton fabrics were measured to examine the influence of fly ash particles on the self-cleaning effect. From Figure 28(b), the contact angle hysteresis was found to reduce from 11° to 6° with increase of fly ash concentration from 1wt% to 3 wt%. This indicated the formation of discontinuous, unstable, and contorted air/solid/liquid contact line at higher concentration of fly ash particles. By depositing high density of fly ash particles, solid-liquid-air contact line can further become more discontinuous and a larger amount of air film can be trapped leading to superhydrophobicity. Based on previous studies, a liquid droplet on a superhydrophobic surface can fulfill either Wenzel state or Cassie-Baxter state, or both [47]. A liquid impregnates the rough surface to form a completely wetted contact with the surface in the Wenzel state, whereas the liquid does not completely fill up the rough surface and there are air pockets trapped at the solid-liquid interface in the Cassie-Baxter state [106]. Therefore, the superhydrophobicity of the fly ash-OTMS coated cotton fabrics can be believed in Cassie-Baxter state where spherical water drop cannot penetrate entire fabric surface due to large amount of air trapped in the structure [70]. For verification of Cassie-Baxter state, the fly ash-OTMS coated cotton fabric was immersed into water by an external force (see Figure 22). A silver mirror-like bright and reflective surface was observed, which was attributed to the plastron layer formed by the trapped air between the water and the superhydrophobic fabric [112].

The physical self-cleaning behavior of 3 wt% fly ash-OTMS coated cotton fabrics was examined due to their superhydrophobic nature and low roll off angles. The orange dye was used

as contaminants to test the self-cleaning ability. From Figure 29, the water drop was found to roll over the surface of the superhydrophobic fabric maintaining a spherical shape and subsequently the dye particles were taken away, leaving a clean trace on the superhydrophobic fabric [113]. This further confirmed the low surface energy of coated fabric samples and therefore more attraction of dye particles to the running liquid than to the solid surface itself. This characteristic of lotus effect can allow the surface to be cleaned of dust particles by the rolling liquid.

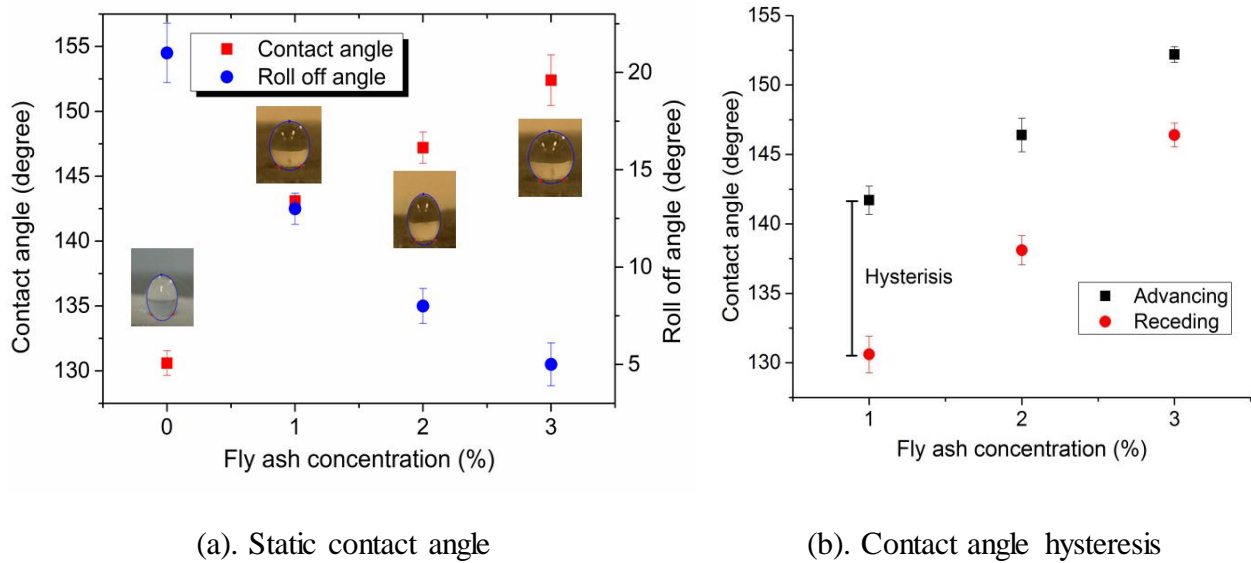


Figure 28. Effect of fly ash concentration on contact angle

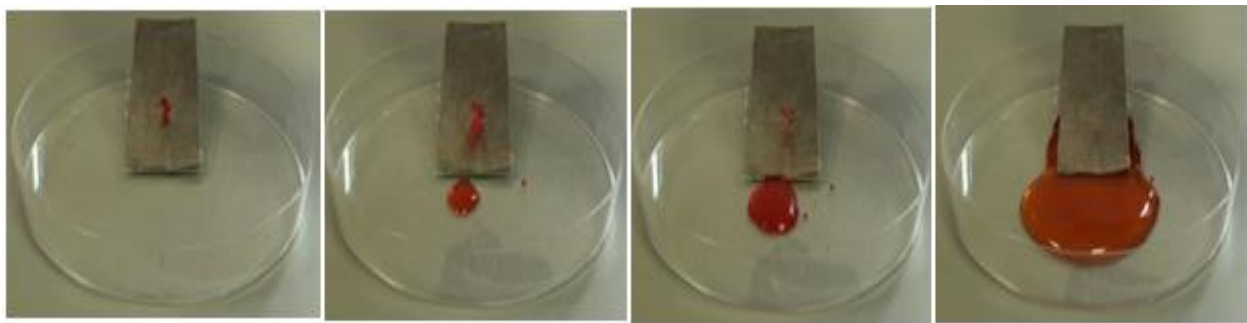


Figure 29. Self-cleaning property of 3 wt% fly ash-OTMS coated cotton fabric

5.1.7. Analysis of superhydrophobicity of fly ash-OTMS coated cotton fabrics

From Cassie–Baxter model, the area fraction of a water droplet (f) in contact with a fabric surface (i.e. wetted solid fraction) can be estimated based on the relationship between the apparent contact angle (θ^*) observed on a rough surface and the equilibrium contact angle (θ) obtained on a smooth surface.

From Figure 30 (a), the wetted solid fraction was found to decrease with increase in surface density of fly ash particles. The increase in unwetted fraction of the air pocket trapped in the interspaces among the fly ash particles was estimated to be 43%, 55% and 67% respectively for 1, 2 and 3 wt% of fly ash particles. This confirmed that the layer of fly ash particles created a rougher surface for the air storage to resist liquid penetration.

Furthermore, the movement of liquid droplets on hydrophobic surfaces was described by calculation of work of adhesion (W_{ad}) according to the Young–Duprè equation [53] (see Equation 11).

$$W_{ad} = \gamma_L (1 + \cos\theta) \quad (11)$$

Where γ_L is the surface tension of the liquid drops (i.e. 72.8 mN/m).

Figure 30 (b) shows the inverse relationship between work of adhesion and the surface density of fly ash particles. The work of adhesion for OTMS coated cotton fabric was measured around 25.42 mN/m. On the other hand, values of work of adhesion for fly ash-OTMS coated cotton fabrics ranged from 14.58 to 8.28 mN/m. The fabric surface decorated with 3 wt% fly ash exhibited lowest work of adhesion value, which indicated smallest work required for the movement of the water drop on its surface. Thus, an efficient way to improve the water repellency of cotton fabric was confirmed by creation of a fly ash layer with subsequent OTMS treatment.

By equating the work of adhesion and the work of separation, the maximum force of attraction can be achieved [47]. By accepting the force versus distance relationship of attraction

and repulsion, the attractive force (F_a) and repulsive force (F_r) at equilibrium can be written as given in Equation (12) and Equation (13), respectively.

$$F_a = (F_a)_e \left(\frac{d}{x}\right)^3 \quad (12)$$

$$F_r = (F_r)_e \left(\frac{d}{x}\right)^8 \quad (13)$$

Where x is the separation distance and d is the equilibrium distance

Under equilibrium conditions

$$(F_a)_e = (F_r)_e$$

Therefore, the work of adhesion can be expressed as given in Equation (14) and Equation (15) [53].

$$W_{ad} = \int_d^{\infty} (F_e) \left(\frac{d}{x}\right)^3 dx - \int_d^{\infty} (F_e) \left(\frac{d}{x}\right)^8 dx \quad (14)$$

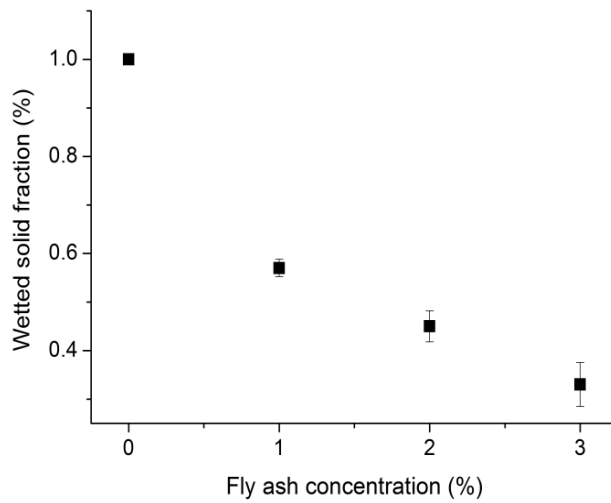
Which is equal to

$$W_{ad} = F_e \left[\frac{d}{2} - \frac{d}{7} \right] \quad (15)$$

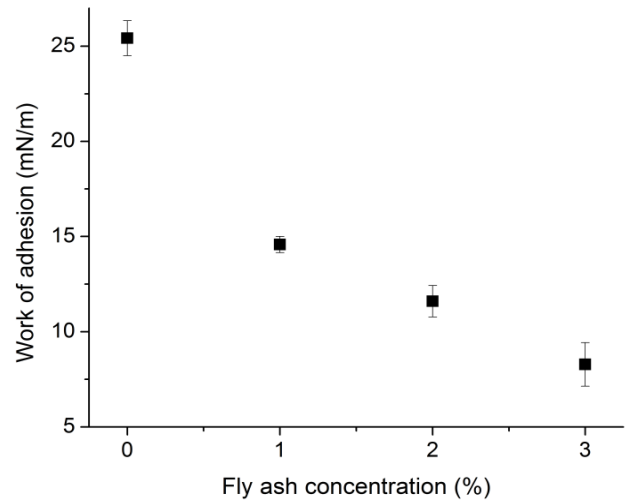
In this way, the force of attraction F_e can be determined by knowing the values of work of adhesion W_{ad} and equilibrium distance d . The distance between the molecular centers of a liquid can be estimated from the specific gravity and molecular weight of the liquids. For example, the equilibrium distance of 3.1 Å can be used for estimation of distance between the molecular centers of water. The interfacial tension of liquid and the natural characteristics of the

substrate, such as surface geometry or porosity, polarity, and chemical composition, affect the absorption of solid–liquid interface [111].

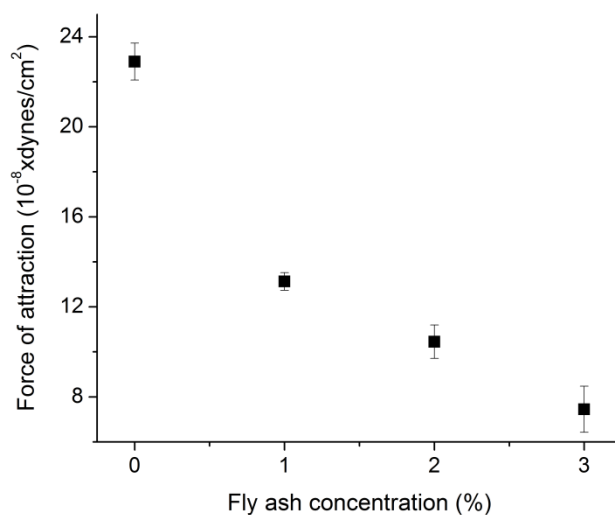
The force of attraction was calculated from the values of work of adhesion based on Equation (14) and Equation (15). From Figure 30 (c), the force of attraction was found to decrease with increase in fly ash concentration. The force of attraction for OTMS coated cotton fabric was measured around $22.9 (10^{-8} \text{dyne/cm}^2)$. However, for cotton fabrics decorated with fly ash particles, the force of attraction ranged from 13.13 to $7.45 (10^{-8} \text{dyne/cm}^2)$. This suggested that it required only about half the force to move a water drop on the fabric decorated with 3 wt% fly ash compared to that with 1 wt% fly ash.



(a). Cassie-Baxter prediction



(b). Work of adhesion



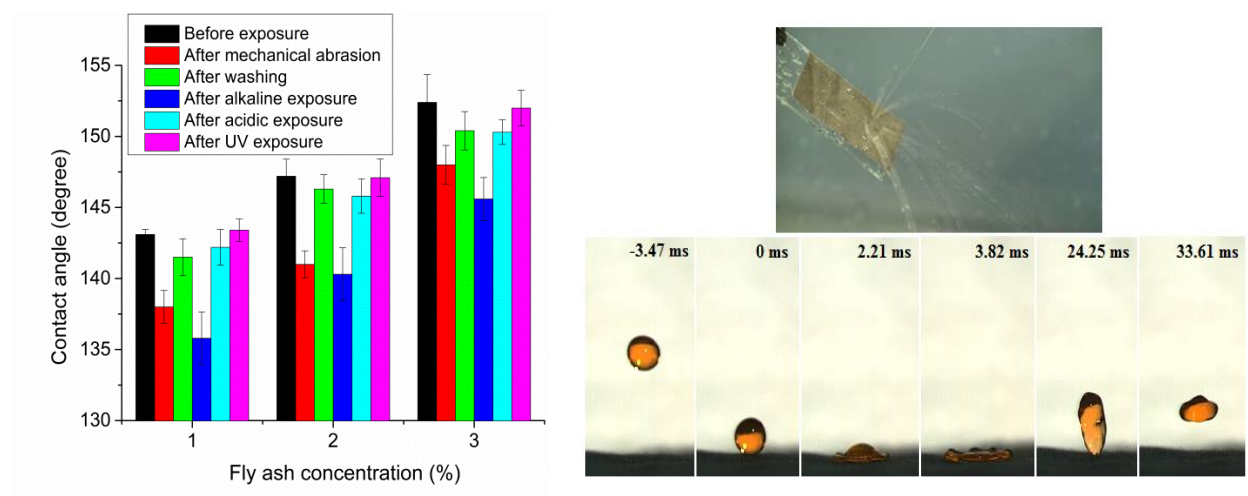
(c). Force of attraction

Figure 30. Analysis of superhydrophobicity of fly ash-OTMS coated cotton fabrics

5.1.8. Durability of superhydrophobic properties of fly ash-OTMS coated cotton fabrics

Figure 31 (a) shows the results of contact angle measurements for characterization of durability of fly ash-OTMS coated cotton fabrics against mechanical abrasion, laundering, chemical and UV action. It was observed that the water contact angles were reduced to some extent after 20 cycles of sand paper abrasion, but still maintained their superhydrophobicity especially at higher deposition of fly ash particles. Similarly, the contact angle was reduced for all the concentration of fly ash after five laundering cycles. However, it was still higher than 150° for 3 wt% fly ash sample. This demonstrated that fly ash particles were robust and stable on cotton surfaces, and only few fly ash particles were removed due to shearing and friction forces of laundering process [8]. When chemical durability of superhydrophobic fly ash-OTMS coated cotton fabrics was studied, all samples showed significant reduction of contact angle against alkaline conditions (pH=13) whereas negligible reduction against acidic conditions (pH=1). In order to improve the durability of contact angle, one of the solutions is going from two-tier surface roughness to the three-tier surface roughness characteristics. The ultraviolet durability of

superhydrophobic fly ash-OTMS coated cotton fabrics was studied as many types of materials lose their superhydrophobicity when exposed to ultraviolet irradiation [75]. The water contact angle had no obvious decrease for all the fly ash concentration, which indicated that fly ash coated samples have great resistance to ultraviolet rays and can be used under solar radiation. Finally, the durability of contact angle when fabric surface was impacted by jet of water can be observed from the time-lapse photographs of water droplets bouncing on the fabric as shown in Figure 31 (b). The water droplets completely left the fabric surface without wetting, which further indicated the development of superhydrophobic fly ash-OTMS coated cotton fabrics.



(a). Contact angle before and after exposure

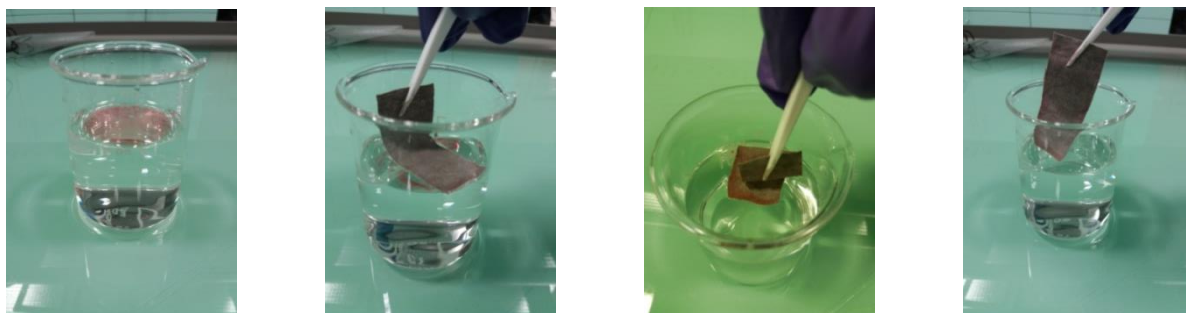
(b). Impact of water jet and bouncing of water droplets

Figure 31. Durability of fly ash-OTMS coated cotton fabrics

5.1.9. Oil in water removal performance of fly ash-OTMS coated cotton fabrics

As fly ash-OTMS coated cotton fabrics were superhydrophobic in nature, therefore further investigation was made on their oil sorption capacity. The toluene as model oil was used to observe the oil separation from the surface of water, whereas chloroform as model oil was used to observe the underwater oil separation performance. A small amount of toluene and

chloroform oil dyed by red orange is added into the water surface. Due to low density of toluene, it was floated on water surface (Figure 32a). Whereas, chloroform reached to bottom of water surface due to its high density (see Figure 32b). When a piece of superhydrophobic fly ash-OTMS coated cotton fabric was immersed into the water, both the oils were completely absorbed into the coated fabric structure within few seconds without leaving any color in water. This improvement of oil retention ability can be attributed to enhanced stability of capillary pressure to prevent the sliding of absorbed oil on fiber surface by creation of rough surfaces by fly ash particles [114].



(a). Photographs of toluene removal from top water surface



(b). Photographs of chloroform removal from underwater surface



(c). Photographs of oil in water separation experiment

Figure 32. Oil in water removal performance of fly ash-OTMS coated cotton fabrics

Furthermore, the oil separation efficiency of fly ash-OTMS coated cotton fabrics was quantitatively estimated in separate experiments (see Figure 32c) using four model oils of different densities (i.e. toluene, n-hexane, chloroform and petro ether). When the mixture of oil (dyed with red orange) and water was poured onto the superhydrophobic textile, the oil was quickly passed through the coated fabric into the small beaker. On the other hand, water was accumulated on the cotton surface, and then decanted into the big beaker from the top of the coated fabric. The separation efficiency of 98%, 96%, 97% and 95% was obtained for toluene/water, n-hexane/water, chloroform/water and petro ether/water, respectively. Moreover, the oil absorption capacity for toluene, n-hexane, chloroform and petro ether was found around 2540, 1750, 3300, 2100 %, respectively. The difference in oil sorption capacity was mainly attributed to the viscosity, density and surface tension of oils [75]. Later, the oil absorption capacities of fly ash-OTMS coated cotton fabrics were compared with previously reported high performance oil-absorbents. For example, SiO_2 /Octadecyltrichlorosilane coated cotton showed the oil absorption capacity of 4500 for chloroform [115], whereas polydimethylsiloxane coated cotton showed the oil absorption capacity of 2485 for toluene [116]. Although few studies showed better oil absorption capacities, however the results from the current study were found encouraging owing to low cost, and good environmental friendliness of fly ash particles.

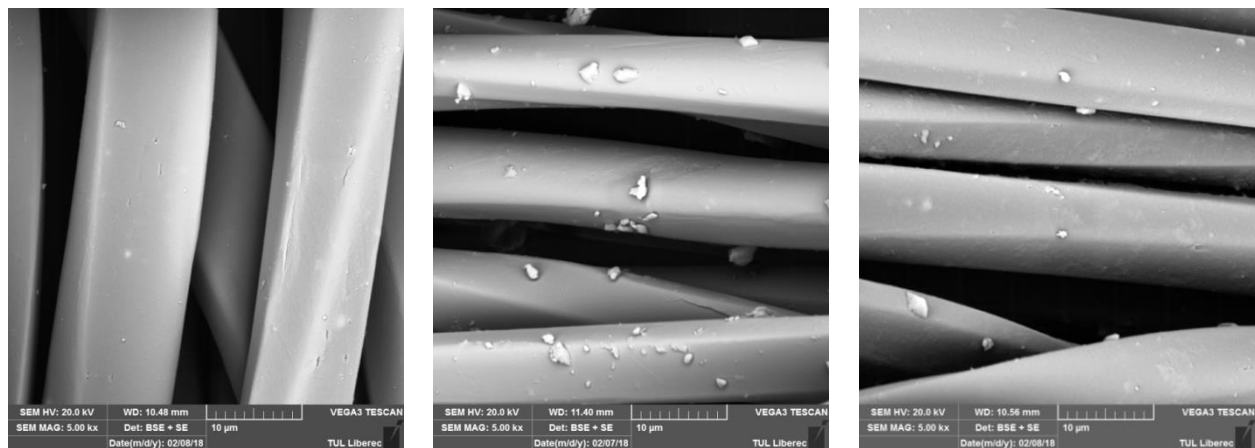
Therefore, the findings of this work could be useful for versatile separation of oil/water mixtures under various conditions (e.g. floating oil layer, underwater oil droplet or oil/water mixtures).

Towards the end, the reusability of superhydrophobic fly ash-OTMS coated cotton fabric was investigated by measuring the separation efficiency for toluene/water and chloroform/water after numerous of water–oil separation recycles. The oil sorption capacities decreased slightly throughout the whole cycles and the separation efficiency of coated fabrics ranged from 98% to 94% for toluene and 97% to 94% for chloroform after 5 cycles. The small decrease of oil sorption capacity can be attributed to the residual oils inside the structure of coated fabrics [117].

5.2. Superhydrophobic fabrics coated with TiO₂ nanoflowers and OTMS

5.2.1. SEM analysis of polyester fabrics coated with TiO₂ nanoflowers

The polyester fiber surface has low surface free energy, low wettability and poor adhesion due to lack of polar groups (COOH and OH) on the main chains. In order to attach TiO₂ nanoseeds on polyester fabric surface, the caustic soda treatment was carried out to generate the polar groups. Although the tensile strength of the polyester fabric decreased by 11 % due to the cleavage of ester linkages and hydrolysis of polyester chains, but it resulted into the formation of hydroxyl and carboxyl acid groups on the fiber surface [118]. From Figure 33b, Oligomers formed due to hydrolysis of polymer chains can be seen as small particles on the surface of the polyester fibers. The attachment of very fine TiO₂ nanoseeds can be observed from the surface of polyester fibers shown in Figure 33c.



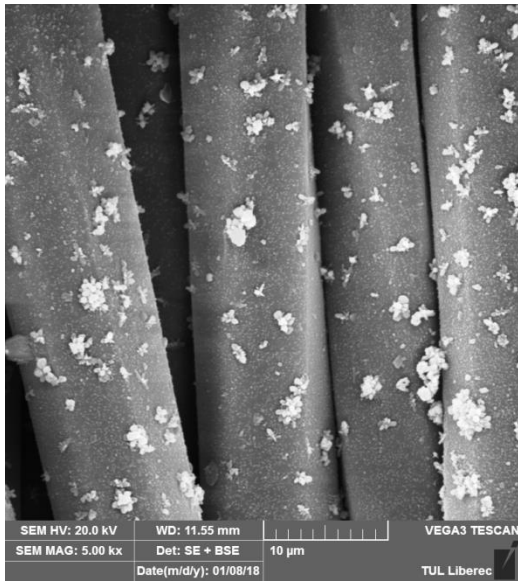
(a) Before caustic soda

(b) After caustic soda

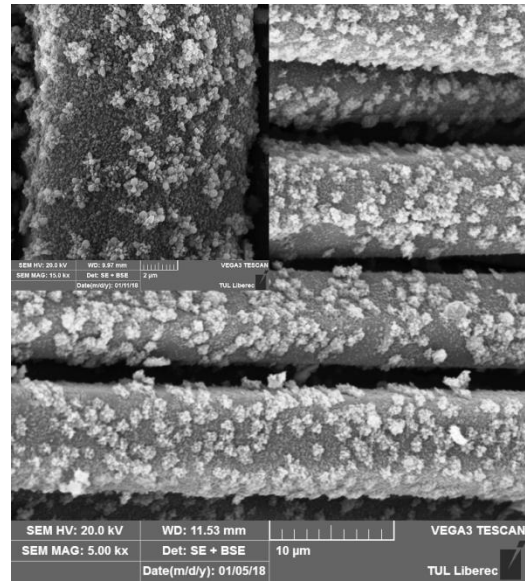
(c) After seeding

Figure 33. SEM micrographs of polyester fabric

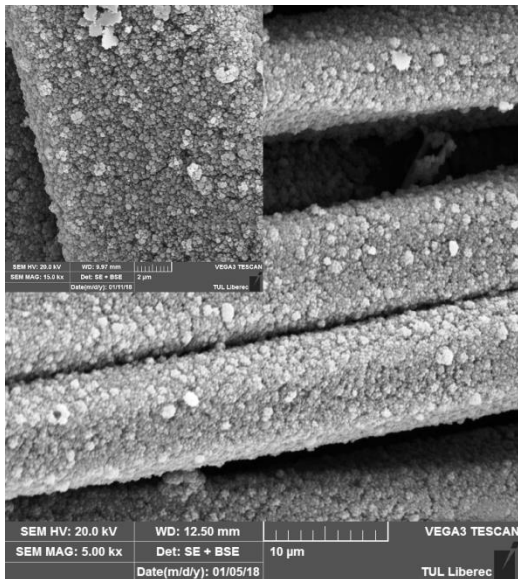
The surface hierarchical structure is important to obtain the superhydrophobic property. The surface structure of coated fabrics was investigated at different TTIP doses (i.e. 0.5 mL, 1 mL, 1.5 mL, and 2 mL) from SEM images shown in Figure 34. It can be seen that the dose of TTIP had a great effect on the growth and structure of TiO_2 nanoflowers. At low dose of TTIP (i.e. 0.5 mL), no TiO_2 flower structures were found on the polyester fiber surface except some tiny crystal nuclei of TiO_2 particles. However, the amount and the size of TiO_2 flower structures greatly increased as the amount of TTIP increased from 1 mL to 1.5 mL (see Figure 34a and Figure 34b). When the TTIP dose was further increased to 2 mL (see Figure 34c), the flower-like structures started to aggregate sharply and a continuous thicker coating was constructed on the polyester fiber surface. A micro/nanoscale surface mimicking the surface of lotus leaf was formed with each fiber of approximately 10 μm diameter, and the TiO_2 particles of below 500 nm sizes. A good adhesion between the TiO_2 particles and polyester fibers can be attributed to the presence of hydroxyl groups and formation of hydrogen bonds between them.



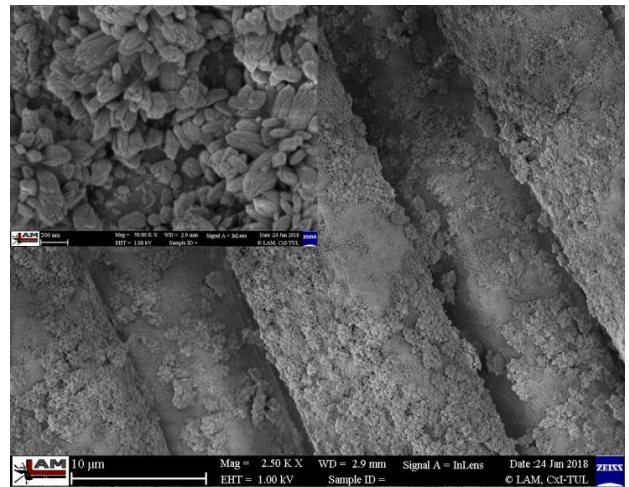
(a) 1 mL TTIP



(b) 1.5 mL TTIP



(c) 2 mL TTIP



(d) 2mL TTIP with high resolution

Figure 34. Effect of Titanium isopropoxide dose on growth of TiO_2 nanoflowers

5.2.2. EDS analysis

It was carried out to know the chemical composition of TiO₂ coated fabric. The EDS spectra in Figure 35 showed the presence of O, C, Ti, and Au as main elements on the surface of TiO₂ coated fabric, whereas the pristine polyester surface mostly consisted of O and C elements. The relative atom ratio for O, C, and Ti was determined about 40.7%, 37.1%, and 22.1%, respectively. The presence of Au element was caused by sputtering of gold on TiO₂ coated sample during SEM characterization.

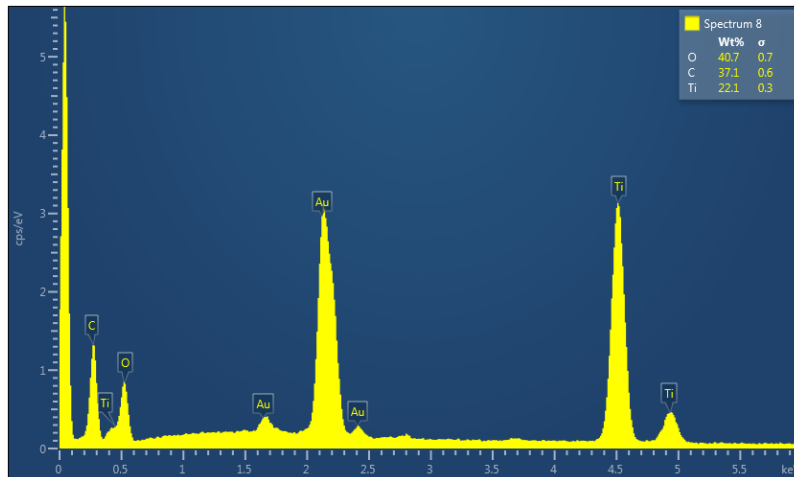


Figure 35. EDS spectrum of flower-like TiO₂ nanoparticles coated on polyester

5.2.3. Raman spectroscopy

It was employed to investigate the crystal structure of TiO₂ flower shaped 3D structures coated on the polyester fabrics. The Raman spectra shown in Figure 36 displayed the vibration modes at about 231, 447, and 608 cm⁻¹, which can be attributed to the second-order Raman scattering of tetragonal structure. The Raman peak observed at 146 cm⁻¹ indicated the formation of the anatase TiO₂ phase [119, 120], whereas the two strong Raman peaks observed at 447 cm⁻¹ and 608 cm⁻¹ confirmed the formation of crystalline rutile phase [121–123]. The intensity and peak positions of observed Raman spectra are in good agreement with the previous studies reported in the literature.

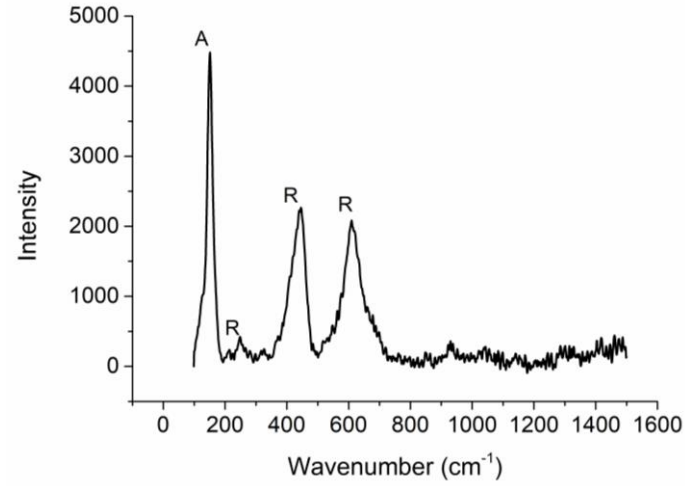


Figure 36. Raman spectra of flower-like TiO_2 nanoparticles coated on polyester fabric

5.2.4. XRD analysis

It was carried out to determine the crystal phase of the complex TiO_2 nanostructures coated onto polyester fabrics. As discussed in previous section of Raman spectroscopy, the existence of both anatase and rutile TiO_2 phases in the synthesized TiO_2 flower structures were confirmed (see Figure 37) [122]. The Bragg peaks observed at 27.08, 36.02, 41.24, 54.26 and 62.89 (2θ) were due to (110), (101), (111), (211) and (002) planes of tetragonal rutile phase (JCPDS no. 76-0317). The peaks observed at 25.29 and 48.01 (2θ) were due to (101) and (200) planes of the anatase phase (JCPDS no. 21-1272) [124, 125]. Further, the shapes of the diffraction peaks suggested the formation of highly crystalline TiO_2 structures. It was found that the ratio R of the intensity of the strongest rutile reflection I_r to the intensity of the strongest anatase reflection I_a (i.e. $R = \frac{I_r}{I_a}$) on XRD pattern can be used for quantification of TiO_2 individual polymorphs content. The weight fraction of anatase x_a can be approximated by Equation (16) [126].

$$x_a = \frac{1}{1.265 R + 1} \quad (16)$$

From the XRD pattern the ratio R was estimated around 0.698 and by using above Equation the weight fraction of anatase x_a of flower-like TiO_2 nanoparticles coated on polyester fabric was calculated 0.532.

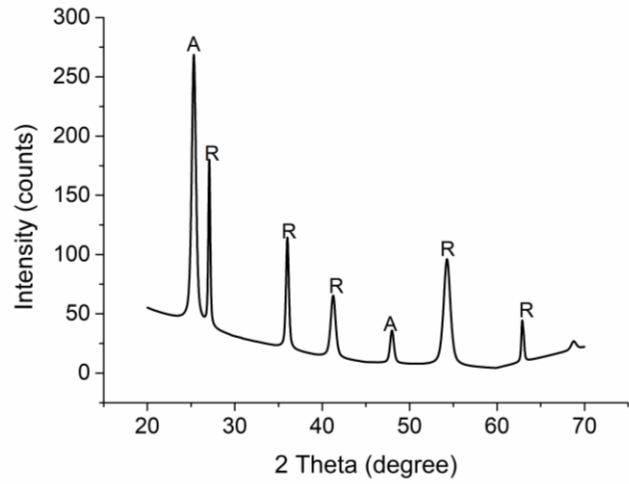
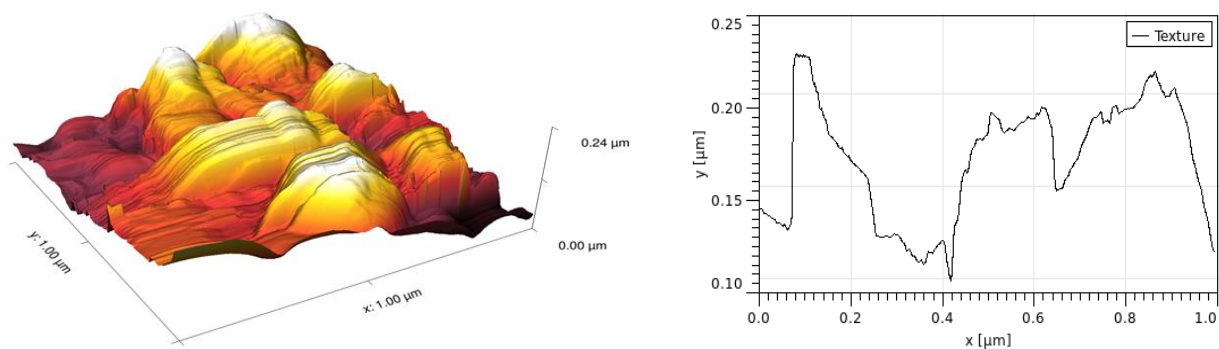


Figure 37. XRD pattern of flower-like TiO_2 nanoparticles coated on polyester fabric

5.2.5. AFM analysis

Figure 38 shows the topographical AFM images and surface profiles of the TiO_2 coated polyester fabrics. The increase in surface roughness of the coated polyester fabric can be seen from the topographical image. The average roughness (R_a) of 78.8 ± 9.3 nm was estimated for the flower-like TiO_2 nanoparticles coated polyester. Such surface roughness is sufficient to fabricate the physical self-cleaning (lotus effect) combined with hydrophobic surface chemistry by OTMS coating. The micro/nano structures enhance the roughness, which is necessary to form air cushion and validation of the Cassie–Baxter equation.



(a). 3D AFM image

(b). Surface profile

Figure 38. AFM analysis of the flower-like TiO_2 nanoparticles coated polyester

5.2.6. Physical properties of TiO_2 -OTMS coated polyester fabrics

The add-on of coated fabrics at different TiO_2 -OTMS coatings were calculated, and it was found to increase in linear pattern with increase in TTIP dose (Table 5). The final dry add-on of the coated fabrics was measured as 1.8 % for 1 mL TTIP, 4.2 % for 1.5 mL TTIP and 7.3 % for 2 mL TTIP doses.

Table 5. Add-on (%) of TiO_2 -OTMS coated polyester fabrics

Sample	Add-on (%)
1 mL TTIP	1.8 (± 0.21)
1.5 mL TTIP	4.2 (± 0.34)
2 mL TTIP	7.3 (± 0.41)

Subsequently, the hand (i.e. comfort) properties of the coated fabrics were assessed from the measurements of stiffness values. Stiffness is a tendency of the fabric to keep standing without support. It is a special property of the fabric for desirable draping and also influences the physical comfort of clothing [107, 109, 127]. It can be evaluated from bending properties of the fabric using bending length and flexural rigidity. Despite large increments in add-on of coated fabrics at higher TTIP dose, the stiffness values were found to increase marginally (Table 6). The stiffness of uncoated polyester fabric was 0.93 N m, whereas it was measured as 1.16, 1.32 and 1.42 N m for TiO₂+OTMS coated polyester fabrics at 1 mL, 1.5 mL and 2 mL TTIP respectively. This indicated no loss in draping behavior of TiO₂-OTMS coated polyester fabrics and therefore satisfactory physical comfort behavior.

Table 6. Stiffness of the TiO₂-OTMS coated polyester fabrics

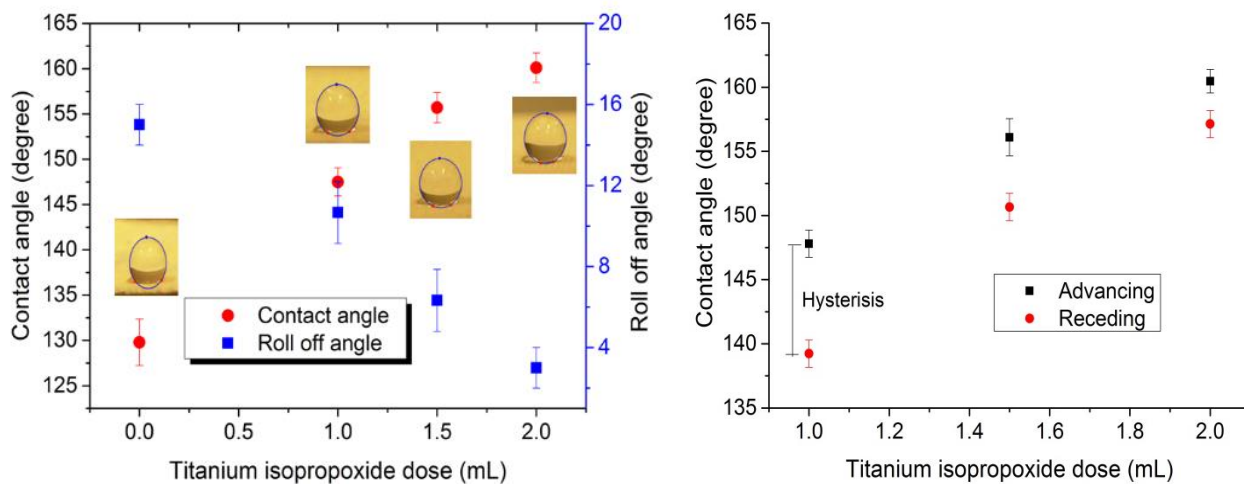
Sample	Stiffness (N m)
Control	0.93 (±0.11)
1 mL TTIP	1.16 (±0.14)
1.5 mL TTIP	1.32 (±0.09)
2 mL TTIP	1.42 (±0.12)

5.2.7. Superhydrophobic properties of TiO₂ nanoflowers coated polyester fabrics

The measurements of static water contact angle, roll-off angle and contact angle hysteresis were made to understand the effect of surface decoration of TiO₂ flowers on surface wettability of TiO₂-OTMS coated polyester fabrics (Figure 39). The water droplet depicted a spherical shape on the surface of TiO₂-OTMS coated textile. On the contrary, the surface of uncoated polyester fabric was partially wetted by the water droplet. Without any decoration of TiO₂ flowers and with only coating of OTMS on polyester surface, the static water contact angle

and roll off angle were measured around 129.8° and 15° respectively. This indicated the hydrophobic behavior of polyester fabrics after OTMS coating alone. However, this surface was not suited for physical self-cleaning action as the water droplets were difficult to roll off showing the strong adhesion between the water droplet and the coating surface. When polyester fabric surface was decorated with 3D shaped TiO_2 flowers and subsequent treatment of OTMS, the enhancement in contact angle and simultaneous reduction in roll off angle was found. The increase in contact angle and reduction in roll of angle was observed with the increase of TTIP dose during the hydrothermal deposition of TiO_2 flowers (Figure 39a).

The maximum static contact angle of 160.1° and minimum roll off angle of 3° was found for 2 mL TTIP dose. Therefore, the improvement in water repellency from surface hydrophobicity to superhydrophobicity can be confirmed when polyester fabric surface is decorated with TiO_2 nanoflowers before the OTMS coating. This phenomenon can be attributed to the formation of unique two-tier structural surface combined with the microscaled polyester fibers ($10\ \mu\text{m}$) and the nanoscaled TiO_2 flowers ($500\ \text{nm}$).



(a) Static contact angle

(b) Contact angle hysteresis

Figure 39. Effect of Titanium isopropoxide dose on contact angle

Due to surface roughness and heterogeneity of textile surfaces, the measured contact angle after the liquid drop advances is usually greater than the contact angle that results after the droplet recedes from a previously wetted surface [70, 106]. Therefore, the measurement of static contact angle results can be misleading for assessment of physical self-cleaning action. The contact angle hysteresis (i.e. difference between the advancing and receding contact angles) plays an important role in the sliding behavior of water droplets for self-cleaning effect [44, 110]. Here, the advancing and receding angles of TiO₂-OTMS coated polyester fabrics were measured to examine the influence of TiO₂ flower structures on the self-cleaning effect. From Figure 39b, the contact angle hysteresis was found to reduce from 9° to 3° with increase of TTIP dose from 1 mL to 2 mL, which indicated the formation of discontinuous, unstable, and contorted air/solid/liquid contact line due to the decoration of TiO₂ flowers. For superhydrophobicity, the solid–liquid–air contact line can further become more discontinuous and a larger amount of air film can be trapped by depositing high density of TiO₂ flowers using higher dose of TTIP.

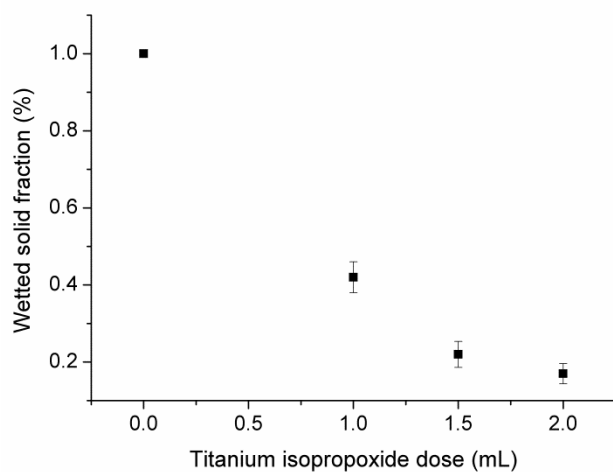
5.2.8. Analysis of superhydrophobicity of coated polyester fabrics

Based on previous studies, the wetting behavior of liquids can be explained either by Wenzel state or Cassie–Baxter state [47]. In Wenzel state, a liquid impregnates the rough surface to form a completely wetted contact with the surface, whereas the liquid does not completely fill up the rough surface due to air pockets in the Cassie–Baxter state. Therefore, the superhydrophobicity of the TiO₂-OTMS coated polyester fabrics can be believed in Cassie–Baxter state where spherical water drop cannot penetrate entire fabric surface due to large amount of air trapped in the structure [70]. Further, the Cassie–Baxter state of TiO₂-OTMS coated polyester fabric was verified by immersing the coated fabrics into water. The trapped air between the water and the superhydrophobic fabric resulted into the formation of plastron layer and thus showed the silver mirror-like bright and reflective surface [112]. The Cassie–Baxter model can be used to estimate the area fraction of a water droplet (f) in contact with a fabric surface (i.e. wetted solid fraction) from the relationship between the apparent contact angle (θ^*) observed on a rough surface and the equilibrium contact angle (θ) obtained on a smooth surface. It can be seen from Figure 40(a) that the wetted solid fraction was decreased with increase in

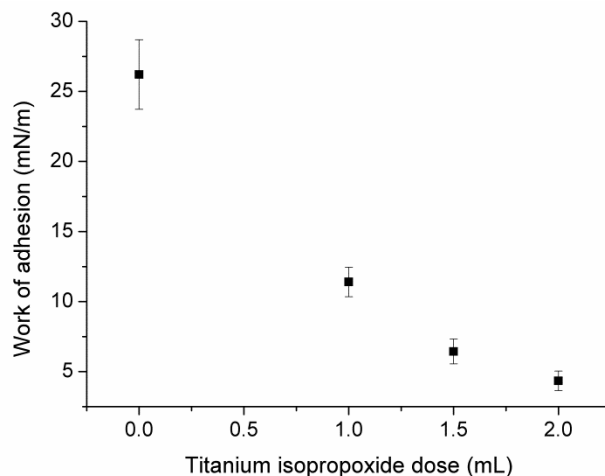
surface density of TiO₂ nanoflowers. The increase of 58%, 78% and 83% unwetted fraction of the air pocket was observed for the dose of 1 mL, 1.5 mL and 2 mL TTIP respectively, which further confirmed that the layer of TiO₂ nanoflowers created a rougher surface for the air storage to resist liquid penetration.

Furthermore, the Young–Duprè equation was employed to describe the movement of liquid droplets on hydrophobic surfaces by calculation of work of adhesion (W_{ad}). The work of adhesion was found to reduce with increase in surface density of TiO₂ nanoflowers (see Figure 40b). The polyester fabric coated with OTMS alone depicted the work of adhesion around 26.2 mN/m, whereas it ranged from 11.4 to 4.34 mN/m for TiO₂-OTMS coated polyester fabrics at respective doses of TTIP from 1 to 2 mL. The least work of adhesion (or smallest work required for the movement of the water drop) was shown by fabric surface after decoration of TiO₂ nanoflowers at 2 mL TTIP dose.

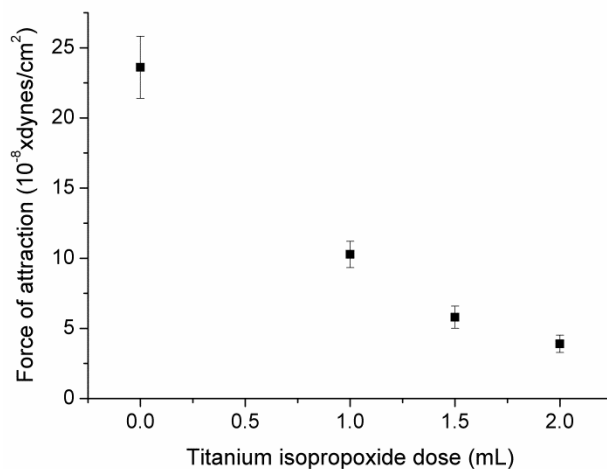
At the end, the force of attraction F_e was estimated by knowing the values of work of adhesion W_{ad} and equilibrium distance d given. Here, the equilibrium distance of 3.1 Å was used for estimation of distance between the molecular centers of water. Likewise in previous discussions, the force of attraction was found to decrease with increased deposition of TiO₂ nanoflowers on the surface (Figure 40c). The force of attraction for polyester fabric coated with OTMS alone was measured around 23.6 (10^{-8} dyne/cm²). But, the force of attraction ranged from 10.27 to 3.9 (10^{-8} dyne/cm²) after the decoration of TiO₂ flower structures at TTIP doses of 1 to 2 mL. This indicated less force required for movements of water drops on the fabric surface coated with increased amount of TiO₂ flowers and OTMS.



(a). Cassie-Baxter prediction



(b). Work of adhesion



(c). Force of attraction

Figure 40. Analysis of superhydrophobicity of TiO₂-OTMS coated polyester fabrics

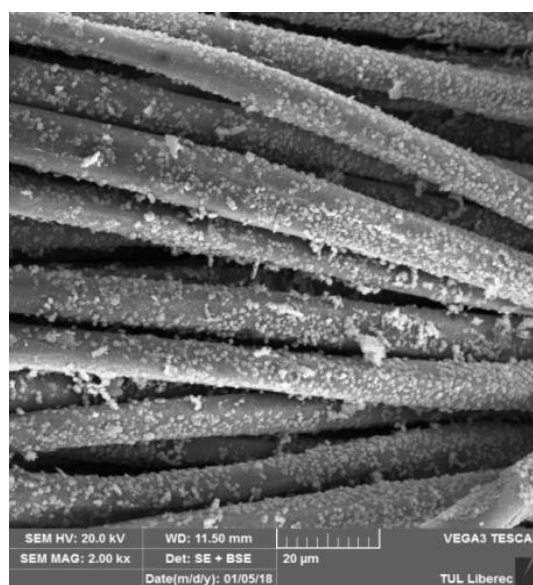
5.2.9. Durability of superhydrophobic properties of coated polyester fabrics

The durability of TiO₂-OTMS coated polyester fabrics against mechanical abrasion, laundering, chemical and UV action can be seen from the results of contact angle measurements

shown in Figure 42(a). After 20 cycles of sand paper abrasion, the water contact angles were reduced for all the samples of different TiO_2 depositions. However, the samples coated with TTIP doses of 1.5 and 2 mL continued to maintain their superhydrophobicity and presented the respective contact angles of 153° and 156° after mechanical abrasions. Likewise, the action of five laundering cycles resulted in the decrease of contact angles, but still higher than 150° for the samples coated with more than 1.5 mL TTIP. The removal of only few particles for samples coated with TTIP dose of 1.5 and 2 mL against laundering indicated the robust and stable coating of TiO_2 particles over polyester fabrics (see Figure 41) [8].



(a) 2 mL

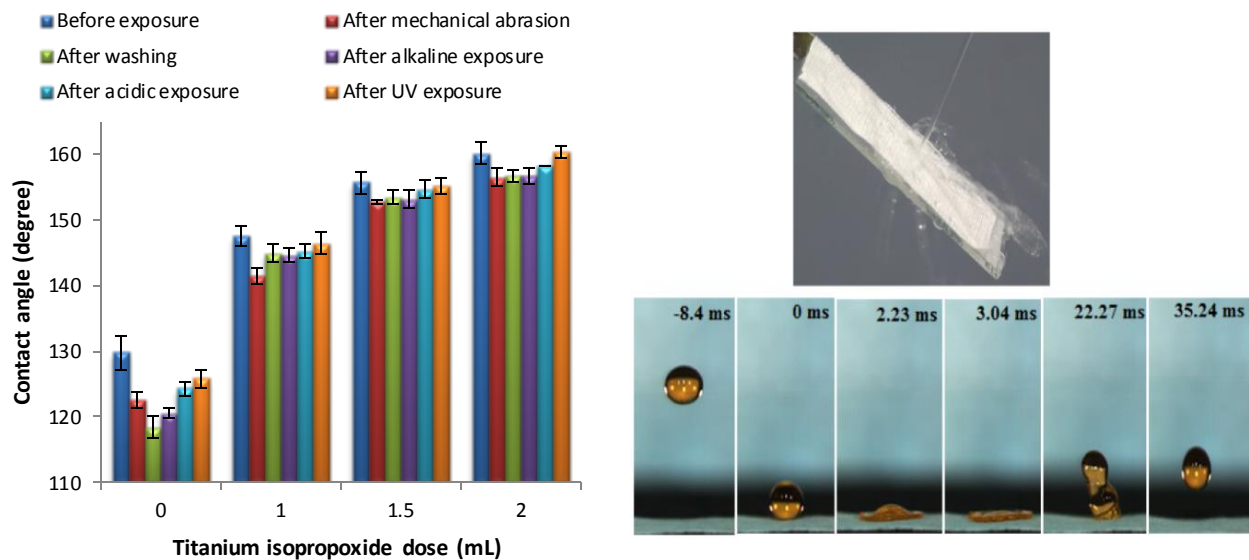


(b) 1.5 mL

Figure 41. Durability of surface microstructure TiO_2 -OTMS coated fabrics

Further, all samples showed acceptable reductions in superhydrophobic properties after exposure to chemical environment. The reductions in contact angle after exposure to alkaline environment was found greater than the acidic environments due to the itching of polyester fiber surfaces in presence of alkali. As many types of materials lose their superhydrophobicity when exposed to ultraviolet irradiation, therefore the ultraviolet durability of superhydrophobic TiO_2 -

OTMS coated polyester fabrics was also studied [75]. Compared to mechanical and chemical actions, the water contact angle of coated fabrics was not affected after exposure to ultraviolet rays and thus suitable for use under the solar radiations (Figure 42a). Lastly, the effect of jet of water when impacted on coated fabric surface was examined to verify the durability of contact angles. The time-lapse photographs of water droplets bouncing on the fabric are shown in Figure 42(b), where water droplets completely left the fabric surface without wetting and thus confirmed their super hydrophobic behavior.



(a). Contact angle before and after exposure

(b). Impact of water jet and bouncing of water droplets

Figure 42. Durability of TiO₂-OTMS coated polyester fabrics

5.2.10. Physical self-cleaning properties of coated fabrics

Due to the superhydrophobic behavior and low roll off angles, the utility of TiO₂-OTMS coated polyester fabrics was studied for physical self-cleaning performance. The methyl orange dye was used as contaminant to demonstrate the self-cleaning action. When the water droplets were dropped on the contaminated fabric, it rolled over the surface and maintained the spherical

shape. During the sliding process of water droplets, the dye particles were immediately picked up and taken away leaving behind a clear surface as seen in Figure 43 [113]. This behavior was attributed to the creation of lotus effect by high water surface tension and low surface energy of coated fabrics [128].

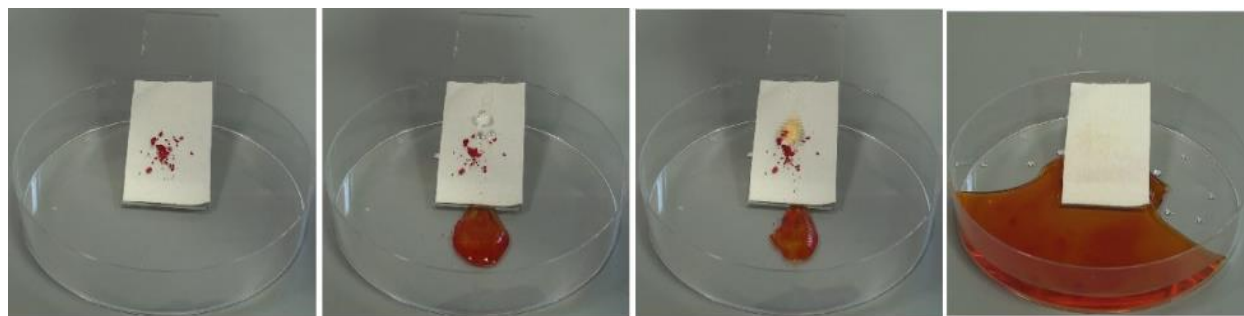


Figure 43. Physical self-cleaning property of TiO_2 -OTMS coated polyester fabric

5.2.11. Chemical self-cleaning properties of coated fabrics

The chemical self-cleaning properties of coated fabrics were examined based on two aspects (i.e. stain degradation and solution discoloration tests). For stain degradation performance, the methyl orange dye was applied as stain on the coated fabrics and their photo degradation behavior towards the dye was observed at different time intervals of exposure to the ultraviolet light. From Figure 44, the significant degradation of methyl orange dye was found for all the coated samples decorated with different concentrations of 3D shaped TiO_2 flowers. The reasons for low deviation under 30 min could be due to different locations of dyes and photocatalyst. When the dye stain was deposited on the coated fabric, the part of it which was on top of the TiO_2 nanoflowers degraded quickly because it was completely exposed to UV light. On the other hand, the dye deposited on the sides of nanoflowers required more time to degrade. The stains disappeared mostly within 3 h and the samples became approximately white after 4 h. Furthermore, the degradation rate was found to increase with increased density of TiO_2 flowers coated onto fabric and also with increased time of UV exposure. On the other hand, the pristine polyester fabrics showed no change in stain reduction even after the exposure to UV light for more than 4 h.

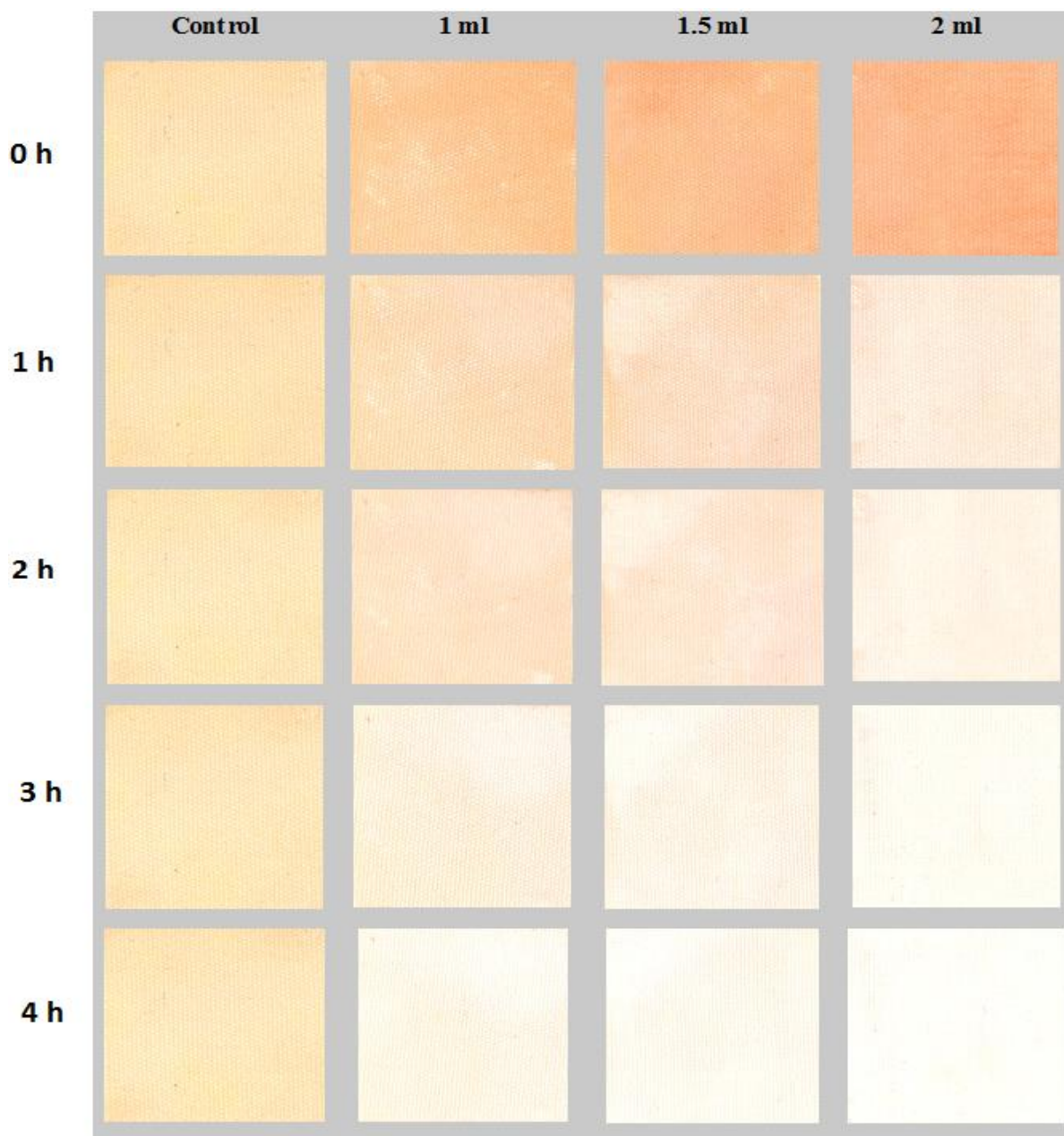


Figure 44. Photocatalytic stain degradation of TiO₂-OTMS coated polyester fabric

Later, the photocatalytic degradation rate of methyl orange dye was quantitatively estimated by measuring the color intensity of samples on ImageJ software. When the sample becomes whiter, the value (counts) of color intensity increases that mean it is measuring the whiteness of the sample. The increase in measured color intensity from this software can be correlated to increase in the whiteness index (see Figure 45). Interestingly, the depth of stains

were found much higher before the start of UV irradiation on samples decorated with TiO₂ flowers than the alone OTMS coated sample. This can be attributed to hydrophilic nature of TiO₂ particles deposited onto the polyester fabrics. However, from the measurements of color intensity, the dye degradation of samples decorated with TiO₂ flowers was found to increase after the UV irradiation. Whereas, the sample coated with OTMS alone showed a straight line and thus no degradation of dyes in absence of TiO₂ particles. The photocatalytic activity of TiO₂ coated textiles can be attributed to the decomposition of dyes by generation of highly oxidative radicals under the UV light [13].

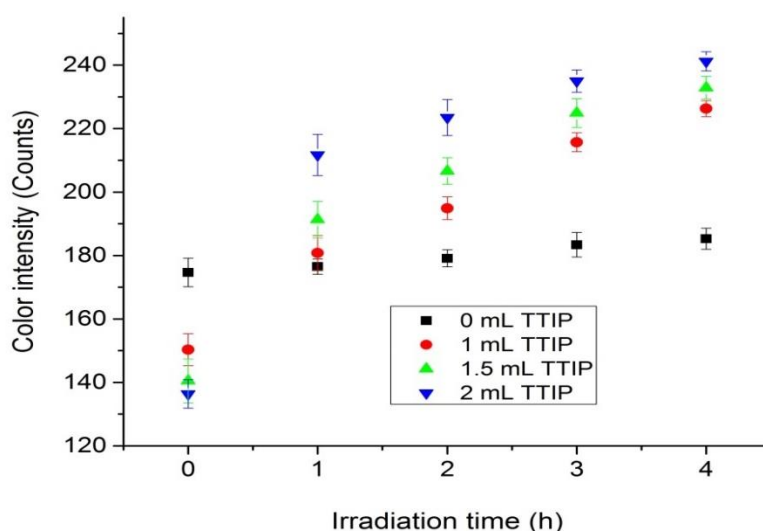


Figure 45. Evaluation of TiO₂-OTMS coated polyester fabric after photocatalytic degradation

Another test of solution discoloration was also employed to characterize the chemical self-cleaning properties of coated fabrics. Here, the coated samples were added into the dye solution and then the dye concentration was measured by recording the UV-Vis spectra. Figure 46(a) showed the absorbance spectra of the dye solution at different UV illumination time. The straight line obtained for the pristine polyester fabric indicated the absence of any photocatalytic activity by polyester itself. The absorbance value of methyl orange dye in the solution was measured by observing the peak intensity at 485 nm. The decrease in absorbance value with the passage of time indicated the decrease in the concentration of dye due to its photocatalytic degradation. The samples coated with 2 mL TTIP decolorized the dye solution in 150 min, whereas the samples coated with 1 mL and 1.5 mL TTIP took almost 300 and 210 min

respectively. The higher rate of dye degradation in case of 2 mL of TTIP can be attributed to the decoration of high density 3D shaped TiO₂ flowers on the fiber surface. Furthermore, the photocatalytic efficiency of the sample coated with 2 mL TTIP was examined for repeated discolorations of dye solution. From Figure 46(b), no change in photocatalytic efficiency of treated fabric was found during the five successive discoloration cycles which confirmed its potential use for several times in the application.

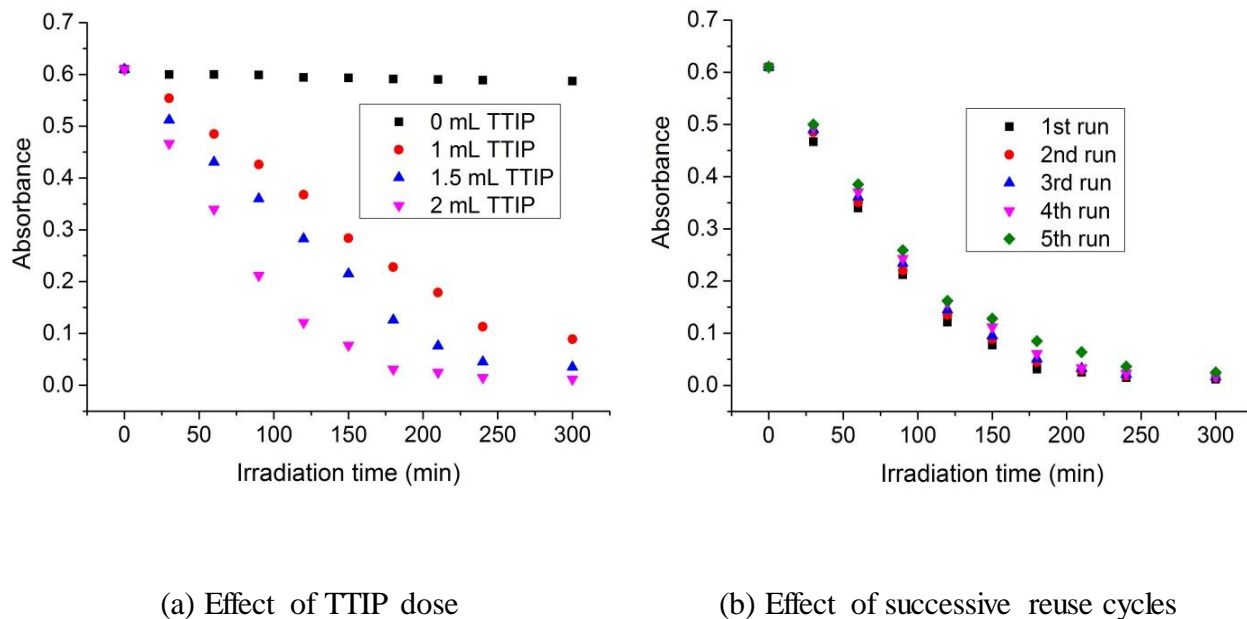


Figure 46. Solution discoloration properties of TiO₂-OTMS coated polyester fabrics

Mechanism of photocatalytic dye degradation. When TiO₂ was illuminated by light energy higher than its band gaps, the electrons in TiO₂ jumped from the valence band to the conduction band and then formed electron (e⁻) and electric hole (h⁺) pairs on the surface of the photocatalyst. The negative electrons and oxygen combined into O₂⁻, whereas the positive electric holes and water generated hydroxyl radicals. When the organic compound falls on the surface of the photo catalyst, it can combine with O₂⁻ and OH[•] respectively, and turn into carbon dioxide and water. In present study, the degradation of dye was started with the azo bond cleavage by highly oxidizing hydroxyl radicals and was followed by the hydroxylation of the aromatic ring.

5.3. Superhydrophobic fabrics coated with ZnO nanorods and OTMS

5.3.1. Morphological analysis and growth mechanism

The low surface energy and hierarchical micro/nanostructures are important factors to fabricate superhydrophobic textile surfaces. Microwave hydrothermal method was used for rapid growth of ZnO nanorods on the fiber surfaces to develop micro/nanostructures and then subsequently treated with low surface energy material (OTMS) to produce superhydrophobic surface. The surface of the pristine cotton fabric was completely wetted by the water droplet without any contact angle (inset, Figure 47a). From SEM image uniform and continuous layer of nanorods can be seen on the surface of the cotton fiber (Figure 47b), whereas; the water droplet exhibited a spherical shape on the surface of OTMS modified ZnO nanorods decorated cotton fabric (inset, Figure 47b). AFM image show topography of the grown ZnO nanorods on fibers of the cotton fabrics (Figure 47c). These results show the uniform patterned growth of the nanorods on the surface of the cotton fabrics. The grown nanorods enhance the surface roughness, which is necessary to form air pockets. According to Cassie–Baxter model, to fabricate a superhydrophobic surface, it is important to design the rough surface for enlarging the contact area of liquid and air [129–131].

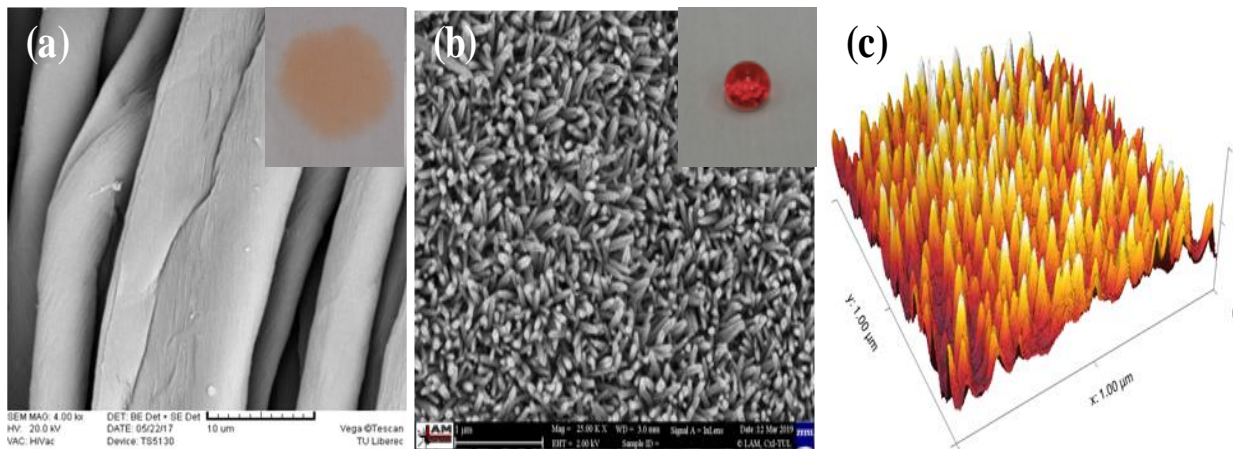


Figure 47. SEM image of the (a) pristine cotton fabric, (b) ZnO nanorods grown fabric surface and (c) 3D AFM image of the ZnO nanorods decorated fabric surface. Insets (a) and (b) are images of water droplet on the corresponding fabric surfaces.

The reaction taking place in the presence of $\text{Zn}(\text{NO}_3)_2 \cdot 6\text{H}_2\text{O}$ and HMTA during the growth of ZnO nanorods onto cotton fiber are given in equations (17) – (22).



The hydrolysis of HMTA in aqueous solutions generates NH_4^+ and OH^- ions as shown in the Equation (18). The Zn^{2+} and 2NO_3^- ions released from hydrolysis of $\text{Zn}(\text{NO}_3)_2$ as shown in Equation (19). The reaction of Zn^{2+} ions with OH^- ions to produce $\text{Zn}(\text{OH})_2$ is given in eqn. (20). When $\text{Zn}(\text{OH})_2$ is heated to 100 °C ZnO nanorods is formed as given in Equation (21). Moreover, the rest of Zn^{2+} ions and the ammonia formed in previous eqn. (17) react to form the $[\text{Zn}(\text{NH}_3)_4]^{2+}$ complex ions, as given in Equation (22). The nanoseeds prior to growth of nanorods actually provide the site for nucleation which is prerequisite for growth of nanorods. Another important thing which favors the seeded growth is the presence of -OH groups on seeds which are similar to those present on (0001) face of ZnO crystals. The ZnO crystal in hexagonal wurtzite type structure has polar and nonpolar planes. The top polar (0001) plane is positively charged and exhibits high surface energy. The ZnO crystal growth under hydrothermal condition has fastest rate in this direction (0001). The shape and orientation of the grown ZnO nanocrystals are mainly influenced by the type and concentration of the ZnO precursors,

additives, and pretreatment of substrate and deposition parameters, such as microwave power and deposition time [132–134].

The surface morphology of all ZnO nanorods grown cotton fabrics was directly observed by SEM. To investigate the influence of the zinc nitrate hexahydrate and HMTA concentration on the growth and morphology of ZnO nanorods, a set of experiments was performed. The attachment of very fine ZnO nanoseeds can be seen on the surface of cotton fibers as shown in Figure 48(a). It was found that concentration of zinc nitrate hexahydrate and HMTA had a great influence on the size and structure of grown nanorods. At a low zinc nitrate hexahydrate and HMTA concentration of 10mM (Figure 48b), no ZnO nanorods were found on the surface of cotton fiber but only few tiny ZnO crystals were sparsely coated on cotton fiber surface.

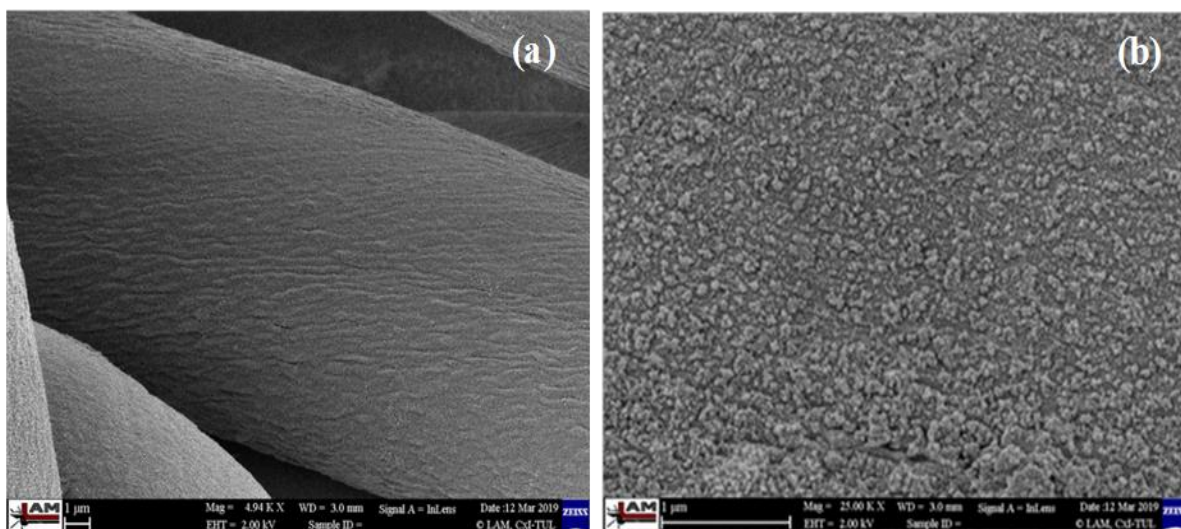


Figure 48. SEM images of (a) ZnO seeded cotton fiber and, (b) 10 mM zinc nitrate hexahydrate concentration treated cotton fiber

Figure 49 shows the SEM images of grown nanorods on cotton fiber surface at different level of concentrations (i.e., 25 mM to 100 mM). A uniform and continuous layer of grown ZnO nanorods can be seen on all the samples synthesized at different concentration using microwave hydrothermal method except sample with 10 mM of concentration. SEM images and Image J software was used for the calculation of the nanorods dimensions. An average value of the dimensions was calculated from 100 individual nanorods. The hexagon shaped morphology of

the as-grown nanorods can be seen from SEM images. It is clear that the solution concentration plays a vital role in determining the shape and size of the ZnO nanostructures [135].

It was found that diameter (D) and length (L) of the as-grown nanorods increased with increased in concentration of zinc nitrate hexahydrate/HMTA (Table 7). The diameter and length of the as-prepared nanorods were found in the range of 35-55 nm (Diameter) and 190-300 nm (Length), respectively. The average diameter of the grown nanorods was increased from 35 nm to 55 nm, as the concentration increased from 25 mM to 100 mM. The maximum length (300 nm) of the as-grown nanorods was achieved, when the 50 mM concentration of zinc nitrate hexahydrate/HMTA was used. When the ZnO rods were grown at higher concentration (i.e. 75 mM, 100 mM), more thick nanorods were obtained as compared to the lower concentration (i.e. 25 mM, 50 mM). These results shows that at higher concentration the growth increases more along the, $10\bar{1}0$ or $01\bar{1}0$ ZnO crystal planes that form the sides of ZnO hexagonal rods rather than the length direction (0001). Our results reveal that concentration plays an important role in the formation of the ZnO nanorods. The higher concentration led to the supersaturation and formation of many nuclei of small size which results in fast nucleation and slow growth rate. Thus, this will hinder the growth rate of the (0001) plane and making nanorods thicker [136–138].

Table 7. Dimension of nanorods grown at various concentrations

Zn(NO₃)₂ ·6H₂O Concentration (mM/L)	Nanorods average diameter (nm)	Nanorods Average length (nm)
25	35 ±3.5	190 ±11.5
50	41 ±5.4	300 ±14.6
75	50 ±4.2	262 ±12.6
100	55 ±6.1	260 ±15.4

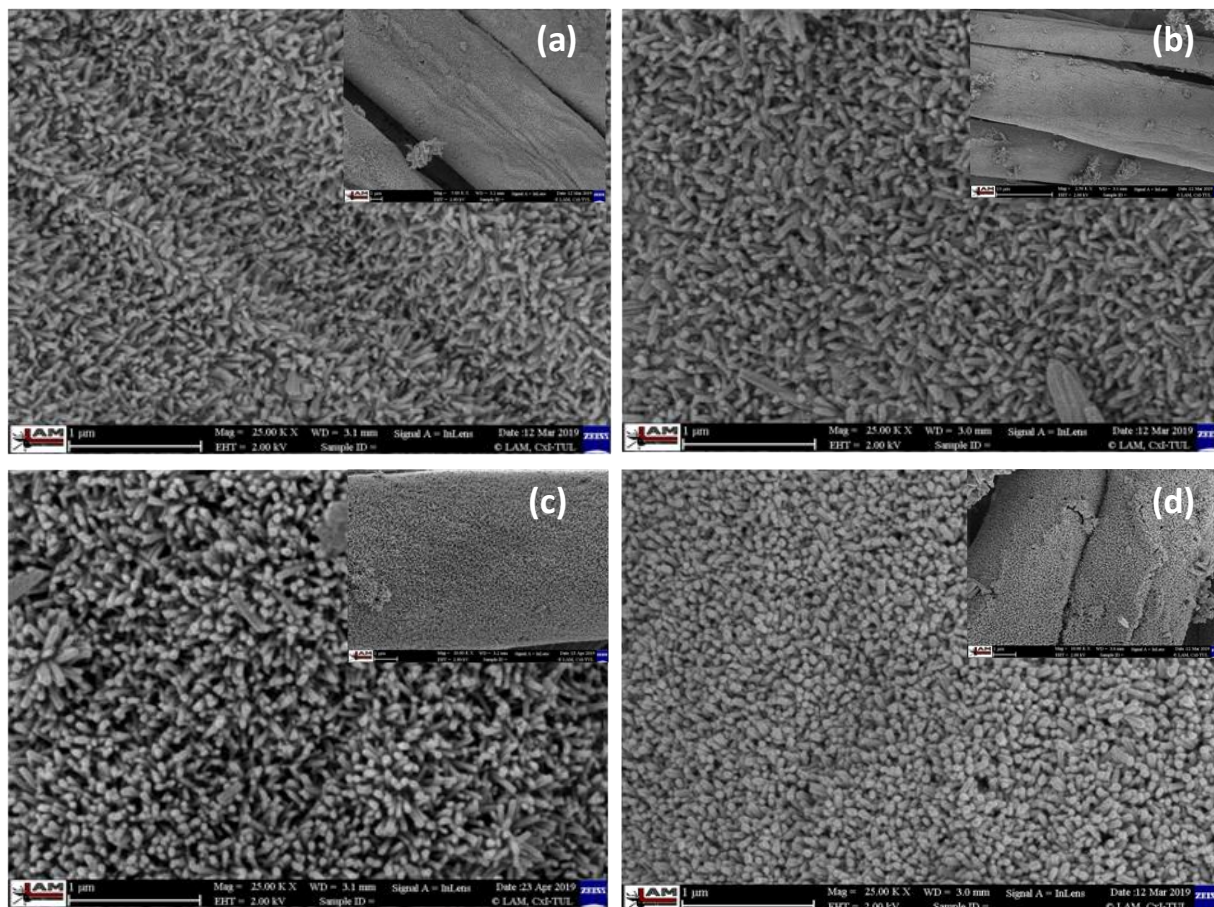


Figure 49. SEM images of ZnO nanorods grown onto cotton fabric in microwave reactor at 360 W (60 %) for 10 min under various concentration of zinc nitrate hexahydrate/HMTA: (a) 25 mM, (b) 50 mM, (c) 75 mM, and (d) 100 mM. Insets are the corresponding low magnification images

Figure 50 shows the SEM images of the as-prepared nanorods grown on the ZnO seeded cotton fibers after microwave hydrothermal reaction at different reaction time. It can be clearly seen that the cotton fibers is completely covered with the uniform and dense film of ZnO nanorods. The as-prepared ZnO nanorods were well faceted, with the diameter of 35–54 nm and an axial length of 190–295 nm under different reaction time (Figure 50). The length (L) and diameter (D) was increased with increase in reaction time. For instance, length and diameter increases from 190 nm to 295 nm and 35 nm to 55 nm respectively, when the reaction time

increases from 10 min to 30 min. Therefore, the reaction time is also an important factor to control the size of the nanorods [139, 140].

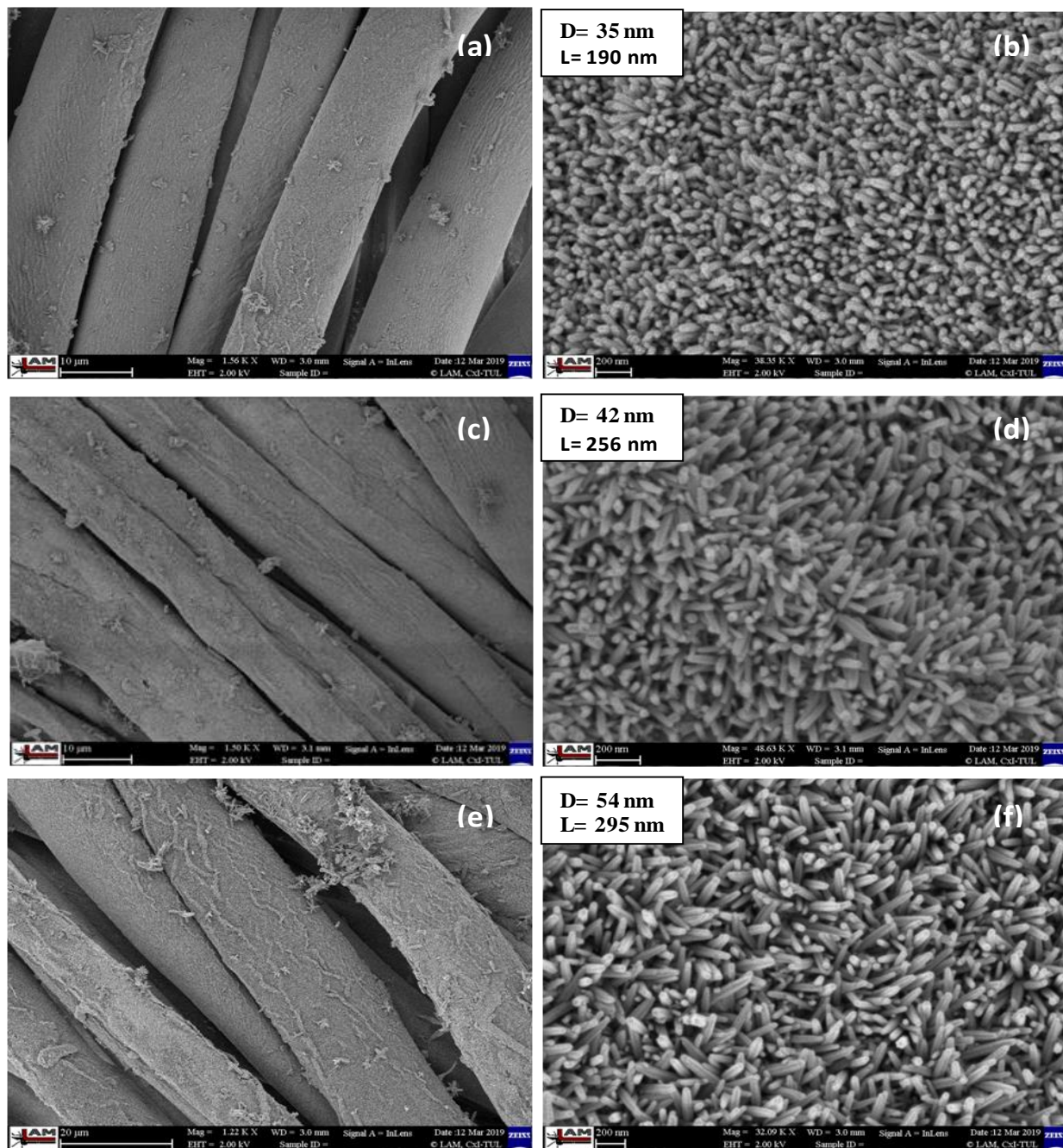


Figure 50. SEM images of ZnO nanorods grown on cotton surfaces treated with 25 mM of Zinc nitrate hexahydrate/HMTA in microwave reactor at 360 W (60 %) for different reaction time: (a, b) 10 min, (c, d) 20 min and (e, f) 30 min

The effect of microwave power on the growth rate of nanorods was also studied. The microwave power was found to have great influence on both the axial and lateral growth rates of the nanorods. The microwave power level was found to be proportional to the growth rate of the nanorods. This is mainly due to the rapid heating of the precursors to its crystallization temperature and quick dissolution of the precipitated hydroxides [141]. It was observed that longer and thicker nanorods can be obtained at higher microwave power levels. Figure 51(a-f) shows the SEM images of as-grown nanorods at different microwave power levels (360 W, 420 W and 480 W) for 10 min. A homogenous and continuous film of ZnO nanorods can be seen on cotton fiber surface. The nanorods grown at high microwave power (480 W) had higher diameter (44 nm) and length (308 nm) as compared to nanorods grown at 360 W and 420 W of microwave powers (Figure 51e, f). The nanorods having averaged diameter of 40 nm and length of 270 nm were grown at microwave power of 420 W (Figure 51c, d). The increase in microwave power causes the rapid heating of the solution simultaneously, which enhance the nucleation and growth of the ZnO crystal [142, 143]. Thus, rapid growth of longer and thicker nanorods can be achieved by increasing the microwave power. It can be concluded that microwave powers has great influence on enhancing the dimensions of the nanorods.

The above discussion indicated that ZnO nanorods film can be successfully prepared on the cotton fibers. The size and morphology of the as-prepared nanorods can be controlled by changing salt concentrations, reaction time and microwave power levels. Therefore, we can conclude that an increase in the concentration of zinc nitrate hexahydrate/HMTA induces the changes in the kinetics of nucleation and growth, which may results in a change of size and density of the ZnO nanorods on the fiber surfaces. Similarly, the reaction time and microwave power also had great effect on the size and density of the ZnO nanorods. In particular, these parameters influence the growth rate of the nanorods along different planes resulting in vary sizes of ZnO nanorods. Finally, a controlled and uniform film of ZnO nanorods of desired shape and size can be developed under optimized parameters.

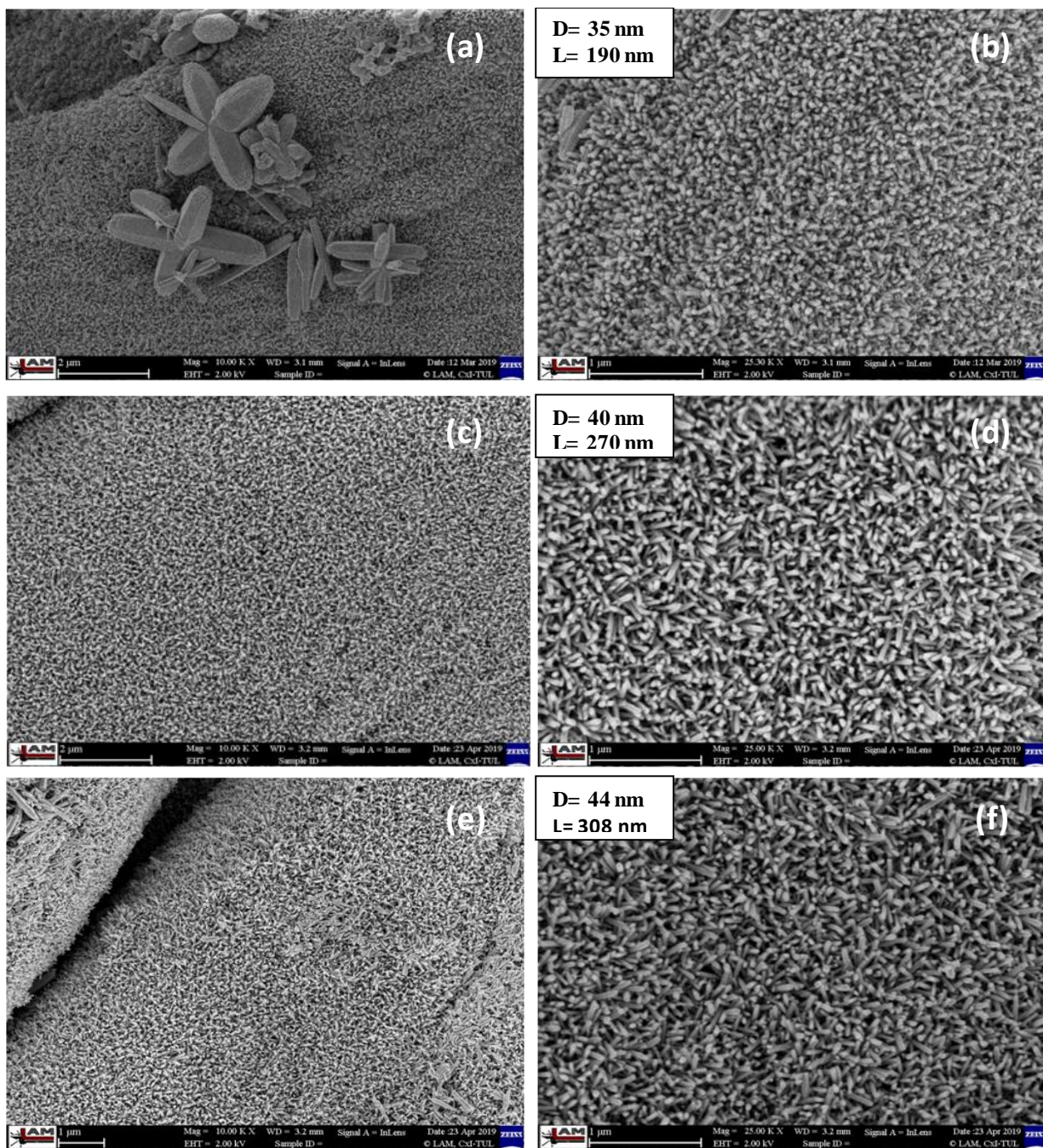


Figure 51. SEM images of ZnO nanorods grown on cotton surfaces treated with 25 mM of Zinc nitrate hexahydrate/HMTA in microwave reactor for 10 min at different microwave powers (watt): (a, b) 360 W (60 %), (c, d) 420 W (70 %) and (e, f) 480 W (80 %). Magnifications: 10.00 KX (a, c, e) and 25.00 KX (b, d, f)

5.3.2. Add-on analysis

The add-on (%) of ZnO-OTMS coated fabrics at different concentrations of zinc nitrate hexahydrate was calculated. The add-on was found to increase with increase of zinc nitrate hexahydrate concentration. This indicates an efficient coating of the surface. The final dry add-on of the ZnO-OTMS coated fabrics are given in Table 8.

Table 8. Add-on (%) of ZnO-OTMS coated cotton fabrics

Zn(NO ₃) ₂ · 6H ₂ O Concentration (mM/L)	Add-on (%)
10	3.6 (±0.31)
25	8.5 (±0.23)
50	9.1 (±0.40)
75	9.4 (±0.19)
100	9.9 (±0.27)

5.3.3. EDS analysis

To confirm the composition of these as-grown nanorods, the samples were investigated by energy disperse spectroscopy (EDS). The EDS analysis clearly showed that these uniformly distributed nanorods were mainly composed of Zn and O elements (Figure 52). Samples treated with various concentration of zinc nitrate hexahydrate showed almost similar amount of Zn content as shown in Table 9. Additionally, the amount of Zn content on the different coated fabrics can be attributed to the crystallinity of the grown nanorods [144]. The presence of Pt

element was caused by sputtering of platinum on ZnO coated sample during SEM characterization.

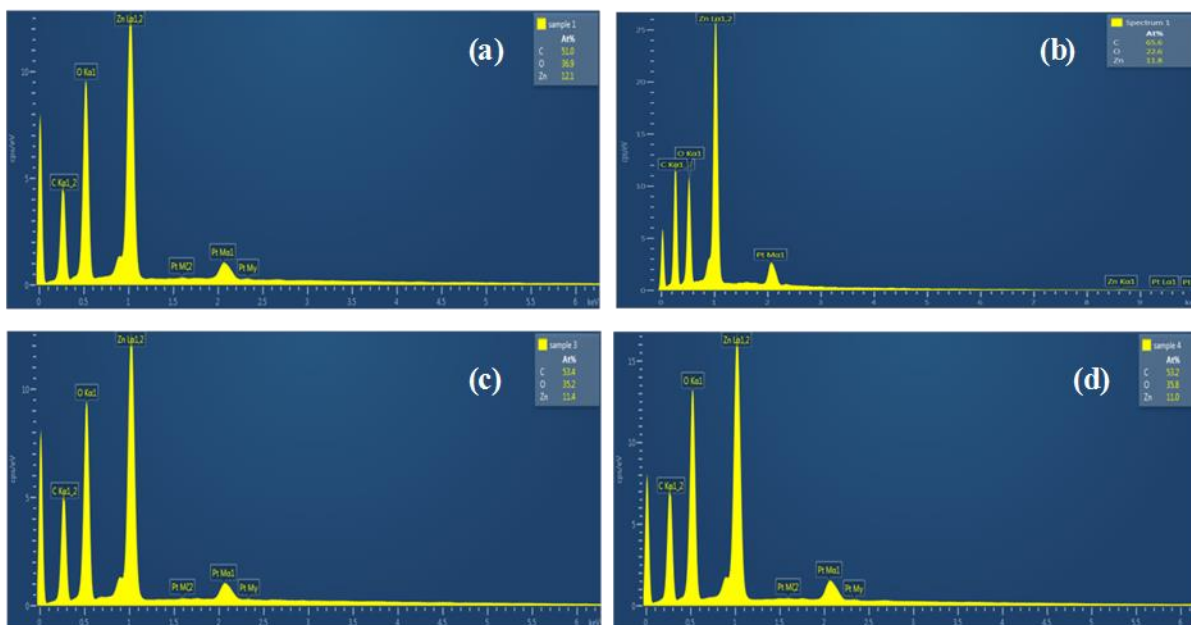


Figure 52. EDS spectra of ZnO nanorods coated cotton fabrics at various concentration of Zinc nitrate hexahydrate/HMTA for 10 min: (a) 25 mM, (b) 50 mM, (c) 75 mM, and (d) 100 mM

Table 9. Elemental composition of ZnO nanorods coated cotton fabrics

Element (wt. %)	Sample treated with 25 mM	Sample treated with 50 mM	Sample treated with 75 mM	Sample treated with 100 mM
C	30.71	41.09	32.88	33.11
O	29.57	18.86	28.88	29.65
Zn	39.73	40.05	38.24	37.25

5.3.4. XRD analysis

The ZnO nanorods coated cotton fabric samples exhibited typical diffraction peaks of ZnO at 2θ : 37.0, 40.2, 42.3, 55.8, 66.8, 74.5, 79.9, 80.9 and 82.3 which correspond to the (100), (002), (101), (102), (110), (103), (200), (112), (201) planes of ZnO (Figure 53). All the observed peaks represent the hexagonal wurtzite structure of ZnO nanorods. No extraordinary diffraction peaks were observed in the XRD patterns and three sharp peaks confirmed the presence of highly pure and crystalline nature of ZnO nanorods on the cotton fiber surfaces [135, 145].

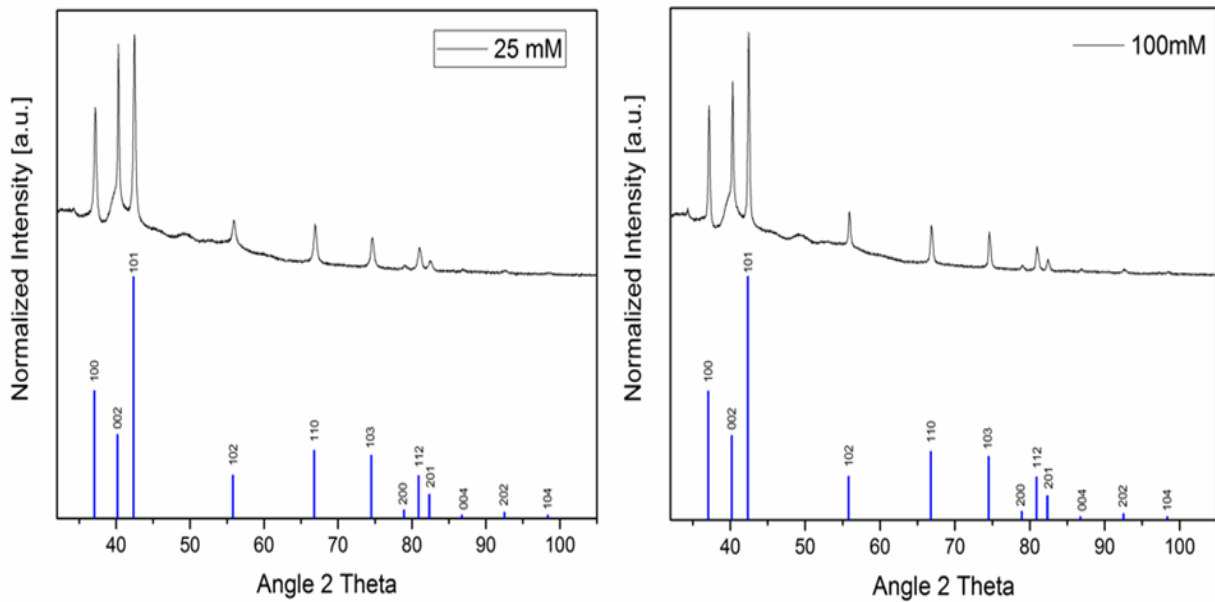


Figure 53. XRD patterns of the ZnO nanorods grown at 25 mM and 100 mM concentration of zinc nitrate hexahydrate/HMTA. All peaks are indexed according to ICDD Card No. 01-083-

6338

5.3.5. Topography and roughness analysis

Figure 54 shows the AFM images and surface profiles of the grown nanorods on cotton fabric surfaces at different level of concentrations (i.e., 25 mM to 100 mM). A uniform and continuous pattern of grown ZnO nanorods can be seen for all the samples. AFM analysis shows that each sample has different roughness and topographic patterns. The growth patterns and orientations of the nanorods changed due to different crystal growth under various concentration

of zinc nitrate hexahydrate. The average roughness (Ra) measured for samples treated with various concentration of zinc nitrate hexahydrate are given in Table 10. The sample coated with 25 mM of concentration exhibited minimum roughness 26.2 nm. The surface roughness of the samples was ranged from 26.2 to 61.3 nm for various concentration of zinc nitrate hexahydrate (25 mM to 100 mM). The sample coated with 100 mM of concentration shows very dense growth of nanorods due to which the tip of AFM cannot go between the nanorods hence the topography is different. The AFM images of sample coated with 25 mM showed the presence of nanorods at a certain distance from each other that allow the movement of micro tip between the nanorods. At less concentration, the distance between the consecutive nanorods increased but a uniform growth pattern was observed. While at high concentration, dense packing of nanorods was observed. The roughness is greatly influenced by the size and growth direction of the nanorods. In previous study, the average roughness was found to increase with increase of nanorods diameter [146]. It has been reported that the roughness depends on the alignment and orientation of the grown nanorods [147]. Similar amount of surface roughness were reported for ZnO nanorods grown superhydrophobic surfaces [148]. It can be concluded that morphology and size of the grown nanorods highly affect the topography and roughness of the surface.

Table 10. Analysis of surface roughness

Zn(NO ₃) ₂ · 6H ₂ O Concentration (mM/L)	Roughness (nm)
25	26.2 (±3.5)
50	36.6 (±2.3)
75	61.3 (±7.1)
100	45.1 (±5.2)

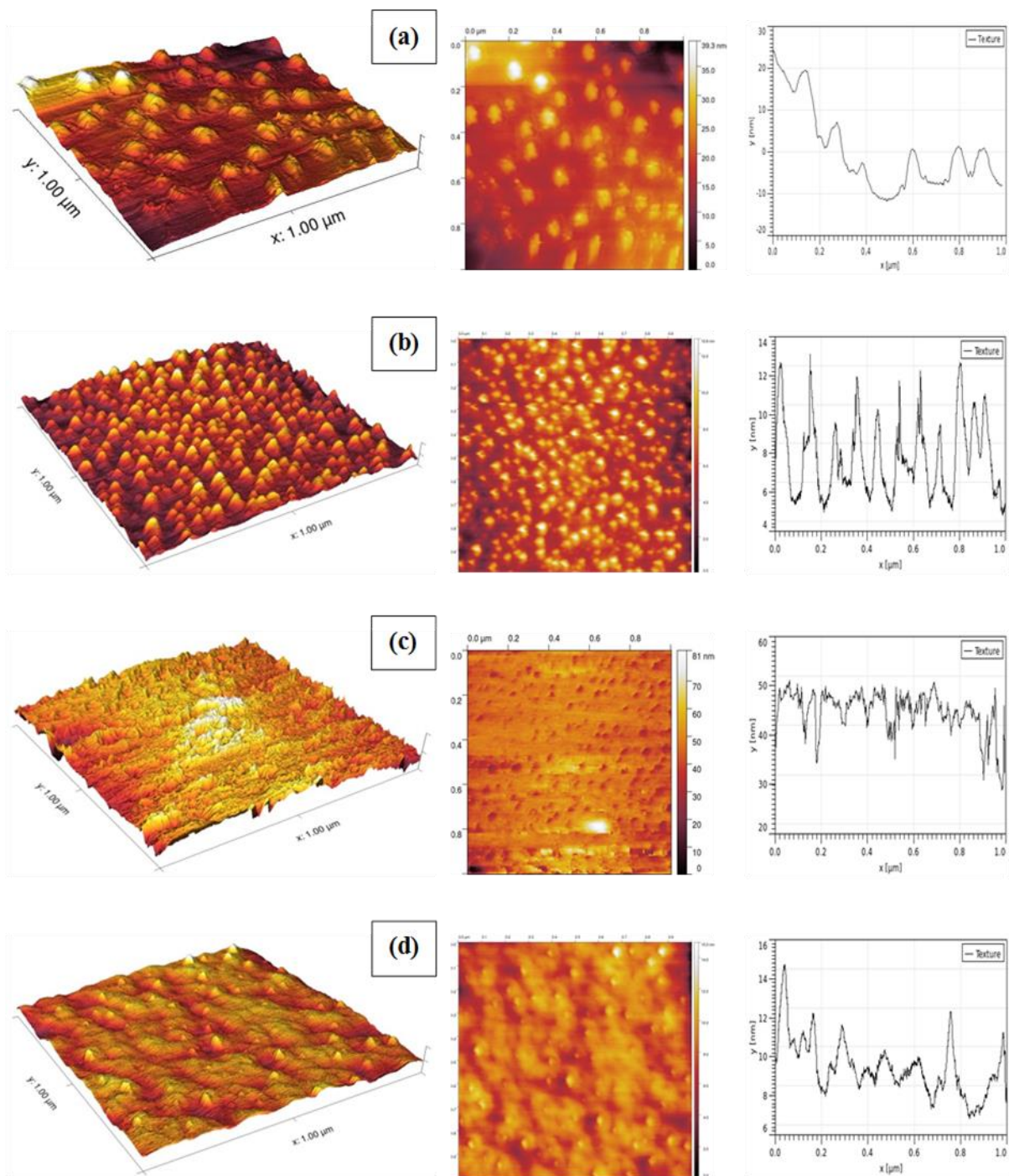


Figure 54. AFM images and surface profiles of ZnO nanorods grown fabrics at various concentration of zinc nitrate hexahydrate, (a) 25 mM, (b) 50 mM, (c) 75 mM, and (d) 100 mM

5.3.6. Superhydrophobic properties of ZnO-OTMS coated cotton fabrics

The static water contact angle and roll-off angle are the most widely used wetting measurements. These measurements were made to study the effect of zinc nitrate hexahydrate concentration on the wettability of the ZnO-OTMS coated cotton fabric (Figure 55). The pristine cotton fabric completely absorbed water droplet due to presence of hydroxyl groups in the structure. Without any deposition of ZnO nanorods and with only coating of OTMS on cotton fabric, the water contact angle and roll off-angle were measured around 130.1° and 19° respectively. This shows the hydrophobic behavior of cotton fabrics after OTMS coating alone. But this surface was not able to perform physical self-cleaning action as the water droplets were difficult to roll off showing the strong adhesion between the water droplet and the coated fiber surface. The increase in contact angle and decrease in roll-off angle was observed, when cotton fabric surface was deposited with ZnO nanorods and subsequent treatment of OTMS.

In our study, the nanorods coated surfaces were found to be superhydrophobic with WCA of greater than 150° . The maximum WCA of 170.2° and minimum roll off angle of 1° was found for 25 mM of zinc nitrate hexahydrate concentration. The WCAs of 164.6° , 161.4° and 158.8° were achieved for 50 mM, 75 mM, and 100 mM of concentrations, respectively. The increase of zinc nitrate hexahydrate concentration was resulted into little decrease of WCA that could be possibly due to increase in diameter and dense packing of the grown nanorods. We noted that the surface roughness in combination with the particle size is important factor for higher water contact angles. In all cases, the coated surfaces were found to be superhydrophobic. Although the sample coated with 25 mM of concentration ($D=35$ nm, $L=190$ nm) did not provide the highest surface roughness, but the size and orientation of the nanorods enhanced the fraction of the air pocket at the composite interface which is in accordance with the Cassie-Baxter state. Therefore, optimum size of nanorods can be grown to achieve the desire superhydrophobicity. These results demonstrate that the size, shape, and orientation of the nanoparticles also play an important role when designing suitable superhydrophobic surfaces [149, 150].

Finally, the development of superhydrophobic surfaces can be achieved when cotton fiber surface is decorated with nanorods and subsequently modified with OTMS. The surface roughness produced by nanorods is responsible for the formation of lotus effect. This

phenomenon can be related to the formation of unique micro/nano structural surface providing necessary roughness and improving the surface hydrophobicity.

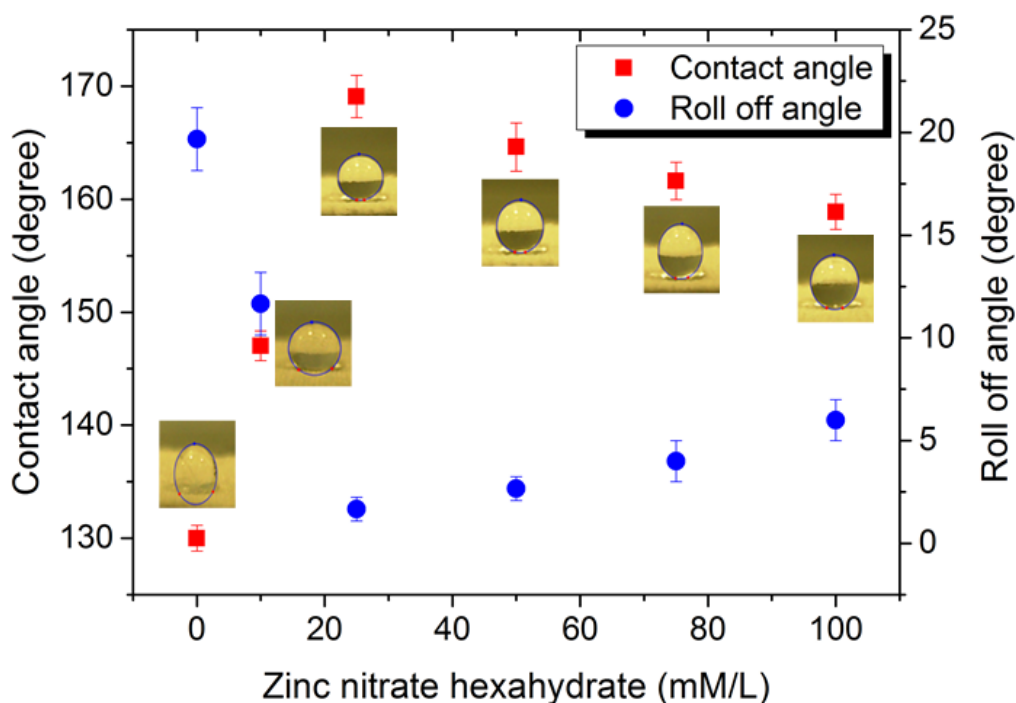


Figure 55. Effect of zinc nitrate hexahydrate concentration on water contact angle

Generally, the surface wettability is explained by three important theories. These commonly known theories are Young model, Wenzel model and Cassie–Baxter model. The Young equation assumes that the surface is totally smooth and the static contact angle is determined by the interfacial energies between the solid–vapor phase, solid–liquid phase, and liquid–vapor phase. However, in reality most of the solid surfaces are rough and this has put a limitation on Young's model in explaining the surface wettability behavior [18]. In previous studies, the surface wetting behavior of liquids can be explained either by Wenzel state or Cassie–Baxter state [47]. In Wenzel state, a liquid impregnates the rough surface to form a completely wetted contact with the surface, whereas in the Cassie–Baxter state the liquid does not completely fill up the rough surface due to the presence of air pockets. Therefore, the superhydrophobicity of the ZnO-OTMS coated cotton fabrics can be believed in Cassie–Baxter state where spherical water drop cannot penetrate entire fabric surface due to large amount of air

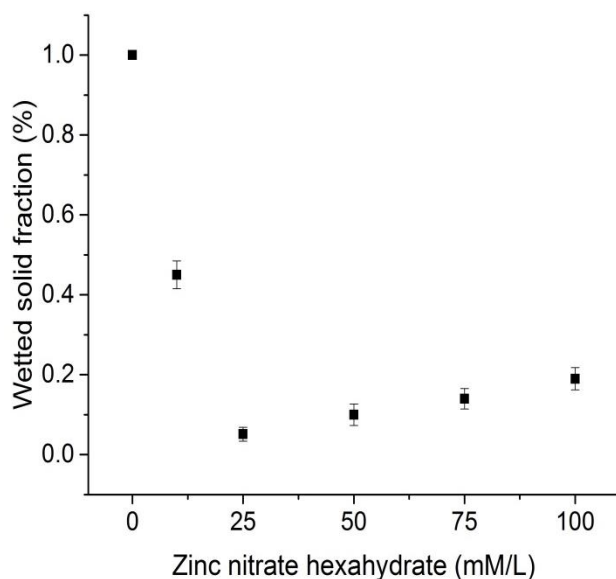
trapped in the structure [70]. Moreover, the Cassie–Baxter state of ZnO-OTMS coated cotton fabric was verified by immersing the coated fabrics into water. The formation of plastron layer due to trapped air between the water and the superhydrophobic fabric and thus showed the silver mirror-like bright and reflective surface [112]. The Cassie–Baxter model can be used to estimate the wetted solid fraction that is area fraction of a water droplet (f) in contact with a fabric surface. Where, θ^* is the apparent contact angle is observed on a rough surface decorated with nanorods and θ is the equilibrium contact angle obtained on an untreated smooth surface. Figure 56(a) shows that the wetted solid fraction was decreased to lowest value for 25 mM of zinc nitrate hexahydrate treated sample and further increase of concentration was resulted into slightly increase of wetted solid fraction, which could be due to increase in size and shape of ZnO nanorods. The significant increase of unwetted fraction of the air pocket was observed for the 25 mM to 100 mM of zinc nitrate hexahydrate concentration except sample treated with 10 mM of concentration. The maximum unwetted fraction of the air pocket of 95% was found for 25 mM of zinc nitrate hexahydrate. These results further confirmed that the continuous and homogenous layer of nanorods constructed a rough surface for the air storage to resist the penetration of liquid.

Moreover, the Young–Duprè equation was used to describe the movement of liquid droplets on highly hydrophobic surfaces by calculation of work of adhesion (W_{ad}) [53]. The work of adhesion was found to reduce with increase in surface density and the change in morphology of the ZnO nanorods (see Figure 56b). The untreated cotton fabric coated with OTMS alone depicted the work of adhesion around 26.01 mN/m, whereas the work of adhesion ranged from 11.7 to 1.34 mN/m for ZnO-OTMS coated cotton fabrics at concentrations of zinc nitrate hexahydrate from 10mM to 100 mM. The fabric surface decorated with nanorods at 25 mM of zinc nitrate hexahydrate concentration exhibited least work of adhesion or smallest work required for the movement of the water drop.

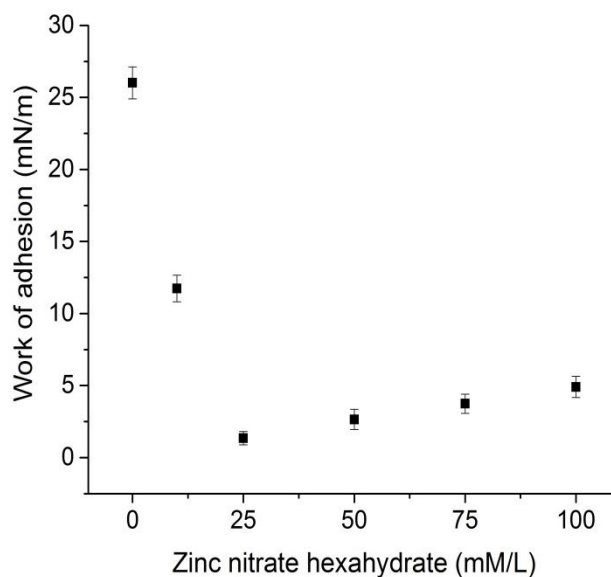
By using the values of work of adhesion W_{ad} and equilibrium distance d , the force of attraction F_e can be calculated. The distance between the molecular centers of a liquid can be estimated from the specific gravity and molecular weight of the liquids. Therefore, the equilibrium distance of 3.1 Å can be used for calculation of distance between the molecular

centers of water. Interfacial tension of liquid and natural characteristics of the substrate, such as surface geometry or porosity, polarity, and chemical composition, affect the absorption of solid–liquid interface [111].

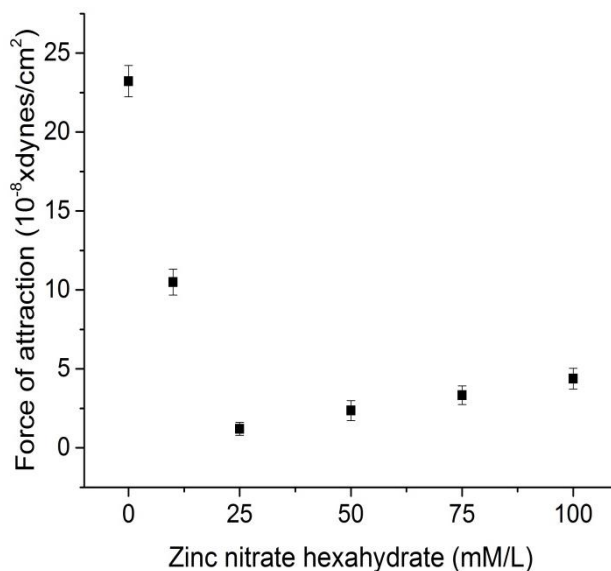
The force of attraction was found to increase with increased size of ZnO nanorods on the surface of cotton fabric (Figure 56c). The cotton fabric coated with OTMS alone, the force of attraction was found around $23.22 (10^{-8} \text{dyne/cm}^2)$. However, the force of attraction was measured from 10.49 to $1.19 (10^{-8} \text{dyne/cm}^2)$ after the decoration of ZnO nanorods at various zinc nitrate hexahydrate concentrations of 10mM to 100 mM. The least force of attraction was found around $1.19 (10^{-8} \text{dyne/cm}^2)$ for the fabric decorated with ZnO nanorods at 25 mM of zinc nitrate hexahydrate concentration. These results showed that less force required for movements of water drops on the fabric surface coated with ZnO nanorods and OTMS.



(a). Cassie-Baxter prediction



(b). Work of adhesion



(c). Force of attraction

Figure 56. Analysis of superhydrophobicity of ZnO-OTMS coated cotton fabrics

5.3.7. Durability of ZnO-OTMS coated cotton fabrics

The durability of ZnO-OTMS coated cotton fabrics against mechanical abrasion, laundering, chemical and UV action was evaluated and contact angle results after exposure are shown in Figure 57. The contact angle of the ZnO-OTMS coated cotton fabrics was studied after 20 cycles of sand paper abrasion. All the coated samples showed reduction in water contact angle, but the WCAs were still higher than 150° except sample coated with 10 mM of zinc nitrate hexahydrate. The sample coated with 25 mM of zinc nitrate hexahydrate showed greater reduction in WCA and exhibited WCA of 156.5° after mechanical abrasions. The sample with 50 mM of concentration exhibited good stability after mechanical actions with a WCA of 158.4° . The samples deposited with nanorods showed acceptable reduction in water contact angle after five laundering cycles. However, the sample coated with 50mM maintained highest water contact angle of 160.2° . These results shows the robustness and durability of the nanorods grown samples against mechanical and friction forces [8].

It has been observed that the samples showed acceptable reduction of WCAs and retained their hydrophobicity after exposure to chemical environment. Reduction of WCA after alkali exposure was greater than acidic environment. The durability of ZnO-OTMS coated cotton fabrics against ultraviolet rays was also evaluated and it was seen that the contact angle of the ZnO-OTMS coated fabrics was not affected after exposure to ultraviolet rays. Thus, it is suitable to use under solar irradiations.

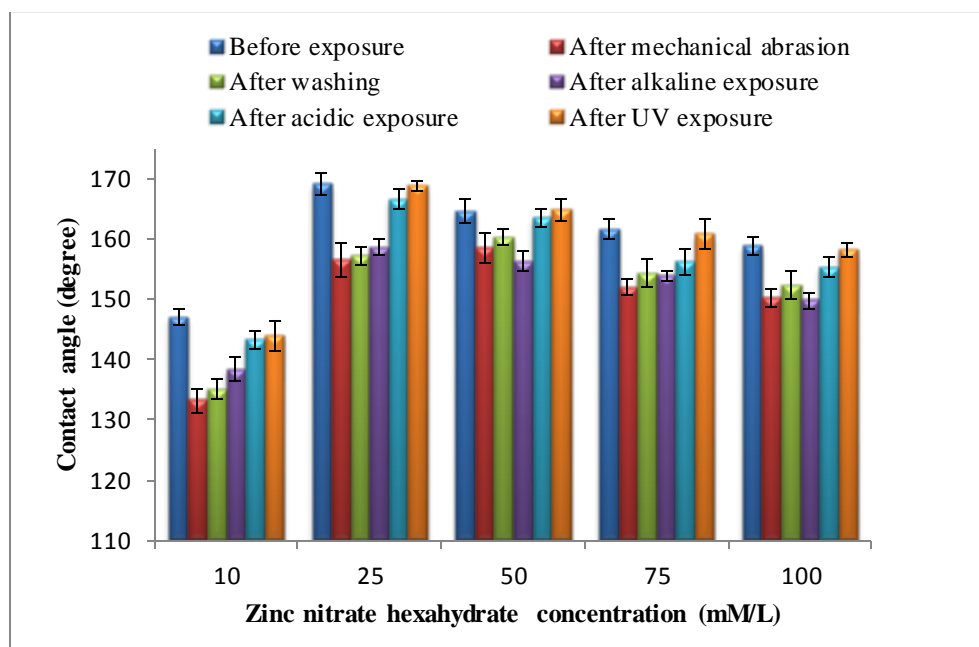


Figure 57. Durability of ZnO-OTMS coated cotton fabrics

5.3.8. Physical self-cleaning properties of ZnO-OTMS coated cotton fabrics

To demonstrate the self-cleaning property of the superhydrophobic ZnO-OTMS coated cotton fabrics methyl orange dye was used as a contaminant. The superhydrophobic fabric was fixed on a transparent glass slides that leans against a round dish with a small angle of inclination (Figure 58). When the water droplets were dropped on the contaminated fabric, it rolled over the surface and maintained the spherical shape. During the sliding process of water droplets, the dye particles were immediately picked up and taken away leaving behind a clear surface. Digital images were obtained at different moment. This behavior was attributed to the creation of lotus effect by high water surface tension and low surface energy of coated fabrics [128].

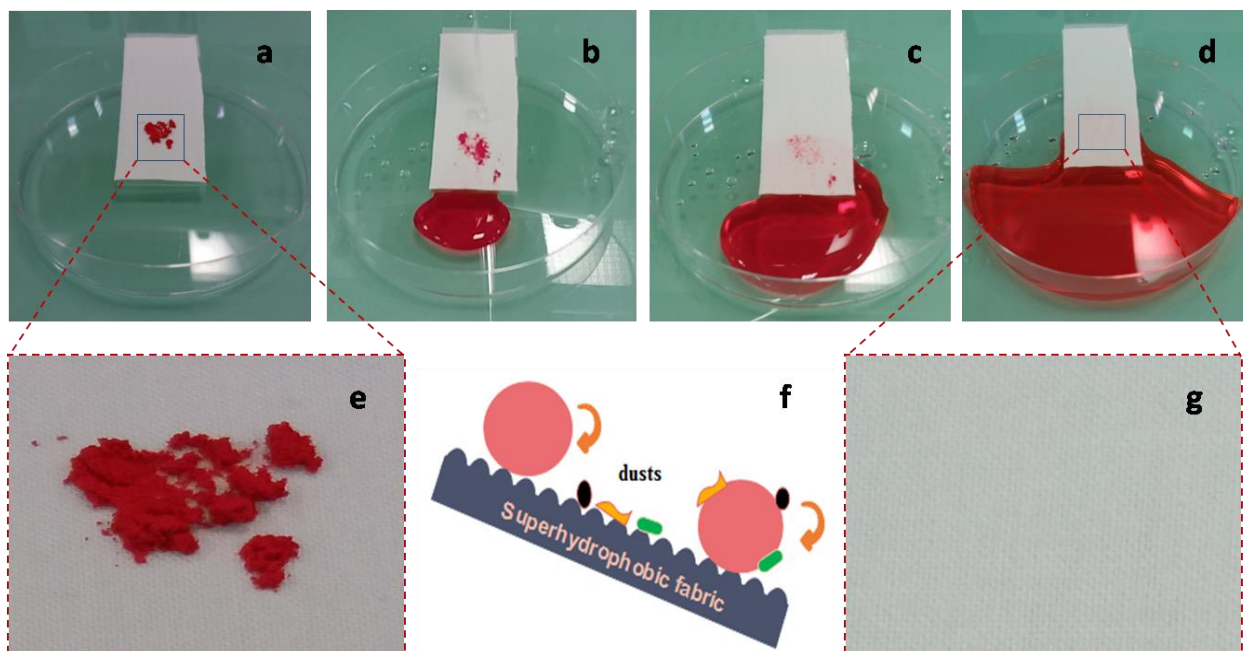
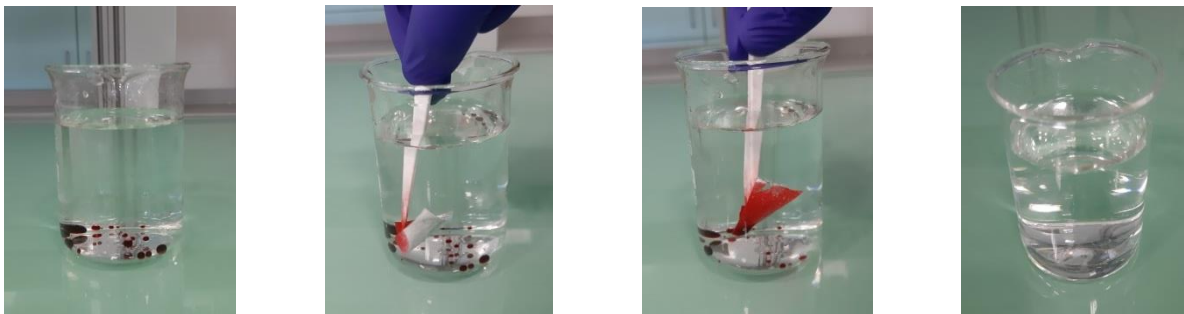


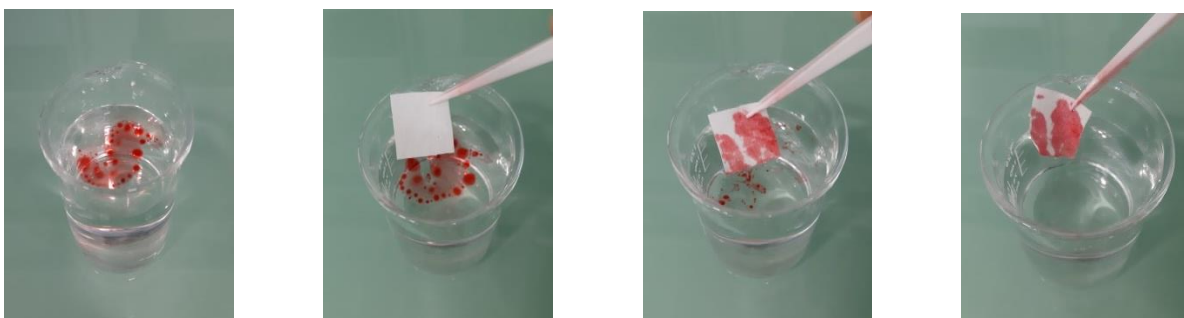
Figure 58. The self-cleaning process of ZnO-OTMS coated cotton fabric (a–d). The high magnify optical images of ZnO-OTMS coated cotton fabric before self-cleaning (e), and after self-cleaning (g), and corresponding schematic illustration of the self-cleaning process (f)

5.3.9. Oil in water removal performance of ZnO-OTMS coated cotton fabrics

Based on superhydrophobic nature of the ZnO-OTMS coated cotton fabrics, the coated samples were further tested for their oil sorption capacity. The ZnO-OTMS coated fabrics can be used for removal of oil from water/oil mixture due to their special wettability. The underwater oil removal was observed by using chloroform, whereas toluene was used to observe the oil removal performance from the surface of water. A small amount of toluene and chloroform was dyed with Oil Red O for better experimental observation. The chloroform due to its high density reached to the bottom of the water layer (Figure 59a) and toluene was floating on the water surface due its low density (see Figure 59b). A piece of ZnO-OTMS coated cotton fabric was immersed into the water and oil was quickly absorbed by the superhydrophobic fabric without leaving any traces of oil in the water. The coated fabric becomes red which shows the presence of red oils. This improvement of oil retention ability could be related to enhanced stability of capillary pressure to prevent the rolling of absorbed oil on the coated fiber surface by creation of rough surfaces by ZnO nanorods [114].



(a). Photographs of chloroform removal from underwater surface



(b). Photographs of toluene removal from top water surface



(c). Photographs of oil/water separation experiment

Figure 59. Oil in water removal performance of ZnO-OTMS coated cotton fabrics

For further quantitative estimation of the oil separation efficiency of ZnO-OTMS coated cotton fabrics were carried out in separate experiments (see Figure 59c). Four model oils with different densities that include chloroform, n-hexane, petro ether and toluene were used to estimate the oil separation efficiency. The mixture of oil (dyed with Oil Red O) and water was poured onto the ZnO-OTMS coated cotton fabric, the oil was quickly passed through the superhydrophobic fabric into the small beaker and leaved water on the top of the superhydrophobic fabric surface. The accumulated water on the top of the superhydrophobic fabric was then decanted into the big beaker. The separation efficiency of 99%, 98%, 98% and 96% was obtained for chloroform/water, n-hexane/water, petro ether/water and toluene/water, respectively. Additionally, the reusability of superhydrophobic ZnO-OTMS coated cotton fabric was investigated by evaluating the separation efficiency for chloroform/water and toluene/water after five recycles of oil/water separation. The oil sorption capacities of the coated fabric reduced slightly during the whole cycles. After five cycles of reusability of coated fabrics, the separation efficiency was ranged from 99% to 96% for chloroform and 96% to 92% for toluene after 5 cycles. This small decrease of oil sorption capacity can be attributed to the presence of residual oils inside the structure of coated fabrics [117].

CHAPTER 6

6. CONCLUSIONS AND FUTURE WORK

6.1. Conclusions

The following conclusions have been drawn from each study.

In first study, fly ash particles were utilized to create superhydrophobic and UV protective cotton fabrics. The surface of fly ash was mechanically activated by ball milling process. The unmilled fly ash with particle diameter of 3547 nm was converted to smaller particles of below 1000 nm diameter after 30 min dry pulverization. The milled fly ash particles were then coated on cotton fabric surfaces at 1, 2 and 3 wt% concentration. Due to presence of hydroxyl groups, the fly ash particles showed better adhesion with cotton fiber surfaces. When the utility of fly ash coated fabrics was investigated for UV protection properties, maximum UV blocking was observed in case of cotton fabric coated with 3 wt% fly ash. The untreated cotton fabric showed a low UPF of 9.49, however all the cotton fabrics decorated with fly ash particles exhibited large increase in UPF values due to their high refractive index and presence of metal oxide constituents. The topography of fly ash coated cotton fabric was characterized using AFM and surface roughness was found to increase with increase in fly ash concentration. In order to achieve superhydrophobic properties, the non-fluorinated silane was applied on previous fly ash coated fabrics. The water contact angle was measured around 130° for coated fabrics of OTMS alone. However, when fly ash concentration of 1, 2 and 3 wt % was applied; the contact angle was improved to 143° , 147° and 153° , respectively. The enhancement in water repellency was attributed to the formation of unique two-tier structural surface combined with the microscaled cotton fibers and the nanoscaled fly ash particles. Based on Cassie-Baxter theories, 43%, 55% and 67% increase in the unwetted fraction of the air pocket trapped in the interspaces among the fly ash particles was estimated for 1, 2 and 3 wt% of fly ash particles respectively. Further, 14.58 to 8.28 mN/m ranges for work of adhesion and 13.13 to 7.45 dyne/cm² ranges for force of attraction were estimated with increased density of fly ash coating. When the utility of fly ash-OTMS coated cotton fabrics was investigated for oil in water separation performance, 98%,

96%, 97% and 95% of separation efficiency was obtained for toluene/water, n-hexane/water, chloroform/water and petro ether/water, respectively. This showed the ability of fly ash coated fabrics for versatile separation of oil/water mixtures under various conditions (e.g. floating oil layer, underwater oil droplet or oil/water mixtures).

In second study, the amount of TTIP was found to have a great effect on the growth and structure of TiO₂ nanoflowers. The assembly of TiO₂ particles in flower shape was not found at low dose of TTIP. However, the amount and the size of TiO₂ flower structures were greatly increased by further increase in TTIP dose from 1 mL to 2.0 mL. The maximum roughness value (Ra) of 78.8 nm was calculated for the flower-like TiO₂ nanoparticles coated polyester. The increase in contact angle and reduction in roll off angle was observed with the increase of TTIP dose, where maximum static contact angle of 160.1° and minimum roll off angle of 3° was found for 2 mL TTIP dose. Furthermore, the formation of discontinuous, unstable, and contorted air/solid/liquid contact line was found as the contact angle hysteresis reduced from 9° to 3° with increase in TTIP dose. From Cassie–Baxter state superhydrophobicity, 58%, 78% and 83% increase in unwetted fraction of the air pocket was calculated for 1 mL, 1.5 mL and 2 mL TTIP dose respectively. Moreover, the reduction in work of adhesion (11.4 to 4.34 mN/m) and force of attraction (10.27 to 3.9 10⁻⁸ dyne/cm²) indicated less force required for movements of water drops on the polyester fabric surface decorated with more number of TiO₂ flowers. The surface of TiO₂-OTMS coated polyester fibers also showed the promising results to maintain the superhydrophobic durability against mechanical abrasion, laundering, chemical and UV action. When the coated fabrics were examined for physical self-cleaning, the methyl orange dye particles were immediately picked up and taken away by the rolling water droplets. The coated fabrics also exhibited the chemical self-cleaning action as the stains of methyl orange dye disappeared mostly within 3 h and the samples became approximately white after 4 h.

In third study, a novel microwave hydrothermal method was used to grow aligned ZnO nanorods on cotton fabrics. It was found that the salt concentration, reaction time and microwave irradiation power have great effect on the size and growth of ZnO nanorods. The growth of ZnO nanorods were not found at 10 mM of zinc nitrate hexahydrate. However, the growth and the size of ZnO nanorods were greatly increased by increase in zinc nitrate hexahydrate concentration

from 25mM to 100 mM. Similarly, size of ZnO nanorods was increased when reaction time and microwave power was increased from 10 min to 30 min and 360 W to 480 W, respectively. Moreover, the non-fluorinated silane (OTMS) was applied on the ZnO nanorods coated fabrics to incorporate superhydrophobic properties. The AFM analysis showed that the nano-roughness changed with the change in concentration of zinc nitrate hexahydrate. The maximum water contact angle of 170.2° and minimum roll off angle of 1° was found for 25 mM of zinc nitrate hexahydrate concentration. The slight decrease in contact angle and increase in roll of angle was observed with the increase of zinc nitrate hexahydrate concentration. Furthermore, from Cassie–Baxter state the maximum unwetted fraction of the air pocket of 95% was found for 25 mM of zinc nitrate hexahydrate. Moreover, the reduction in work of adhesion and force of attraction also indicated less force required for movements of water drops on the ZnO nanorods and OTMS coated fabric. The ZnO-OTMS coated cotton fabrics also showed the promising results to maintain the superhydrophobic durability against mechanical abrasion, laundering, chemical and UV action. The methyl orange dye was quickly picked up by rolling water droplets during physical self-cleaning of the ZnO-OTMS coated cotton fabrics. The ZnO-OTMS coated cotton fabrics also showed great oil/water separation performance when investigated for mixture of chloroform/water, n-hexane/water, petro ether/water and toluene/water, respectively.

6.2. Future work

- In future, durable superhydrophobic surfaces can be developed through single step approach by using fly ash, TiO_2 and ZnO particles.
- Further investigations are needed in future on precisely controlling surface roughness and structure in both small and large scales.
- New theoretical model also needs to be developed apart from Cassie and Wenzel to gain deep insight regarding the mechanism of superhydrophobicity.
- More work is needed to investigate how to enhance the durability of superhydrophobic surfaces.
- The future trend is to develop durable self-healing superhydrophobic surfaces that can automatically restore original characteristics after having been damaged.

REFERENCES

- [1] V. Pandiyarasan, S. Suhasini, J. Archana, M. Navaneethan, A. Majumdar, Y. Hayakawa, and H. Ikeda, "Fabrication of hierarchical ZnO nanostructures on cotton fabric for wearable device applications," *Appl. Surf. Sci.*, vol. 418, pp. 352–361, 2017.
- [2] N. Valipour M., F. C. Birjandi, and J. Sargolzaei, "Super-non-wettable surfaces: A review," *Colloids Surfaces A Physicochem. Eng. Asp.*, vol. 448, no. 1, pp. 93–106, 2014.
- [3] M. Zhang and C. Wang, "Fabrication of cotton fabric with superhydrophobicity and flame retardancy," *Carbohydr. Polym.*, vol. 96, no. 2, pp. 396–402, 2013.
- [4] H. Li, J. Yang, P. Li, T. Lan, and L. Peng, "A facile method for preparation superhydrophobic paper with enhanced physical strength and moisture-proofing property," *Carbohydr. Polym.*, vol. 160, pp. 9–17, 2017.
- [5] M. Zhang, C. Wang, S. Wang, and J. Li, "Fabrication of superhydrophobic cotton textiles for water-oil separation based on drop-coating route," *Carbohydr. Polym.*, vol. 97, no. 1, pp. 59–64, 2013.
- [6] A. Esfandiari, "PPy covered cellulosic and protein fibres using novel covering methods to improve the electrical property," *World Appl. Sci. J.*, vol. 3, no. 3, pp. 470–475, 2008.
- [7] M.-E. Y. Amirhossein Esfandiari, Hossein Nazokdast, AboSaeed Rashidi, "Review of Polymer-Organoclay Nanocomposites," *J. Appl. Sci.*, vol. 8, no. 3, pp. 545–561, 2008.
- [8] S. Li, J. Huang, M. Ge, C. Cao, S. Deng, S. Zhang, G. Chen, K. Zhang, S. S. Al-Deyab, and Y. Lai, "Robust Flower-Like TiO₂@Cotton Fabrics with Special Wettability for Effective Self-Cleaning and Versatile Oil/Water Separation," *Adv. Mater. Interfaces*, vol. 2, no. 14, p. 1500220, 2015.
- [9] Z. Du, C. Cheng, L. Tan, J. Lan, S. Jiang, L. Zhao, and R. Guo, "Enhanced photocatalytic activity of Bi₂WO₆/TiO₂ composite coated polyester fabric under visible light irradiation," *Appl. Surf. Sci.*, vol. 435, pp. 626–634, 2018.
- [10] M. Z. Khan, V. Baheti, J. Militky, A. Ali, and M. Vikova, "Superhydrophobicity, UV protection and oil/water separation properties of fly ash/Trimethoxy(octadecyl)silane coated cotton fabrics," *Carbohydr. Polym.*, vol. 202, no. August, pp. 571–580, 2018.

- [11] M. Z. Khan, V. Baheti, M. Ashraf, T. Hussain, A. Ali, A. Javid, and A. Rehman, "Development of UV Protective, Superhydrophobic and Antibacterial Textiles Using ZnO and TiO₂ Nanoparticles," *Fibers Polym.*, vol. 19, no. 8, pp. 1647–1654, 2018.
- [12] L. Yao and J. He, "Recent progress in antireflection and self-cleaning technology - From surface engineering to functional surfaces," *Prog. Mater. Sci.*, vol. 61, pp. 94–143, 2014.
- [13] S. Afzal, W. A. Daoud, and S. J. Langford, "Superhydrophobic and photocatalytic self-cleaning cotton," *J. Mater. Chem. A*, vol. 2, no. 42, pp. 18005–18011, 2014.
- [14] S. Das, S. Kumar, S. K. Samal, S. Mohanty, and S. K. Nayak, "A Review on Superhydrophobic Polymer Nanocoatings: Recent Development and Applications," *Ind. Eng. Chem. Res.*, vol. 57, no. 8, pp. 2727–2745, 2018.
- [15] Z. G. and W. Liu, "Biomimic from the Superhydrophobic Plant Leaves in Nature: Binary Structure and Unitary Structure," *Plant Sci.*, pp. 1103–1112, 2007.
- [16] K. Koch, B. Bhushan, and W. Barthlott, "Multifunctional surface structures of plants: An inspiration for biomimetics," *Prog. Mater. Sci.*, vol. 54, no. 2, pp. 137–178, 2009.
- [17] W. Barthlott and C. Neinhuis, "Purity of the sacred lotus, or escape from contamination in biological surfaces," *Planta*, vol. 202, no. 1, pp. 1–8, 1997.
- [18] S. Li, J. Huang, Z. Chen, G. Chen, and Y. Lai, "A review on special wettability textiles: theoretical models, fabrication technologies and multifunctional applications," *J. Mater. Chem. A*, vol. 5, no. 1, pp. 31–55, 2017.
- [19] A. M. Rather, N. Jana, S. Begum, H. K. Srivastava, and U. Manna, "Exceptional control on physical properties of a polymeric material through alcoholic solvent-mediated environment-friendly Michael addition reaction," *Green Chem.*, vol. 19, no. 19, pp. 4527–4532, 2017.
- [20] J. Ju, X. Yao, X. Hou, Q. Liu, Y. S. Zhang, and A. Khademhosseini, "A highly stretchable and robust non-fluorinated superhydrophobic surface," *J. Mater. Chem. A*, vol. 5, no. 31, pp. 16273–16280, 2017.
- [21] M. Zhang, J. Li, D. Zang, Y. Lu, Z. Gao, J. Shi, and C. Wang, "Preparation and characterization of cotton fabric with potential use in UV resistance and oil reclaim," *Carbohydr. Polym.*, vol. 137, pp. 264–270, 2016.

- [22] A. Panda, P. Varshney, S. S. Mohapatra, and A. Kumar, "Development of liquid repellent coating on cotton fabric by simple binary silanization with excellent self-cleaning and oil-water separation properties," *Carbohydr. Polym.*, vol. 181, no. November 2017, pp. 1052–1060, 2018.
- [23] G. Broasca, G. Borcia, N. Dumitrascu, and N. Vrinceanu, "Characterization of ZnO coated polyester fabrics for UV protection," *Appl. Surf. Sci.*, vol. 279, pp. 272–278, 2013.
- [24] B. Xu, J. Ding, L. Feng, Y. Ding, F. Ge, and Z. Cai, "Self-cleaning cotton fabrics via combination of photocatalytic TiO₂ and superhydrophobic SiO₂," *Surf. Coatings Technol.*, vol. 262, pp. 70–76, 2015.
- [25] H. Song, T. Chen, Y. L. Sun, X. Q. Zhang, and X. H. Jia, "Controlled synthesis of porous flower-like TiO₂ nanostructure with enhanced photocatalytic activity," *Ceram. Int.*, vol. 40, no. 7 PART B, pp. 11015–11022, 2014.
- [26] A. Esfandiari, E. Firouzi-Pouyaei, and P. Aghaei-Meibodi, "Effect of enzymatic and mechanical treatment on combined desizing and bio-polishing of cotton fabrics," *J. Text. Inst.*, vol. 105, no. 11, pp. 1193–1202, 2014.
- [27] A. Sobczyk-Guzenda, H. Szymanowski, W. Jakubowski, A. Błasińska, J. Kowalski, and M. Gazicki-Lipman, "Morphology, photocleaning and water wetting properties of cotton fabrics, modified with titanium dioxide coatings synthesized with plasma enhanced chemical vapor deposition technique," *Surf. Coatings Technol.*, vol. 217, pp. 51–57, 2013.
- [28] S. Banerjee, D. D. Dionysiou, and S. C. Pillai, "Self-cleaning applications of TiO₂ by photo-induced hydrophilicity and photocatalysis," *Appl. Catal. B Environ.*, vol. 176–177, pp. 396–428, 2015.
- [29] S. Nishimoto and B. Bhushan, "Bioinspired self-cleaning surfaces with superhydrophobicity, superoleophobicity, and superhydrophilicity," *RSC Adv.*, vol. 3, no. 3, pp. 671–690, 2013.
- [30] S. Banerjee, S. C. Pillai, P. Falaras, K. E. O'shea, J. A. Byrne, and D. D. Dionysiou, "New insights into the mechanism of visible light photocatalysis," *J. Phys. Chem. Lett.*, vol. 5, no. 15, pp. 2543–2554, 2014.
- [31] W. Fu, G. Li, Y. Wang, S. Zeng, Z. Yan, J. Wang, S. Xin, L. Zhang, S. Wu, and Z. Zhang,

- “Facile formation of mesoporous structured mixed-phase (anatase/rutile) TiO₂ with enhanced visible light photocatalytic activity,” *Chem. Commun.*, vol. 54, no. 1, pp. 58–61, 2017.
- [32] J. T. Carneiro, T. J. Savenije, J. A. Moulijn, and G. Mul, “How phase composition influences optoelectronic and photocatalytic properties of TiO₂,” *J. Phys. Chem. C*, vol. 115, no. 5, pp. 2211–2217, 2011.
- [33] L. Oberli, D. Caruso, C. Hall, M. Fabretto, P. J. Murphy, and D. Evans, “Condensation and freezing of droplets on superhydrophobic surfaces,” *Adv. Colloid Interface Sci.*, vol. 210, pp. 47–57, 2014.
- [34] H. Liu, S. W. Gao, J. S. Cai, C. L. He, J. J. Mao, T. X. Zhu, Z. Chen, J. Y. Huang, K. Meng, K. Q. Zhang, S. S. Al-Deyab, and Y. K. Lai, “Recent progress in fabrication and applications of superhydrophobic coating on cellulose-based substrates,” *Materials (Basel)*, vol. 9, no. 3, pp. 1–37, 2016.
- [35] B. B. and W. B. K. Koch, “Diversity of Structure, Morphology and Wetting of Plant Surfaces,” *Soft Matter*, pp. 1943–1963, 2008.
- [36] T. Huhtamäki, X. Tian, J. T. Korhonen, and R. H. A. Ras, “Surface-wetting characterization using contact-angle measurements,” *Nat. Protoc.*, vol. 13, no. 7, pp. 1521–1538, 2018.
- [37] T. Darmanin and F. Guittard, “Superhydrophobic and superoleophobic properties in nature,” *Mater. Today*, vol. 18, no. 5, pp. 273–285, 2015.
- [38] D. R. and M. C.-C. X.-M. Li, “What Do We Need for a Superhydrophobic Surface? A Review on the Recent Progress in the Preparation of Superhydrophobic Surfaces,” *Chem. Soc. Rev.*, pp. 1350–1368, 2007.
- [39] R. Ramachandran and M. Nosonovsky, “Vibrations and Spatial Patterns Change Effective Wetting Properties of Superhydrophobic and Regular Membranes,” *Biomimetics*, vol. 1, no. 1, p. 4, 2016.
- [40] J. Jeevahan, M. Chandrasekaran, G. Britto Joseph, R. B. Durairaj, and G. Mageshwaran, “Superhydrophobic surfaces: a review on fundamentals, applications, and challenges,” *J. Coatings Technol. Res.*, vol. 15, no. 2, pp. 231–250, 2018.
- [41] B. Bhushan and Y. C. Jung, “Natural and biomimetic artificial surfaces for

- superhydrophobicity, self-cleaning, low adhesion, and drag reduction,” *Prog. Mater. Sci.*, vol. 56, no. 1, pp. 1–108, 2011.
- [42] J. T. Simpson, S. R. Hunter, and T. Aytug, “Superhydrophobic materials and coatings: A review,” *Reports Prog. Phys.*, vol. 78, no. 8, p. 86501, 2015.
- [43] C. M. Grozea, M. Rabnawaz, G. Liu, and G. Zhang, “Coating of silica particles by fluorinated diblock copolymers and use of the resultant silica for superamphiphobic surfaces,” *Polym. (United Kingdom)*, vol. 64, pp. 153–162, 2015.
- [44] B. Xu and Z. Cai, “Fabrication of a superhydrophobic ZnO nanorod array film on cotton fabrics via a wet chemical route and hydrophobic modification,” *Appl. Surf. Sci.*, vol. 254, no. 18, pp. 5899–5904, 2008.
- [45] M. Ashraf, F. Dumont, C. Campagne, P. Champagne, A. Perwuelz, A. Leriche, and N.-E. Chihib, “Development of Antibacterial Polyester Fabric by Growth of ZnO Nanorods,” *J. Eng. Fiber. Fabr.*, vol. 9, no. 1, pp. 15–22, 2014.
- [46] L. Zou, C. Lan, X. Li, S. Zhang, Y. Qiu, and Y. Ma, “Superhydrophobization of cotton fabric with multiwalled carbon nanotubes for durable electromagnetic interference shielding,” *Fibers Polym.*, vol. 16, no. 10, pp. 2158–2164, 2015.
- [47] M. Ashraf, C. Campagne, A. Perwuelz, P. Champagne, A. Leriche, and C. Courtois, “Development of superhydrophilic and superhydrophobic polyester fabric by growing Zinc Oxide nanorods,” *J. Colloid Interface Sci.*, vol. 394, no. 1, pp. 545–553, 2013.
- [48] D. Xiong, G. Liu, L. Hong, and E. J. S. Duncan, “Superamphiphobic diblock copolymer coatings,” *Chem. Mater.*, vol. 23, no. 19, pp. 4357–4366, 2011.
- [49] M. A. Shirgholami, M. Shateri Khalil-Abad, R. Khajavi, and M. E. Yazdanshenas, “Fabrication of superhydrophobic polymethylsilsesquioxane nanostructures on cotton textiles by a solution-immersion process,” *J. Colloid Interface Sci.*, vol. 359, no. 2, pp. 530–535, 2011.
- [50] H. Liu, S. W. Gao, J. S. Cai, C. L. He, J. J. Mao, T. X. Zhu, Z. Chen, J. Y. Huang, K. Meng, K. Q. Zhang, S. S. Al-Deyab, and Y. K. Lai, “Recent progress in fabrication and applications of superhydrophobic coating on cellulose-based substrates,” *Materials (Basel)*, vol. 9, no. 3, pp. 1–37, 2016.

- [51] E. Gustafsson, P. A. Larsson, and L. Wågberg, "Treatment of cellulose fibres with polyelectrolytes and wax colloids to create tailored highly hydrophobic fibrous networks," *Colloids Surfaces A Physicochem. Eng. Asp.*, vol. 414, pp. 415–421, 2012.
- [52] N. D. Boscher, V. Vaché, P. Carminati, P. Grysan, and P. Choquet, "A simple and scalable approach towards the preparation of superhydrophobic surfaces-importance of the surface roughness skewness," *J. Mater. Chem. A*, vol. 2, no. 16, pp. 5744–5750, 2014.
- [53] P. Aminayi and N. Abidi, "Imparting super hydro/oleophobic properties to cotton fabric by means of molecular and nanoparticles vapor deposition methods," *Appl. Surf. Sci.*, vol. 287, pp. 223–231, 2013.
- [54] Z. H. Zhang, H. J. Wang, Y. H. Liang, X. J. Li, L. Q. Ren, Z. Q. Cui, and C. Luo, "One-step fabrication of robust superhydrophobic and superoleophilic surfaces with self-cleaning and oil/water separation function," *Sci. Rep.*, vol. 8, no. 1, pp. 1–12, 2018.
- [55] Y. Lu, S. Sathasivam, J. Song, C. R. Crick, C. J. Carmalt, and I. P. Parkin, "Robust self-cleaning surfaces that function when exposed to either air or oil," *Science (80)*, vol. 347, no. 6226, pp. 1132–1135, 2015.
- [56] S. S. Latthe and A. V. Rao, "Superhydrophobic SiO₂ micro-particle coatings by spray method," *Surf. Coatings Technol.*, vol. 207, pp. 489–492, 2012.
- [57] C. W. Yao, D. Sebastian, I. Lian, Ö. Günaydin-Şen, R. Clarke, K. Clayton, C. Y. Chen, K. Kharel, Y. Chen, and Q. Li, "Corrosion resistance and durability of superhydrophobic copper surface in corrosive NaCl aqueous solution," *Coatings*, vol. 8, no. 2, 2018.
- [58] I. S. Bayer, "On the durability and wear resistance of transparent superhydrophobic coatings," *Coatings*, vol. 7, no. 1, 2017.
- [59] M. Joshi and a. Bhattacharyya, "Nanotechnology – a new route to high-performance functional textiles," *Text. Prog.*, vol. 43, no. 3, pp. 155–233, Sep. 2011.
- [60] M. Z. Khan, M. Ashraf, T. Hussain, A. Rehman, M. M. Malik, Z. A. Raza, Y. Nawab, and Q. Zia, "In situ Deposition of TiO₂ Nanoparticles on Polyester Fabric and Study of Its Functional Properties," *Fibers Polym.*, vol. 16, no. 5, pp. 1092–1097, 2015.
- [61] B. Haydon, *Nanomaterials and their Applications in Textiles – Domestic Standardization for Canadian Manufacturers and Importers and International Standardization*

Developments. 2012.

- [62] a Yadav, V. Prasad, a a Kathe, S. Raj, D. Yadav, C. Sundaramoorthy, and N. Vigneshwaran, "Functional finishing in cotton fabrics using zinc oxide nanoparticles," *Bull. Mater. Sci.*, vol. 29, no. 6, pp. 641–645, 2006.
- [63] Z. Mao, Q. Shi, L. Zhang, and H. Cao, "The formation and UV-blocking property of needle-shaped ZnO nanorod on cotton fabric," *Thin Solid Films*, vol. 517, no. 8, pp. 2681–2686, 2009.
- [64] A. Becheri, M. Durr, P. Lo Nostro, and P. Baglioni, "Synthesis and characterization of zinc oxide nanoparticles: Application to textiles as UV-absorbers," *J. Nanoparticle Res.*, vol. 10, no. 4, pp. 679–689, 2008.
- [65] I. Perelshtein, G. Applerot, N. Perkas, E. Wehrschetz-Sigl, A. Hasmann, G. M. Guebitz, and A. Gedanken, "Antibacterial properties of an in situ generated and simultaneously deposited nanocrystalline ZnO on fabrics," *ACS Appl. Mater. Interfaces*, vol. 1, no. 2, pp. 361–366, 2009.
- [66] H. Y. Lee, H. K. Park, Y. M. Lee, K. Kim, and S. B. Park, "A practical procedure for producing silver nanocoated fabric and its antibacterial evaluation for biomedical applications.," *Chem. Commun.*, no. 28, pp. 2959–2961, 2007.
- [67] S. Selvam, R. Rajiv Gandhi, J. Suresh, S. Gowri, S. Ravikumar, and M. Sundrarajan, "Antibacterial effect of novel synthesized sulfated -cyclodextrin crosslinked cotton fabric and its improved antibacterial activities with ZnO, TiO₂ and Ag nanoparticles coating," *Int. J. Pharm.*, vol. 434, no. 1–2, pp. 366–374, 2012.
- [68] R. Dastjerdi and M. Montazer, "A review on the application of inorganic nano-structured materials in the modification of textiles: focus on anti-microbial properties.," *Colloids Surf. B. Biointerfaces*, vol. 79, no. 1, pp. 5–18, Aug. 2010.
- [69] C.-H. Xue, S.-T. Jia, H.-Z. Chen, and M. Wang, "Superhydrophobic cotton fabrics prepared by sol–gel coating of TiO₂ and surface hydrophobization," *Sci. Technol. Adv. Mater.*, vol. 9, no. 3, p. 035001, Jul. 2008.
- [70] C. Te Hsieh, F. L. Wu, and S. Y. Yang, "Superhydrophobicity from composite nano/microstructures: Carbon fabrics coated with silica nanoparticles," *Surf. Coatings*

- Technol.*, vol. 202, no. 24, pp. 6103–6108, 2008.
- [71] Y. Wang, Z. Mo, C. Zhang, P. Zhang, R. Guo, H. Gou, R. Hu, and X. Wei, “Morphology-controllable 3D flower-like TiO₂ for UV shielding application,” *J. Ind. Eng. Chem.*, vol. 32, pp. 172–177, 2015.
- [72] H. Joo Kim, H. Raj Pant, J. Hee Kim, N. Jung Choi, and C. Sang Kim, “Fabrication of multifunctional TiO₂-fly ash/polyurethane nanocomposite membrane via electrospinning,” *Ceram. Int.*, vol. 40, no. 2, pp. 3023–3029, 2014.
- [73] A. N. Ökte, D. Karamanis, and D. Tuncel, “Dual functionality of TiO₂-flyash nanocomposites: Water vapor adsorption and photocatalysis,” *Catal. Today*, vol. 230, pp. 205–213, 2014.
- [74] B. Wang, C. Li, J. Pang, X. Qing, J. Zhai, and Q. Li, “Novel polypyrrole-sensitized hollow TiO₂/fly ash cenospheres: Synthesis, characterization, and photocatalytic ability under visible light,” *Appl. Surf. Sci.*, vol. 258, no. 24, pp. 9989–9996, 2012.
- [75] J. Wang, F. Han, and S. Zhang, “Durably superhydrophobic textile based on fly ash coating for oil/water separation and selective oil removal from water,” *Sep. Purif. Technol.*, vol. 164, pp. 138–145, 2016.
- [76] S. Ge, B. Wang, D. Li, W. Fa, Z. Yang, Z. Yang, G. Jia, and Z. Zheng, “Surface controlled photocatalytic degradation of RhB over flower-like rutile TiO₂ superstructures,” *Appl. Surf. Sci.*, vol. 295, pp. 123–129, 2014.
- [77] J. Yuenyongsuwan, N. Nithiyakorn, P. Sabkird, E. A. O’Rear, and T. Pongprayoon, “Surfactant effect on phase-controlled synthesis and photocatalyst property of TiO₂ nanoparticles,” *Mater. Chem. Phys.*, vol. 214, pp. 330–336, 2018.
- [78] Y. Li, J. Liu, and Z. Jia, “Morphological control and photodegradation behavior of rutile TiO₂ prepared by a low-temperature process,” *Mater. Lett.*, vol. 60, no. 13–14, pp. 1753–1757, 2006.
- [79] Q. E. Zhao, W. Wen, Y. Xia, and J. M. Wu, “Photocatalytic activity of TiO₂ nanorods, nanowires and nanoflowers filled with TiO₂ nanoparticles,” *Thin Solid Films*, vol. 648, no. December 2017, pp. 103–107, 2018.
- [80] Z. Wu, Q. Wu, L. Du, C. Jiang, and L. Piao, “Progress in the synthesis and applications of

- hierarchical flower-like TiO₂ nanostructures,” *Particuology*, vol. 15, pp. 61–70, 2014.
- [81] M. Hasanpoor, M. Aliofkhazraei, and H. Delavari, “Microwave assisted synthesis of Zinc oxide nanoparticles,” *Procedia Mater. Sci.*, vol. 8, no. 11, pp. 320–325, 2015.
- [82] X. L. Hu, Y. J. Zhu, and S. W. Wang, “Sonochemical and microwave-assisted synthesis of linked single-crystalline ZnO rods,” *Mater. Chem. Phys.*, vol. 88, no. 2–3, pp. 421–426, 2004.
- [83] A. Kajbafvala, S. Zanganeh, E. Kajbafvala, H. R. Zargar, M. R. Bayati, and S. K. Sadrnezhad, “Microwave-assisted synthesis of narciss-like zinc oxide nanostructures,” *J. Alloys Compd.*, vol. 497, no. 1–2, pp. 325–329, 2010.
- [84] S. Fujita, B. M. Bhanage, M. Arai, P. Tambade, and K. D. Bhatte, “Microwave-assisted additive free synthesis of nanocrystalline zinc oxide,” *Powder Technol.*, vol. 203, no. 2, pp. 415–418, 2010.
- [85] K. Manoharan and S. Bhattacharya, “Superhydrophobic surfaces review: Functional application, fabrication techniques and limitations,” *J. Micromanufacturing*, vol. 2, no. 1, pp. 59–78, 2019.
- [86] C. H. Xue, J. Chen, W. Yin, S. T. Jia, and J. Z. Ma, “Superhydrophobic conductive textiles with antibacterial property by coating fibers with silver nanoparticles,” *Appl. Surf. Sci.*, vol. 258, no. 7, pp. 2468–2472, 2012.
- [87] J. Y. Huang, S. H. Li, M. Z. Ge, L. N. Wang, T. L. Xing, G. Q. Chen, X. F. Liu, S. S. Al-Deyab, K. Q. Zhang, T. Chen, and Y. K. Lai, “Robust superhydrophobic TiO₂ @fabrics for UV shielding, self-cleaning and oil–water separation,” *J. Mater. Chem. A*, vol. 3, no. 6, pp. 2825–2832, 2015.
- [88] M. Ashraf, P. Champagne, C. Campagne, a. Perwuelz, F. Dumont, and a. Leriche, “Study the multi self-cleaning characteristics of ZnO nanorods functionalized polyester fabric,” *J. Ind. Text.*, pp. 1–17, 2014.
- [89] N. Preda, M. Enculescu, I. Zgura, M. Socol, E. Matei, V. Vasilache, and I. Enculescu, “Superhydrophobic properties of cotton fabrics functionalized with ZnO by electroless deposition,” *Mater. Chem. Phys.*, vol. 138, no. 1, pp. 253–261, 2013.
- [90] B. Xu, Y. Ding, S. Qu, and Z. Cai, “Applied Surface Science Superamphiphobic cotton

- fabrics with enhanced stability,” *Appl. Surf. Sci.*, vol. 356, pp. 951–957, 2015.
- [91] X. J. Guo, C. H. Xue, M. Li, X. Li, and J. Z. Ma, “Fabrication of robust, superhydrophobic, electrically conductive and UV-blocking fabrics: Via layer-by-layer assembly of carbon nanotubes,” *RSC Adv.*, vol. 7, no. 41, pp. 25560–25565, 2017.
- [92] F. Ahmad, F. Idrees, Fazal-e-Aleem, and F. Idrees, “Recent Advancements in Microwave-Assisted Synthesis of NiO Nanostructures and their Supercapacitor Properties: A Comprehensive Review,” *Curr. Nanomater.*, vol. 3, no. 1, pp. 5–17, 2018.
- [93] A. Mirzaei and G. Neri, “Microwave-assisted synthesis of metal oxide nanostructures for gas sensing application: A review,” *Sensors Actuators, B Chem.*, vol. 237, pp. 749–775, 2016.
- [94] S. C. Motshekga, S. K. Pillai, S. Sinha Ray, K. Jalama, and R. W. M. Krause, “Recent trends in the microwave-assisted synthesis of metal oxide nanoparticles supported on carbon nanotubes and their applications,” *J. Nanomater.*, vol. 2012, p. 15, 2012.
- [95] S. Faheem, V. Baheti, M. Tunak, J. Wiener, and J. Militky, “Comparative performance of flame retardancy, physiological comfort, and durability of cotton textiles treated with alkaline and acidic casein suspension,” *J. Ind. Text.*, p. 152808371775088, 2017.
- [96] A. Das, J. Deka, A. M. Rather, B. K. Bhunia, P. P. Saikia, B. B. Mandal, K. Raidongia, and U. Manna, “Strategic Formulation of Graphene Oxide Sheets for Flexible Monoliths and Robust Polymeric Coatings Embedded with Durable Bioinspired Wettability,” *ACS Appl. Mater. Interfaces*, vol. 9, no. 48, pp. 42354–42365, 2017.
- [97] D. Parbat, S. Gaffar, A. M. Rather, A. Gupta, and U. Manna, “A general and facile chemical avenue for the controlled and extreme regulation of water wettability in air and oil wettability under water,” *Chem. Sci.*, vol. 8, no. 9, pp. 6542–6554, 2017.
- [98] A. M. Rather and U. Manna, “Stretchable and durable superhydrophobicity that acts both in air and under oil,” *J. Mater. Chem. A*, vol. 5, no. 29, pp. 15208–15216, 2017.
- [99] X. N. Tang, A. E. Berman, R. A. Swanson, and M. A. Yenari s, “Digitally quantifying cerebral hemorrhage using Photoshop® and Image J,” *J. Neurosci. Methods*, vol. 190, no. 2, pp. 240–243, 2010.
- [100] V. Baheti, J. Militky, R. Mishra, and B. K. Behera, “Thermomechanical properties of glass

- fabric/epoxy composites filled with fly ash,” *Compos. Part B Eng.*, vol. 85, pp. 268–276, Feb. 2015.
- [101] P. Cataldi, I. S. Bayer, R. Cingolani, S. Marras, R. Chellali, and A. Athanassiou, “A Thermochromic Superhydrophobic Surface,” *Sci. Rep.*, vol. 6, no. February, pp. 1–11, 2016.
- [102] X. Dong, S. Gao, J. Huang, S. Li, T. Zhu, Y. Cheng, Y. Zhao, Z. Chen, and Y. Lai, “A self-roughened and biodegradable superhydrophobic coating with UV shielding, solar-induced self-healing and versatile oil-water separation ability,” *J. Mater. Chem. A*, vol. 7, no. 5, pp. 2122–2128, 2019.
- [103] X. Luo, Y. Weng, S. Wang, J. Du, H. Wang, and C. Xu, “Superhydrophobic and oleophobic textiles with hierarchical micro-nano structure constructed by sol–gel method,” *J. Sol-Gel Sci. Technol.*, vol. 89, no. 3, pp. 820–829, 2019.
- [104] H. R. Pant, M. P. Bajgai, K. T. Nam, Y. A. Seo, D. R. Pandeya, S. T. Hong, and H. Y. Kim, “Electrospun nylon-6 spider-net like nanofiber mat containing TiO₂ nanoparticles: A multifunctional nanocomposite textile material,” *J. Hazard. Mater.*, vol. 185, no. 1, pp. 124–130, 2011.
- [105] C. Pan, L. Shen, S. Shang, and Y. Xing, “Preparation of superhydrophobic and UV blocking cotton fabric via sol-gel method and self-assembly,” *Appl. Surf. Sci.*, vol. 259, pp. 110–117, 2012.
- [106] Y. Zhao, Z. Xu, X. Wang, and T. Lin, “Superhydrophobic and UV-blocking cotton fabrics prepared by layer-by-layer assembly of organic UV absorber intercalated layered double hydroxides,” *Appl. Surf. Sci.*, vol. 286, pp. 364–370, 2013.
- [107] A. Ali, V. Baheti, J. Militky, and Z. Khan, “Utility of silver-coated fabrics as electrodes in electrotherapy applications,” *J. Appl. Polym. Sci.*, vol. 135, no. 23, 2018.
- [108] A. Ali, V. Baheti, J. Militky, Z. Khan, V. Tunakova, and S. Naeem, “Copper coated multifunctional cotton fabrics,” *J. Ind. Text.*, vol. 0, no. 00, p. 152808371773207, 2017.
- [109] A. Ali, N. H. A. Nguyen, V. Baheti, M. Ashraf, J. Militky, T. Mansoor, M. T. Noman, and S. Ahmad, “Electrical conductivity and physiological comfort of silver coated cotton fabrics,” *J. Text. Inst.*, vol. 109, no. 5, pp. 620–628, 2018.

- [110] Y. Zhao, Y. Tang, X. Wang, and T. Lin, "Superhydrophobic cotton fabric fabricated by electrostatic assembly of silica nanoparticles and its remarkable buoyancy," *Appl. Surf. Sci.*, vol. 256, no. 22, pp. 6736–6742, 2010.
- [111] P. Aminayi and N. Abidi, "Ultra-oleophobic cotton fabric prepared using molecular and nanoparticle vapor deposition methods," *Surf. Coatings Technol.*, vol. 276, pp. 636–644, 2015.
- [112] X. Zhu, Z. Zhang, B. Ge, X. Men, X. Zhou, and Q. Xue, "A versatile approach to produce superhydrophobic materials used for oil-water separation," *J. Colloid Interface Sci.*, vol. 432, pp. 105–108, 2014.
- [113] B. Jiang, Z. Chen, Y. Sun, H. Yang, H. Zhang, H. Dou, and L. Zhang, "Fabrication of superhydrophobic cotton fabrics using crosslinking polymerization method," *Appl. Surf. Sci.*, vol. 441, pp. 554–563, 2018.
- [114] J. Wang, G. Geng, A. Wang, X. Liu, J. Du, Z. Zou, S. Zhang, and F. Han, "Double biomimetic fabrication of robustly superhydrophobic cotton fiber and its application in oil spill cleanup," *Ind. Crops Prod.*, vol. 77, pp. 36–43, 2015.
- [115] F. Liu, M. Ma, D. Zang, Z. Gao, and C. Wang, "Fabrication of superhydrophobic/superoleophilic cotton for application in the field of water/oil separation," *Carbohydr. Polym.*, vol. 103, no. 1, pp. 480–487, 2014.
- [116] Y. Jin, P. Jiang, Q. Ke, F. Cheng, Y. Zhu, and Y. Zhang, "Superhydrophobic and superoleophilic polydimethylsiloxane-coated cotton for oil-water separation process: An evidence of the relationship between its loading capacity and oil absorption ability," *J. Hazard. Mater.*, vol. 300, pp. 175–181, 2015.
- [117] J. Wang and G. Geng, "Highly recyclable superhydrophobic sponge suitable for the selective sorption of high viscosity oil from water," *Mar. Pollut. Bull.*, vol. 97, no. 1–2, pp. 118–124, 2015.
- [118] A. Cammarano, G. De Luca, and E. Amendola, "Surface modification and adhesion improvement of polyester films," *Cent. Eur. J. Chem.*, vol. 11, no. 1, pp. 35–45, 2013.
- [119] P. Soundarrajan, K. Sankarasubramanian, T. Logu, K. Sethuraman, and K. Ramamurthi, "Growth of rutile TiO₂ nanorods on TiO₂ seed layer prepared using facile low cost

- chemical methods," *Mater. Lett.*, vol. 116, pp. 191–194, 2014.
- [120] G. Nagaraju, K. Manjunath, T. N. Ravishankar, B. S. Ravikumar, H. Nagabhushan, G. Ebeling, and J. Dupont, "Ionic liquid-assisted hydrothermal synthesis of TiO₂ nanoparticles and its application in photocatalysis," *J. Mater. Sci.*, vol. 48, no. 24, pp. 8420–8426, Aug. 2013.
- [121] X. Gan, X. Gao, J. Qiu, P. He, X. Li, and X. Xiao, "TiO₂ nanorod-derived synthesis of upstanding hexagonal kassite nanosheet arrays: An intermediate route to novel nanoporous TiO₂ nanosheet arrays," *Cryst. Growth Des.*, vol. 12, no. 1, pp. 289–296, 2012.
- [122] M. R. Subramaniam, S. Devanathan, and D. Kumaresan, "Synthesis of micrometer-sized hierarchical rutile TiO₂ flowers and their application in dye sensitized solar cells," *RSC Adv.*, vol. 4, no. 69, pp. 36791–36799, 2014.
- [123] A. M. Selman, Z. Hassan, and M. Husham, "Structural and photoluminescence studies of rutile TiO₂ nanorods prepared by chemical bath deposition method on Si substrates at different pH values," *Meas. J. Int. Meas. Confed.*, vol. 56, pp. 155–162, 2014.
- [124] N. Li, Q. Zhang, J. B. Joo, Z. Lu, M. Dahl, Y. Gan, and Y. Yin, "Water-assisted crystallization of mesoporous anatase TiO₂ nanospheres," *Nanoscale*, vol. 8, no. 17, pp. 9113–9117, 2016.
- [125] M. Li, Y. Jiang, R. Ding, D. Song, H. Yu, and Z. Chen, "Hydrothermal Synthesis of Anatase TiO₂ Nanoflowers on a Nanobelt Framework for Photocatalytic Applications," *J. Electron. Mater.*, vol. 42, no. 6, pp. 1290–1296, 2013.
- [126] R. . Spurr and H. Myers, "Quantitative Analysis of Anatase-Rutile Mixtures with an X-Ray Diffractometer," *Anal. Chem.*, vol. 29, no. 5, pp. 760–762, 1957.
- [127] A. Ali, V. Baheti, J. Militky, Z. Khan, V. Tunakova, and S. Naeem, "Copper coated multifunctional cotton fabrics," *J. Ind. Text.*, vol. 48, no. 2, pp. 448–464, 2018.
- [128] J. Y. Huang, S. H. Li, M. Z. Ge, L. N. Wang, T. L. Xing, G. Q. Chen, X. F. Liu, S. S. Al-Deyab, K. Q. Zhang, T. Chen, and Y. K. Lai, "Robust superhydrophobic TiO₂@fabrics for UV shielding, self-cleaning and oil-water separation," *J. Mater. Chem. A*, vol. 3, no. 6, pp. 2825–2832, 2015.

- [129] A. B. Gurav, S. S. Latthe, R. S. Vhatkar, J. G. Lee, D. Y. Kim, J. J. Park, and S. S. Yoon, "Superhydrophobic surface decorated with vertical ZnO nanorods modified by stearic acid," *Ceram. Int.*, vol. 40, no. 5, pp. 7151–7160, 2014.
- [130] B. Xu, Z. Cai, W. Wang, and F. Ge, "Preparation of superhydrophobic cotton fabrics based on SiO₂ nanoparticles and ZnO nanorod arrays with subsequent hydrophobic modification," *Surf. Coatings Technol.*, vol. 204, no. 9–10, pp. 1556–1561, 2010.
- [131] S. Riaz, M. Ashraf, T. Hussain, M. T. Hussain, and A. Younus, "Fabrication of Robust Multifaceted Textiles by Application of Functionalized TiO₂ Nanoparticles," *Colloids Surfaces A Physicochem. Eng. Asp.*, vol. 581, no. August, p. 123799, 2019.
- [132] F. Xu, Y. Lu, Y. Xie, and Y. Liu, "Controllable morphology evolution of electrodeposited ZnO nano/micro-scale structures in aqueous solution," *Mater. Des.*, vol. 30, no. 5, pp. 1704–1711, 2009.
- [133] R. Nandi and S. S. Major, "The mechanism of growth of ZnO nanorods by reactive sputtering," *Appl. Surf. Sci.*, vol. 399, pp. 305–312, 2017.
- [134] M. Skompska and K. Zarębska, "Electrodeposition of ZnO nanorod arrays on transparent conducting substrates-a review," *Electrochim. Acta*, vol. 127, pp. 467–488, 2014.
- [135] M. He, W. Li, J. Ran, D. Cheng, J. Wu, G. Cai, and X. Wang, "Hydrothermal growing of cluster-like ZnO nanoparticles without crystal seeding on PET films via dopamine anchor," *Appl. Surf. Sci.*, vol. 467–468, no. August 2018, pp. 534–542, 2018.
- [136] V. R. Shinde, T. P. Gujar, T. Noda, D. Fujita, A. Vinu, M. Grandcolas, and J. Ye, "Growth of shape- and size-selective zinc oxide nanorods by a microwave-assisted chemical bath deposition method: Effect on photocatalysis properties," *Chem. - A Eur. J.*, vol. 16, no. 34, pp. 10569–10575, 2010.
- [137] K. Edalati, A. Shakiba, J. Vahdati-Khaki, and S. M. Zebarjad, "Low-temperature hydrothermal synthesis of ZnO nanorods: Effects of zinc salt concentration, various solvents and alkaline mineralizers," *Mater. Res. Bull.*, vol. 74, pp. 374–379, 2016.
- [138] H. Zhang, D. Yang, X. Ma, N. Du, J. Wu, and D. Que, "Straight and thin ZnO nanorods: Hectogram-scale synthesis at low temperature and cathodoluminescence," *J. Phys. Chem. B*, vol. 110, no. 2, pp. 827–830, 2006.

- [139] R. Wahab, Y. S. Kim, K. Lee, and H. S. Shin, "Fabrication and growth mechanism of hexagonal zinc oxide nanorods via solution process," *J. Mater. Sci.*, vol. 45, no. 11, pp. 2967–2973, 2010.
- [140] D. Polsongkram, P. Chamninok, S. Pukird, L. Chow, O. Lupan, G. Chai, H. Khallaf, S. Park, and A. Schulte, "Effect of synthesis conditions on the growth of ZnO nanorods via hydrothermal method," *Phys. B Condens. Matter*, vol. 403, no. 19–20, pp. 3713–3717, 2008.
- [141] H. E. Unalan, P. Hiralal, N. Rupesinghe, S. Dalal, W. I. Milne, and G. A. J. Amaratunga, "Rapid synthesis of aligned zinc oxide nanowires," *Nanotechnology*, vol. 19, no. 25, 2008.
- [142] A. Ul Hassan Sarwar Rana, M. Kang, and H. S. Kim, "Microwave-assisted Facile and Ultrafast Growth of ZnO Nanostructures and Proposition of Alternative Microwave-assisted Methods to Address Growth Stoppage," *Sci. Rep.*, vol. 6, no. April, pp. 1–13, 2016.
- [143] S. Brahma, K. J. Rao, and S. Shivashankar, "Rapid growth of nanotubes and nanorods of würtzite ZnO through microwave-irradiation of a metalorganic complex of zinc and a surfactant in solution," *Bull. Mater. Sci.*, vol. 33, no. 2, pp. 89–95, 2010.
- [144] M. Küçük and M. L. Öveçoğlu, "Fabrication of SiO₂–ZnO NP/ZnO NR hybrid coated cotton fabrics: the effect of ZnO NR growth time on structural and UV protection characteristics," *Cellulose*, vol. 2, pp. 1773–1793, 2019.
- [145] E. S. Ates and H. E. Unalan, "Zinc oxide nanowire enhanced multifunctional coatings for cotton fabrics," *Thin Solid Films*, vol. 520, no. 14, pp. 4658–4661, 2012.
- [146] H. Ghayour, H. R. Rezaie, S. Mirdamadi, and A. A. Nourbakhsh, "The effect of seed layer thickness on alignment and morphology of ZnO nanorods," *Vacuum*, vol. 86, no. 1, pp. 101–105, 2011.
- [147] T. Dedova, I. O. Acik, M. Krunks, V. Mikli, O. Volobujeva, and A. Mere, "Effect of substrate morphology on the nucleation and growth of ZnO nanorods prepared by spray pyrolysis," *Thin Solid Films*, vol. 520, no. 14, pp. 4650–4653, 2012.
- [148] G. Qi, H. Zhang, and Z. Yuan, "Superhydrophobic brocades modified with aligned ZnO nanorods," *Appl. Surf. Sci.*, vol. 258, no. 2, pp. 662–667, 2011.

- [149] D. Hill, H. Attia, A. R. Barron, and S. Alexander, "Size and morphology dependent surface wetting based on hydrocarbon functionalized nanoparticles," *J. Colloid Interface Sci.*, vol. 543, pp. 328–334, 2019.
- [150] R. G. Karunakaran, C. Lu, Z. Zhang, and S. Yang, "Highly Transparent Superhydrophobic Surfaces from the Coassembly of Nanoparticles (e100 nm)," *Langmuir*, vol. 27, pp. 4594–4602, 2011.

LIST OF PUBLICATIONS

PUBLICATIONS IN IMPACT FACTOR JOURNALS

1. **Muhammad Zaman Khan**, Vijay Baheti, Jiri Militky, Azam Ali, and Martina Vikova. "Superhydrophobicity, UV-protection and oil/water separation properties of fly ash/trimethoxy (octadecyl) silane coated cotton fabrics." *Carbohydrate Polymers* 202 (2018): 571-580. **(Impact factor = 6.04)**
2. **Muhammad Zaman Khan**, Vijay Baheti, Jiri Militky, Jakub Wiener, and Azam Ali. "Self-cleaning properties of polyester fabrics coated with flower-like TiO₂ particles and trimethoxy (octadecyl) silane." *Journal of Industrial Textiles* (2019): doi.org/10.1177/1528083719836938. **(Impact factor = 1.88)**
3. **Muhammad Zaman Khan**, Vijay Baheti, Munir Ashraf, Tanveer Hussain and Azam Ali. "Development of UV Protective, Superhydrophobic and Antibacterial Textiles Using ZnO and TiO₂ Nanoparticles." *Fibers and Polymers* 19, no. 8 (2018): 1647-1654. **(Impact factor = 1.43)**
4. **Muhammad Zaman Khan**, Sajid Hussain, Faisal Siddique, Vijay Baheti, Jiri Militky "Improvement of liquid moisture management in plaited knitted fabrics". *TEKSTİL VE KONFEKSİYON* 28, (2018): 182-188. **(Impact factor = 0.27)**
5. **Muhammad Zaman Khan**, Munir Ashraf, Tanveer Hussain, Abdur Rehman, Muhammad Mohsin Malik, and Qasim Zia. "In situ deposition of TiO₂ nanoparticles on polyester fabric and study of its functional properties." *Fibers and Polymers* 16, no. 5 (2015): 1092-1097. **(Impact factor = 1.43)**
6. Ali, Azam, Vijay Baheti, **Muhammad Zaman Khan**, Munir Ashraf, and Jiri Militky. "Development of electrically conductive composites based on recycled resources." *The Journal of the Textile Institute* 111, no. 1 (2020): 16-25. **(Impact factor = 1.06)**
7. Ali, Azam, Vijay Baheti, Jiri Militky, **Zaman Khan**, and Guocheng Zhu. "Metal Coating on Ultrafine Polyester Non-woven Fabrics and Their Ageing Properties." *Fibers and Polymers* 20, no. 7 (2019): 1347-1359. **(Impact factor = 1.43)**

8. Ali, Azam, Vijay Baheti, Jiri Militky, and **Zaman Khan**. "Utility of silver-coated fabrics as electrodes in electrotherapy applications." *Journal of Applied Polymer Science* 135, no. 23 (2018): 46357. **(Impact factor = 2.18)**
9. Azam Ali, Vijay Baheti, Jiri Militky, **Zaman Khan**, and Syed Qummer Zia Gilani. "Comparative Performance of Copper and Silver Coated Stretchable Fabrics." *Fibers and Polymers* 19, no. 3 (2018): 607-619. **(Impact factor = 1.43)**
10. Azam Ali, Vijay Baheti, Jiri Militky, **Zaman Khan**, Veronika Tunakova, and Salman Naeem. "Copper coated multifunctional cotton fabrics." *Journal of Industrial Textiles* 48, no. 2 (2018): 448-464. **(Impact factor = 1.88)**
11. Azeem, Musaddaq, Jakub Wiener, and **Muhammad Zaman Khan**. "Hydrophobic analysis of nano-filament polyester fabric." *Vlakna a Textil*, 2018.
12. Hussain, Sajid, Viera Glombikova, Antonín Havelka, Hafsa Jamshaid, Syeda Sidra Batool, **Muhammad Zaman Khan**. "MOISTURE TRANSPORT PHENOMENA OF FUNCTIONAL." *Vlakna a Textil*, 2017.
13. **Muhammad Zaman Khan**, Jakub Wiener, Vijay Baheti, Jiri Militky " Development of durable Superhydrophobic and UV protective cotton fabric via TiO₂/Trimethoxy(octadecyl)silane nanocomposite coating" Under Review in *Journal of Textile Institute*.
14. **Muhammad Zaman Khan**, Jiri Militky, Jakub Wiener " Development of Robust Superhydrophobic Cotton Fabrics by Microwave Hydrothermal Synthesis of Zinc Oxide Nanorods " Under Submission.

PUBLICATIONS IN INTERNATIONAL CONFERENCES

1. **Muhammad Zaman Khan**, Vijay Baheti, Jiri Militky, "Superhydrophobicity, UV protection and oil/water separation properties of TiO₂ nanoparticles and Trimethoxy(octadecyl)silane coated cotton fabrics" The Fiber Society Fall 2019 Conference: University of Texas, Austin, USA, October 2019.
2. **Muhammad Zaman Khan**, Vijay Baheti, Jiri Militky, "Development of Superhydrophobic Cotton Fabrics and Their Functional Properties" ICDTC 2019 : 21th

International Conference on Defence Textiles and Clothing, London, United Kingdom, June 2019.

3. **Muhammad Zaman Khan**, Vijay Baheti, Jiri Militky, “Self-cleaning polyester fabrics decorated with flower like TiO_2 particles” CEC 2019: 10th Central European Conference, Lodz, Poland, October 2019.
4. **Muhammad Zaman Khan**, Vijay Baheti, Jiri Militky, “Hydrothermal synthesis of TiO_2 nanoparticles on PET fabric and their functional properties” The 47th Textile Research Symposium, Liberec, Czech Republic, June 2019.
5. **Muhammad Zaman Khan**, Vijay Baheti, Jiri Militky, “ Development of multifunctional polyester fabric functionalized with TiO_2 nanoparticles” 18th World Textile Conference (AUTEX), Istanbul, Turkey, June 2018.
6. **Muhammad Zaman Khan**, Vijay Baheti, Jiri Militky, “Superhydrophobization of cotton fabric with fly ash for durable UV protection and oil/water separation properties.” International PhD Students Day, 22nd Strutex 2018, Liberec, Czech Republic.
7. **Muhammad Zaman Khan**, Vijay Baheti, Jiri Militky, "Study the functional properties of polyester fabric functionalized with TiO_2 nanoparticles." 195th International Conference on Innovative Engineering Technologies (ICIET). Rawalpindi: IRES, 2017.
8. Musaddaq Azeem, Jakub Wiener, and **Muhammad Zaman Khan**. “Hydrophobic treatment of nano-filament polyester fabric.” International Ph.D. Students Day. CEC 2017, Liberec, Czech Republic.

PUBLICATIONS IN BOOK CHAPTERS

1. **Muhammad Zaman Khan**, Vijay Baheti, Jiri Militky, “ Methods for characterization and evaluation of self-cleaning textiles ” Recent Trends in Fibrous Material Science, Vol- 5, September 2019.
2. Ahmed Hassanin, Yuanfeng Wang, **Muhammad Zaman Khan**, Vijay Baheti, Jiri Militky, “ Surface modification of textile fibers by whiskerization ” Recent Trends in Fibrous Material Science, Vol- 5, September 2019.

RESEARCH PROJECTS

1. Leader of the student grant competition (SGS) project 2019, titled, “Conventional and microwave-assisted hydrothermal methods for coating of textiles”, Faculty of Textile Engineering, Technical University of Liberec, Czech Republic.
2. Leader of the student grant competition (SGS) project 2018, titled, “Superhydrophobic textiles with added functionality”, Faculty of Textile Engineering, Technical University of Liberec, Czech Republic.
3. Member of the student grant competition (SGS) project 2017, titled, “Preparation of modified carbon sorbents”, Faculty of Textile Engineering, Technical University of Liberec, Czech Republic.

Citations

Article: Muhammad Zaman Khan, Vijay Baheti, Jiri Militky, Azam Ali, and Martina Vikova. "Superhydrophobicity, UV-protection and oil/water separation properties of fly ash/trimethoxy (octadecyl) silane coated cotton fabrics." *Carbohydrate Polymers* 202 (2018): 571-580. **(Impact factor = 6.04)**

(Cited in)

1. Kang, Lei, et al. "A water solvent-assisted condensation polymerization strategy of superhydrophobic lignocellulosic fibers for efficient oil/water separation." *Journal of Materials Chemistry A* 7.27 (2019): 16447-16457.
2. Ghasemlou, Mehran, et al. "Bio-inspired sustainable and durable superhydrophobic materials: from nature to market." *Journal of Materials Chemistry A* 7.28 (2019): 16643-16670.
3. Yu, Mingguang, et al. "Facile fabrication of magnetic, durable and superhydrophobic cotton for efficient oil/water separation." *Polymers* 11.3 (2019): 442.
4. Ali, Azam, Vijay Baheti, and Jiri Militky. "Energy harvesting performance of silver electroplated fabrics." *Materials Chemistry and Physics* 231 (2019): 33-40.
5. Yang, Yingying, et al. "Fabrication of multifunctional textiles with durable antibacterial property and efficient oil-water separation via in situ growth of zeolitic imidazolate

- framework-8 (ZIF-8) on cotton fabric." *Applied Surface Science* 503 (2020): 144079.
6. Yang, Yingying, et al. "Robust fluorine-free colorful superhydrophobic PDMS/NH 2-MIL-125 (Ti)@ cotton fabrics for improved ultraviolet resistance and efficient oil–water separation." *Cellulose* 26.17 (2019): 9335-9348.
 7. Qiu, Yujuan, and Xiaojun Ma. "Crystallization, mechanical and UV protection properties of graphene oxide/poly (3-hydroxybutyrate-co-3-hydroxyhexanoate) biocomposites." *Journal of Materials Science* 54.23 (2019): 14388-14399.
 8. Yalcinkaya, Fatma, et al. "A Review on Membrane Technology and Chemical Surface Modification for the Oily Wastewater Treatment." *Materials* 13.2 (2020): 493.
 9. Küçük, Merve, and Mustafa Lütfi Öveçoğlu. "Fabrication of SiO₂–ZnO NP/ZnO NR hybrid coated cotton fabrics: the effect of ZnO NR growth time on structural and UV protection characteristics." *Cellulose* 27.3 (2020): 1773-1793.
 10. He, Yali, et al. "Fabrication and characterization of degradable and durable fluoride-free super-hydrophobic cotton fabrics for oil/water separation." *Surface and Coatings Technology* 378 (2019): 125079.
 11. Faheem, Sajid, et al. "Flame Retardancy, Physiological Comfort and Durability of Casein Treated Cotton Fabrics." *Fibers and Polymers* 20.5 (2019): 1011-1020.
 12. Khan, Muhammad Zaman, et al. "Self-cleaning properties of polyester fabrics coated with flower-like TiO₂ particles and trimethoxy (octadecyl) silane." *Journal of Industrial Textiles* (2019): 1528083719836938.

Article: Muhammad Zaman Khan, Vijay Baheti, Munir Ashraf, Tanveer Hussain and Azam Ali. "Development of UV Protective, Superhydrophobic and Antibacterial Textiles Using ZnO and TiO₂ Nanoparticles. " *Fibers and Polymers* 19, no. 8 (2018): 1647-1654. **(Impact factor = 1.43)**

(Cited in)

1. Ogunsona, Emmanuel O., et al. "Engineered nanomaterials for antimicrobial applications: A review." *Applied Materials Today* (2019): 100473.
2. Zhang, Guangyu, et al. "Study on the Photocatalytic and Antibacterial Properties of TiO₂ Nanoparticles-Coated Cotton Fabrics." *Materials* 12.12 (2019): 2010.

3. Verbič, Anja, Marija Gorjanc, and Barbara Simončič. "Zinc oxide for functional textile coatings: Recent advances." *Coatings* 9.9 (2019): 550.
4. Shaheen, Tharwat I., Salem S. Salem, and Saad Zaghoul. "A new facile strategy for multifunctional textiles development through in situ deposition of SiO₂/TiO₂ nanosols hybrid." *Industrial & Engineering Chemistry Research* 58.44 (2019): 20203-20212.
5. Sliman, Hashim, Xue Dong, and Tao Zhao. "Functionalization of polyethylene terephthalate knitted fabric with cowpea protein and biopolymer complex: Applications for enhancing wettability and UV-Protection properties." *Journal of Colloid and Interface Science* 565 (2020): 360-367.
6. Nazari, Ali. "Preparation of Electroconductive, Antibacterial, Photoactive Cotton Fabric Through Green Synthesis of ZnO/reduced Graphene Oxide Nanocomposite." *Fibers and Polymers* 20.12 (2019): 2618-2624.
7. Khan, Muhammad Zaman, et al. "Self-cleaning properties of polyester fabrics coated with flower-like TiO₂ particles and trimethoxy (octadecyl) silane." *Journal of Industrial Textiles* (2019): 1528083719836938.